

2015

Synthesis of 2-Amino- α -Carboline and Analogues Relevant for Structural Investigations of the Corresponding DNA Adducts

Matthew S. Blake
University of Rhode Island, matt486@my.uri.edu

Follow this and additional works at: <https://digitalcommons.uri.edu/theses>

Terms of Use

All rights reserved under copyright.

Recommended Citation

Blake, Matthew S., "Synthesis of 2-Amino- α -Carboline and Analogues Relevant for Structural Investigations of the Corresponding DNA Adducts" (2015). *Open Access Master's Theses*. Paper 794. <https://digitalcommons.uri.edu/theses/794>

This Thesis is brought to you by the University of Rhode Island. It has been accepted for inclusion in Open Access Master's Theses by an authorized administrator of DigitalCommons@URI. For more information, please contact digitalcommons-group@uri.edu. For permission to reuse copyrighted content, contact the author directly.

SYNTHESIS OF 2-AMINO- α -CARBOLINE AND ANALOGUES RELEVANT
FOR STRUCTURAL INVESTIGATIONS OF THE CORRESPONDING DNA
ADDUCTS

BY

MATTHEW BLAKE

A THESIS SUBMITTED IN PARTIAL FULLFILLMENT OF THE
REQUIREMENTS FOR THE DEGREE OF

MASTER OF SCIENCE

IN

PHARMACEUTICAL SCIENCES

UNIVERSITY OF RHODE ISLAND

2015

MASTER OF SCIENCE THESIS
OF
MATTHEW BLAKE

APPROVED:

Thesis Committee:

Major Professor: Bongsup Cho

Deyu Li

Matthew Kiesewetter

Nasser H. Zawia

DEAN OF THE GRADUATE SCHOOL

UNIVERSITY OF RHODE ISLAND

2015

Abstract

In rational drug design, the most effective targets are identified when a mechanism-based understanding of a disease state's proliferation and persistence is available. 2-amino- α -carboline (2-A α C) is a heterocyclic aromatic amine (HAA), which upon metabolic activation *in vivo*, can covalently bind to the C8-position of guanine. This modification elicits a response from the Nucleotide Excision Repair (NER) system but, if left unrepaired, may result in mutations. The metabolites of 2-A α C are significantly more reactive towards adduct formation than those of 4-aminobiphenyl (4-ABP), a confirmed human bladder carcinogen. Furthermore, 2-A α C is found in cigarette smoke at concentrations 1000 times greater than 4-ABP. 2-A α C has been implicated in hepatocellular carcinoma and cancers of the gastrointestinal tract, potentially explaining the increased incidence of liver cancer in smokers. The cause of cancers and many other diseases is attributed to DNA mutations caused by failure of a cell's natural DNA repair mechanisms. NER is a major human repair system among many, all part of a complex network consisting of hundreds of proteins that target different types of damage. The overlapping systems making up this network are dependent on molecular recognition and signaling pathways.

Structural and thermodynamic investigations of abnormal DNA duplexes have yielded valuable mechanism-based information for use in drug discovery. To

perform these studies, the DNA lesion in question must be readily available. Despite powerful implications regarding the role of 2-AαC in cancer, efficient synthetic protocols are not available for 2-AαC or the corresponding adducts. Inefficient biomimetic production of C8-(2-AαC)-guanine adducts has been reported, but is limited by scale and sequence context. This project outlines a more efficient synthesis of 2-AαC and novel analogs necessary for certain structural investigations. Attempts to synthesize a C8-(2-AαC)-guanine oligonucleotide are also described to provide a starting point for future investigations.

Acknowledgements

Thank you to everyone that provided help along the way.

Dr. Bongsup Cho

Dr. Deyu Li and his lab members

Dr. Matthew Kiesewetter

Dr. Mindy Levine

Dr. Al Bach

Dr. Lifang Xu

Ang Cai

Dr. Sathyaraj Gopul

Dr. David Worthen

Dr. Paul Cohen

Dr. Kyle Scully

Aseel Eid

The University of Rhode Island

The College of Pharmacy

The Chemistry Department

INBRE

TABLE OF CONTENTS

Abstract.....	ii
Acknowledgements.....	iv
Table of Contents.....	v
List of Figures.....	vi
1. Introduction	1
2. Synthesis of 2-Amino- α -Carboline and Relevant Analogs.....	20
2.1. Suzuki Coupling Followed by Reductive Cyclization.....	24
2.2. Cu-Catalyzed Buchwald/Hartwig Coupling Followed by Graebe- Ullmann Cylization of Triazole.....	36
3. Adduct Synthesis.....	61
3.1. Total Synthetic Route.....	63
3.2. Biomimetic Synthesis.....	78
4. Experimental.....	84
5. Bibliography.....	99

LIST OF FIGURES

Figure 1: Different types of DNA damage elicit responses from a variety of repair systems.....	1
Figure 2: Adducts of aromatic amines and HAA's	3
Figure 3: (1) Thermodynamic contributions of non-covalent interactions determine stability, structure, and activity of DNA. (2) Thermodynamic parameters determine macromolecular structure and groove dynamics. (3) How do modifications to DNA affect the stability, and structure?	4
Figure 4: For illustrative purposes only. Protein (A) is binding to DNA (B) at different sites. Modification to a DNA base can 1) alter groove dynamics, changing the global shape of the duplex and impact binding and 2) the modification can physically block the binding site.....	5
Figure 5: Metabolism of aromatic amines by P450 produces reactive electrophiles that form adducts with nucleophilic sites on DNA (d). Redox reactions a, b, and c are reversible by separate P450 isoforms and in different oxidation states of the enzymes.....	7
Figure 6: General structure and numbering scheme of carbolines.....	8
Figure 7: Metabolism of 2-AαC. 2-AαC is a pyrolysis product of protein and can be found when protein is exposed to heat, including grilled meat. It also undergoes UGT secondary metabolism where the bulky leaving group increases reactivity.	9
Figure 8: (B conformer) Carcinogen is placed in the major groove, Watson-Crick base pair is maintained. (S conformer) Carcinogen is “stacked”	

inside the duplex and disrupts Watson-Crick base pairing. (W conformer)	
Minor % population, places carcinogen in minor groove.	11
Figure 9: Structural comparison of 2-A α C, 2-AF, and 2-AAF. An existing SAR of 2-AF and 2-AAF indicate the acetyl group of 2-AAF “locks” the adduct in the anti-position of the glycosidic bond. This results in disparate bioactivity. An SAR of 2-A α C and 2-AF provide an opportunity to understand the effect of disparate electronic configurations in otherwise identical structures.	12
Figure 10: Biomimetic synthesis mimics <i>in vivo</i> bioactivation by creating a reactive N-hydroxyl electrophile and incorporating effective leaving groups. It is then reacted directly with ssDNA.	15
Figure 11: Synthesis of a guanosine phosphoramidite modified by 2-aminofluorene (2-AF) at the C8 position in preparation for automated total oligonucleotide synthesis as reported by Gillet Scharer, 2002 ³²	16
Figure 12: Total synthesis of an oligonucleotide using phosphoramidite nucleosides.	17
Figure 13: Electrophile in biomimetic synthesis reacts at the C8 position of guanine. If multiple guanines are present, purification of products is cumbersome.	18
Figure 14: Starting material necessary for 2-A α C-dG adducts by route of synthesis (biomimetic or total synthetic). Analyses such as ¹⁹ F NMR require specific analogs.	19

Figure 15: Recent synthesis of carbolines. (A) Suzuki coupling followed by a Pd-Catalyzed intramolecular coupling with incorporation of an amine. (B) Intramolecular cross-coupling.	21
Figure 16: Abbreviated scheme for 2-A α C synthesis by Matsumoto <i>et al.</i> , 1979 utilizes cyclization of triazole ³⁴	22
The first proposed route seeks to take advantage of high yielding cross-coupling reactions to obtain 2-A α C in two steps from commercially available starting material (figure 17). The second proposed route utilizes the Graebe-Ullman cyclization of triazole, the final step of an existing synthesis for 2-A α C ³⁴ (figure 30). The latter is based on a reasonable assumption that the 2-A α C precursor in the reported synthesis can be obtained from commercially available starting material using a number of coupling strategies that have been developed since the initial report, thus reducing the total number of steps from five to two.	22
Figure 18: Proposed scheme. Suzuki coupling followed by a reductive cyclization may produce 2-A α C (1-4a) in 2-steps.	25
Figure 19: Retrosynthesis of Suzuki coupling/ Cadogan reductive cyclization reveals several combinations of possible starting material. Limitations are based on immediate commercial availability and cost.	26
Figure 20: Free rotation around single bond on product of Suzuki coupling using starting material from figure 19 may result in 2 final products: 2-A α C (1-4a) and 2-A γ C (1-6).	27
Figure 21: Step 1, Suzuki Coupling.	28

Figure 22: Coupling of 2-amino-5-bromopyridine (1-1) and phenylboronic acid (1-7) as reported by González <i>et al.</i> , 2005 was used as a control.....	28
Figure 23: Deboronation of 1-2a during the desired Suzuki coupling.....	29
Figure 24: (A) Symmetry and peak splitting observed in ¹ H NMR in MeOD are consistent with product of homocoupling (1-10) but not confirmed. (B) ¹ H NMR of recovered 2-amino-5-bromopyridine (1-1).....	30
Figure 25: Table and data from Gonzalez <i>et al.</i> , 2005 showing the effect of temperature and Pd(OAc) ₂ on deboronation ⁴⁸	31
Figure 26: ¹ H NMR of crude product in MeOD produced from Suzuki coupling at a range of temperatures. The relative percent ratio of the 6-H pyridine peaks at δ 7.95 (1-1) and δ 8.2 (1-8) were used to determine completion of reaction.....	33
Figure 27: Relative percent ratio of product and starting material present after reaction at different temperatures. Percents were determined from the ¹ H NMR ratio described in figure 26.	33
Figure 28: ¹ H NMR of crude product in MeOD was used as described previously to determine the percent ratio of starting material (1-1) to product (1-8) in the reaction mixture for different catalysts.	34
Figure 29: ¹ H NMR of crude product in MeOD was used as described previously to determine the percent ratio of starting material (1-1) to product (1-8) in the reaction mixture for different variables. When NaHCO ₃ is the base, the reaction does not progress to completion. Not all variables tested are shown.	35

Figure 30: Comparison of previously existing scheme (red) vs proposed (blue) scheme. (A) Scheme by Matsumoto *et al.*, 1978 requires 5 steps to produce 2-A α C. (B) Step 1 of the proposed route, a Cu-catalyzed Buchwald-Hartwig coupling, produces the immediate precursor of 2-A α C from Matsumoto *et al.*, 1978, reducing the overall scheme from 5 to 2 steps^{34,49}..... 37

Figure 31: Production of 2-A α C (1-4a), 2-N α C (1-5a), and fluorinated analogs. (a) NaNO₂, AcOH, H₂O, RT, 20-30 min. (b) H₂SO₄, H₂O₂, H₂O, RT, 24-48 h. (c) CuI (5 mol%), K₃PO₄, N,N'-dimethylethylenediamine (DMEDA), DMF, 110°C, 24-48 h. (d) Polyphosphoric acid (PPA), 180°C, 30 min..... 38

Figure 32: (a) Step 1, CuI (5 mol%), K₃PO₄, DMEDA, DMF, 110° C, 24hrs.... 39

Figure 33: (A) TLC 20% EtOAc/hexane, product R_f = 0.63. (B) Normal phase MPLC chromatogram for reaction c. Gradient (percent EtOAc in hexane) = blue line. Red line = absorption at 260 nm. Purple line = absorption at 260 nm. The desired product (2-5a) is the major peak and elutes from 9-10 min..... 40

Figure 34: ¹H NMR in DMSO-d₆ for 6-(1*H*-benzotriazol-1-yl)-2-nitropyridine (2-5a) after column chromatography..... 41

Figure 35: (d) Step 2, Polyphosphoric acid (PPA), 30 minutes, 180° C 42

Figure 36: TLC for reaction (d) in 20% EtOAc/hexane. Desired product (2-5a) R_f = 0.62. Lane 1 & 3 = crude product from reaction (d), lane 2 = 2-5a after column chromatography..... 43

- Figure 37: ^1H NMR for 2-6a in acetone- d_6 after chromatographic purification. 9H proton at δ 11.0, close-up shown for δ 7.15- 8.55. See experimental section for ^1H NMR spectrum of higher purity in CDCl_3 . The above sample was used to confirm spin systems through COSY ^1H NMR. Acetone- d_6 was used as the solvent due to lack of overlap between peaks..... 44
- Figure 38: 2D ^1H NMR COSY for 2-6a in acetone- d_6 . Peak 3 & 4 make up expected spin system and are assigned based on chemical shift. Proton nearest the nitro group (3) will be most deshielded as is observed by the chemical shift. 45
- Figure 39: 2D ^1H NMR COSY 2-6a in acetone- d_6 . Triplets of 6/7 and doublets of 5/8 make up the expected spin system. Individual assignment cannot be made with ^1H NMR COSY alone. Heteronuclear correlation would be required. ^1H NMR COSY does reveal the relative connectivity of the protons to each other..... 46
- Figure 40: 2D ^1H NMR COSY of 2-6a in acetone- d_6 . Triplets 6/7 and doublets 5/8 make up the expected spin system. Individual assignment cannot be made with COSY. Heteronuclear correlation would be required..... 47
- Figure 41: Step 1, reaction c with amine functionality (2-3). (c) CuI (5 mol%), K_3PO_4 , DMEDA, DMF, 110°C , 48 hrs. 48
- Figure 42: Reconstructed TLC of crude product from reaction c in 40% EtOAc/hexane. Desired product, 2-amino-9H-pyrido[2,3-b]indole, (2-amino- α -carboline, 2-A α C, 2-7a) is spot 1 and represents the major product $R_f = 74$. Spots 2 and 3 represent other major products, remainder

of spots are minor by-products. Reaction with the amine starting material results in more byproducts than the product of the nitro starting material.	49
Figure 43: (A) ¹ H NMR of 2-amino-6-bromopyridine (2-3) in CDCl ₃ recovered after purification of product mixture. (B) ¹ H NMR of desired product, 2-7a, in CDCl ₃	50
Figure 44: MPLC chromatogram from CombiFlash alumina column. EtOAc/hexane, EtOAc = solvent B. Dry pack. Amine starting material is present in small amount (≈10 min). Product elutes from ≈11-15.5 min....	52
Figure 45: (d) Step 2, Polyphosphoric acid (PPA), 30 minutes, 180° C	53
Figure 46: Tautomerization of 6-fluorobenzotriazole (2-2b) can result in an isomeric mixture. 1-5b and 1-5c represent the isomers.....	54
Figure 47: Synthesis of 2-2b as reported by Wasik <i>et al.</i> , 2010 ⁵⁰ Note the product in their scheme is the undesired tautomer. However, the product results in the desired tautomer as measured in NMR solvents on an NMR time scale.....	55
Figure 48: ¹ H NMR (II-F) Acetone D ₆	56
Figure 49: TLC (1-F) Least polar spot in (A) represents 2 products as seen after 2 nd purification in TLC (B).	57
Figure 50: ¹ H NMR in DMSO-d ₆ 1-5b, 1-5c Isomeric mixture.....	58
Figure 51: ¹ H NMR in CDCl ₃ . Pure isomers as shown in TLC figure 49.	59
Figure 52: Justification for ¹ H NMR assignment of isomers. Reaction reported by Liu <i>et al.</i> , 2010 does not permit formation of isomeric mixture ⁵¹ .	

Coupling constants of relevant peaks are highlighted and consistent with isomer assignments.....	60
Figure 53: Automated DNA synthesis showing essential functional groups and their role in solid support polymerization.	64
Figure 54: Synthesis of a nucleoside phosphoramidite modified by 2-AF. 1-5 followed the procedure reported by Gillet and Scharer, 2002 for the 2-AF control. Troubleshooting techniques for step 5 using 2-A α C are outlined in section 3.1.2. 6-11 are for illustrative purposes only and represent the complete scheme reported by Gillet and Scharer, 2002 ³²	68
Figure 55: (A) Purification and (B) Identification by ¹ H NMR: dG-C8-2-AF matches that reported by Gillet and Scharer, 2002 ³²	69
Figure 56: Buchwald Hartwig catalytic cycle with relevant elements for nucleoside synthesis highlighted in red.	70
Figure 57: Possible ionization equilibrium of 2-A α C under Buchwald-Hartwig conditions.....	71
Figure 58: Possible tautomerization of 2-A α C. Secondary amine formation is unfavorable for the BH conditions being utilized.....	75
Figure 59: HPLC chromatogram, 70% MeOH in H ₂ O, isocratic. (A) Partial reduction of 2-FAF to N-hydroxyl-2-fluorofluorene. (B) Comparison of confirmed UV spectra indicate success of the control reaction.	78
Figure 60: Biomimetic control reaction. Scheme from figure 10, route 2 was executed for 2-AF. PDA UV spectrum was compared to confirmed spectra. According to this data all 2-AF control reactions were successful.	

Due to the established protocols and UV spectra in the Cho lab, this was the only means of identification.....	80
Figure 61: Partial reduction of 2-AcC under identical conditions to the control 2-FAF.	81
Figure 62: Chromatogram from partial reduction of 2-AcC. No product formation. Time point 0, before addition of hydrazine. Time point (1-4) 15 minute intervals. Time point 5 +2 hours, time point 6, +24 hours at RT. Excess hydrazine added.	81
Figure 63: Adjustments made based on Novak's model. Explanations in text.	82
Figure 64: Compounds synthesized in the triazole route. New compounds are indicated as such. (a, b) First report for synthesis of 2-7a and 1-4a via proposed route. . (c) First known report of 1-5a <i>not</i> via oxidation of 1-4a.	85
Figure 65: (2-5a).....	86
Figure 66: ^1H NMR in CDCl_3 δ (ppm), J (Hz) 8.61 (1H, d, J= 8.71), 8.29 (1H, d, J= 9.24), 8.13 (1H, d, J= 8.19), 7.79 (1H, t, J= 7.91), 7.66 (1H, td, J= 8.21, 1.14), 7.51 (1H, d, J= 7.91), 7.49 (1H, td, J= 8.15, 0.90). Ethyl Acetate (EtOAc) impurity, NMR solvent (CHCl_3), and TMS are identified in the spectrum.	87
Figure 67: ^{13}C NMR in CDCl_3 δ (ppm) 151.08 (1C), 146.73 (1C), 140.82 (1C), 139.98 (1C), 131.27 (1C), 129.28 (1C), 126.20 (1C), 125.22 (1C), 119.74 (1C), 114.66 (1C), 112.42 (1C). Ethyl Acetate (EtOAc) impurity, NMR solvent (CHCl_3), and TMS are identified in the spectrum.	88

Figure 68: Normal phase MPLC chromatogram for reaction c. Gradient is EtOAc (%B) in hexane shown as a blue line. Red line = absorption at 260 nm. Purple line = absorption at 260 nm. The desired product (2-5a) is the major peak and elutes from 9-10 min.....	88
Figure 69: 1-5a.....	89
Figure 70: ^1H NMR in Acetone- d_6 δ (ppm), J (Hz) 8.42 (1H, d, J= 8.01), 8.17 (1H, d, J= 7.74), 7.60 (1H, d, J= 8.01), 7.51 (1H, td, J= 7.48, 1.21), 7.39 (1H, d, J= 8.01), 7.29 (1H, td, J=7.74, 1.06). Ethyl Acetate (EtOAc) impurity, NMR solvent (Acetone- d_6), vacuum grease, and TMS are identified in the spectrum.	91
Figure 71: 2-7a.....	92
Figure 72 ^1H NMR in CDCl_3 δ (ppm), J (Hz) 8.57 (1H, d, J= 8.31), 8.11 (1H, d, J= 8.31), 7.66 (1H, t, J= 7.90), 7.58 (1H, d), 7.56 (1H, td, J= 8.75, 1.33), 7.42 (1H, td, J=7.40, 0.90) 6.52 (1H, d, J= 7.90), 4.67 (2H, s). NMR solvent (CDCl_3), vacuum grease, and TMS are identified in the spectrum.	93
Figure 73: Normal phase MPLC chromatogram for reaction c to produce 2-7a. Gradient is EtOAc (%B) in hexane shown as a blue line. Red line = absorption at 260 nm. Purple line = absorption at 260 nm. The desired product (2-7a) is the major peak and elutes from 12-16 min.	94
Figure 74: (1-4a)	94
Figure 75: (2-5c)	95

Figure 76: ^1H NMR in DMSO-d_6 δ (ppm) 8.34 (1H, m), 8.29 (1H, d), 8.15 (1H, dd), 8.10 (1H, t), 7.81 (1H, d), 7.51 (1H, dt). Coupling constants are measured in CDCl_3 and explained in section 2. H_2O , NMR solvent (DMSO-d_6), vacuum grease, and TMS are present in the spectrum. (A) Full spectrum, (B) aromatic region, (C) mixture of 2-5b and 2-5c 96

Figure 77: 2-5b..... 96

Figure 78: ^1H NMR in DMSO-d_6 δ (ppm) 8.50 (1-H, dd), 8.30 (1H, d), 8.12 (1H, d), 8.11 (1H, t), 7.82 (1H, d), 7.74 (1H td). Coupling constants are measured in CDCl_3 and explained in section 2. H_2O , NMR solvent (DMSO-d_6), vacuum grease, and TMS are present in the spectrum. Full spectrum, aromatic region, and an isomeric mixture of 2-5b and 2-5c are shown..... 98

1. Introduction

In average human cells, DNA damage occurs over 10,000 times per day¹.

DNA damage is defined as a chemical alteration to a base, sugar, or phosphate backbone². Accurate transcription and replication is dependent on molecular recognition. Depending on the extent and nature of the damage, if left unrepaired, it may disrupt transcription or result in heritable mutations during replication. Select examples of DNA damage are shown in figure 1.

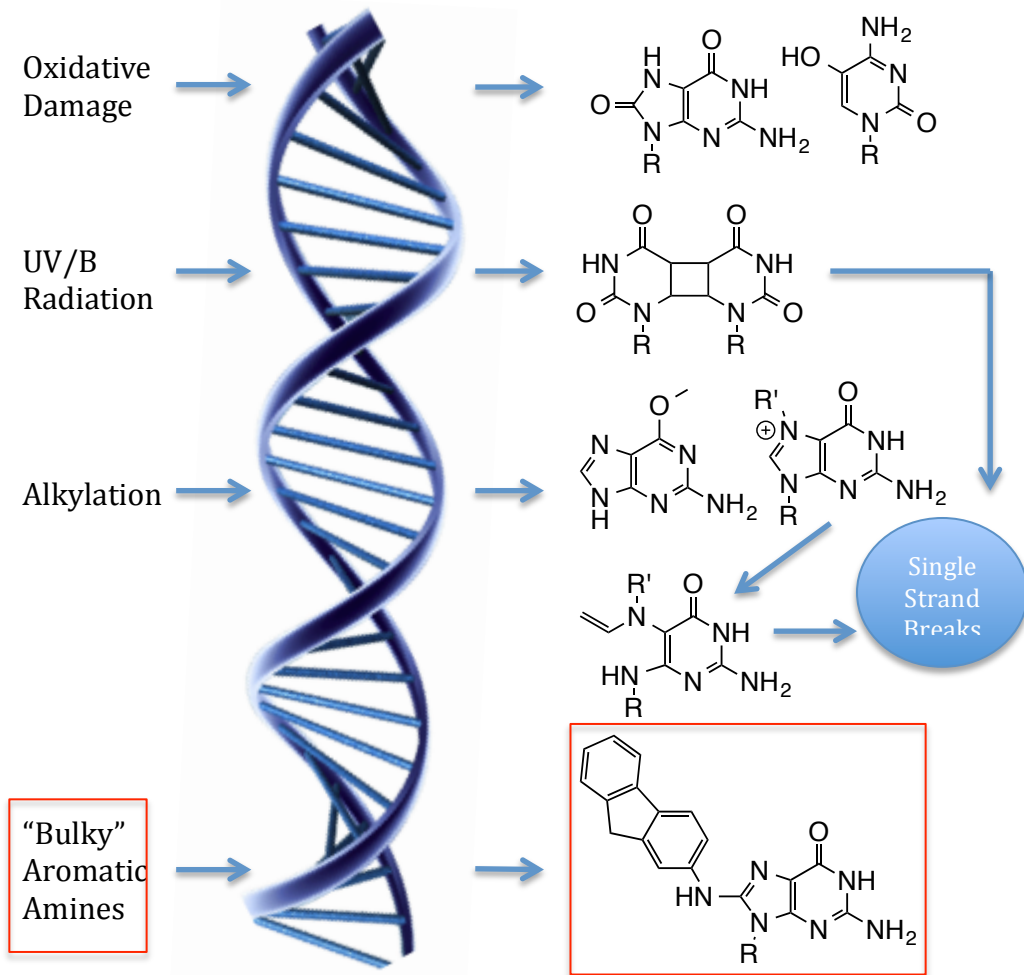
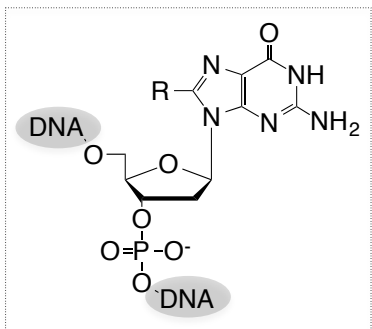


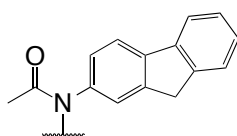
Figure 1: Different types of DNA damage elicit responses from a variety of repair systems.

In order to maintain genome integrity, cells have evolved a complex network of overlapping DNA repair systems composed of hundreds of proteins³. The nature of the chemical alteration will determine which repair system(s), if any, will respond to the change⁴. Failure of repair systems to fix damaged DNA is cited as a major contributing factor to cancers, aging, and other serious disorders⁵.

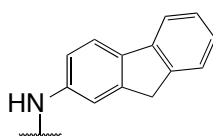
The broad role of Nucleotide Excision Repair (NER) makes the mechanisms of NER a target of interest in medical research⁶. NER responds to bulky adducts that cause global structural changes in the damaged duplex⁷. Common substrates for the NER pathway include adducts formed by polycyclic aromatic hydrocarbons (PAH) and aromatic amines^{6,7}. Figure 2 shows various adducts of aromatic amines and heterocyclic aromatic amines (HAA). Biochemical response can vary widely between these adducts indicating that minor changes in DNA structure can drastically alter outcomes.



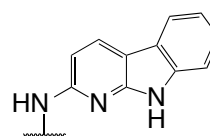
R = aromatic amine, HAA



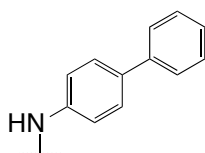
2-acetylaminofluorene
(2-AAF)



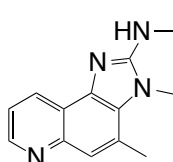
2-aminofluorene
(2-AF)



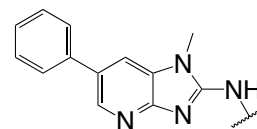
2-amino- α -carboline
(2-A α C)



4-aminobiphenyl
(4-ABP)



2-amino-3,4-dimethylimidazo
[4,5-f]quinoline
(MeIQ)



2-Amino-1-methyl-6-
phenylimidazo[4,5-b]pyridine
(PhIP)

Figure 2: Adducts of aromatic amines and HAA's

The relationship between structure, thermodynamics, and function cannot be overstated. Figure 3 displays a general overview of thermodynamic parameters that contribute to DNA structure and emphasizes the importance of these investigations.

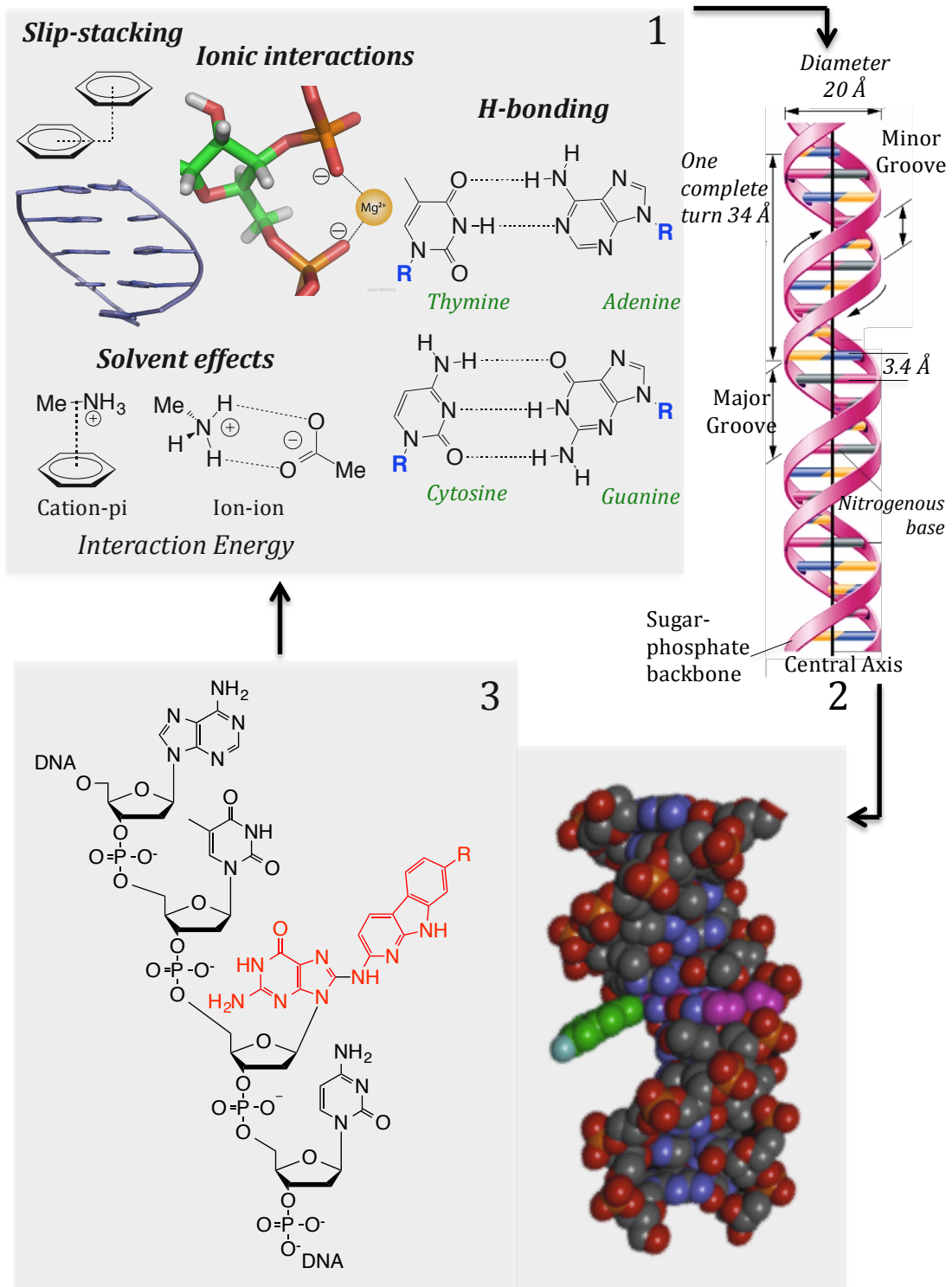


Figure 3: (1) Thermodynamic contributions of non-covalent interactions determine stability, structure, and activity of DNA. (2) Thermodynamic parameters determine macromolecular structure and groove dynamics. (3) How do modifications to DNA affect the stability, and structure?

Adducts that alter DNA structure may change the location, orientation, or strength of non-covalent interactions and, as a result, may impact global DNA conformation. Depending on the location, mutagenicity, and repair efficacy of the adduct, the alteration can have major implications on biological function. The relationship between structure, thermodynamics, and function that has already been discussed means biological phenomenon, such as the mutagenicity and repair efficacy of DNA adducts, can be investigated by measuring changes in the thermodynamic profile of a model duplex.

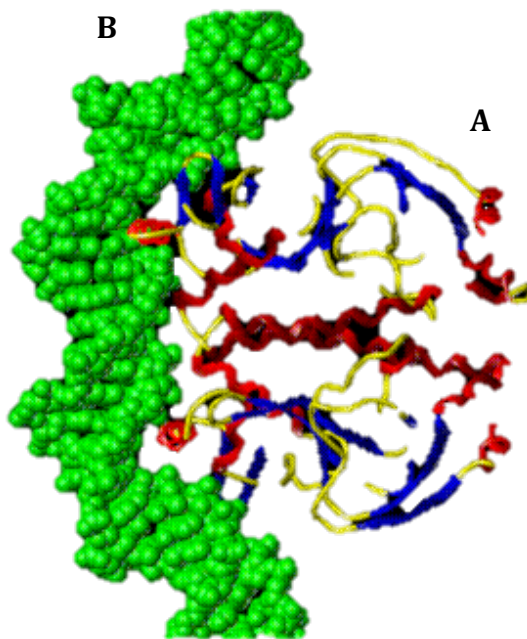


Figure 4: For illustrative purposes only. Protein (A) is binding to DNA (B) at different sites. Modification to a DNA base can 1) alter groove dynamics, changing the global shape of the duplex and impact binding and 2) the modification can physically block the binding site.

As has already been established, DNA adducts cause aberrant biochemical events that can result in cancer initiation^{8,9}. While *some* exposure to aromatic amines is largely unavoidable, knowledge of environmental hazards can help mitigate risk. Adduct formation and mutagenicity are independent variables, thus specific properties of an aromatic amine can impact adduct formation but not mutagenicity and vice versa⁷. In other words, it is possible for adducts to have a high rate of formation *and* a high rate of repair. In this case, the number of mutations per adduct formed will be low. Delineating the mechanism of adduct-formation, and how cells respond to them, increases the likelihood of successful medical interventions after exposure has occurred.

Adduct formation with respect to NER substrates usually requires bio activation¹⁰. Cytochrome P450 (CYP for specific subfamilies, or P450 for the enzyme family) is a major metabolic enzyme for aromatic compounds such as PAHs and HAAs¹¹. The amine compounds in figure 2 are characteristic substrates for various CYP isoforms that catalyze enzymatic redox reactions whereby amine groups are partially oxidized to the reactive N-hydroxyl (figure 5).

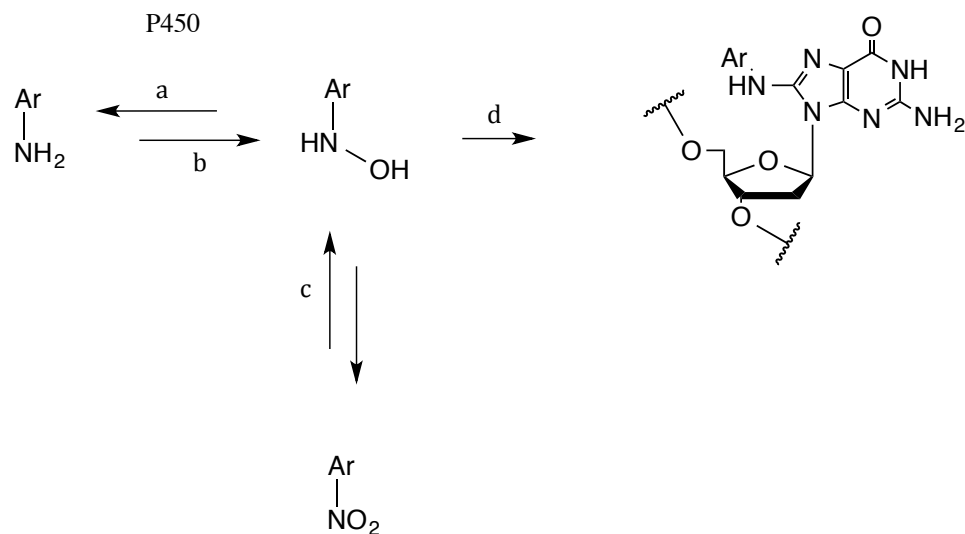


Figure 5: Metabolism of aromatic amines by P450 produces reactive electrophiles that form adducts with nucleophilic sites on DNA (d). Redox reactions a, b, and c are reversible by separate P450 isoforms and in different oxidation states of the enzymes.

The efficiency of NER is dependent on the thermodynamic favorability of binding events between the DNA adduct and repair proteins⁶. If the adduct is not repaired in a timely manner, mutations may occur during the next round of replication. Depending on the nature and location of the mutation along with other variables, this can result in cancer^{7,9}. Delineating these mechanisms is, by definition, a necessary step in rational drug design^{12,13}. Structural, thermodynamic, and kinetic properties that describe biochemical events are an essential foundation for developing drug targets¹³⁻¹⁶

2-Amino- α -carboline (2-A α C, figures 2 and 6) is an adduct-forming HAA implicated in hepatocellular carcinoma and GI tract cancers¹⁷⁻¹⁹. The suspected carcinogen is present in cigarette smoke and overcooked meat at concentrations greater than other confirmed animal carcinogens¹⁷⁻²⁰. Although

factors other than adduct formation are involved in cancer initiation, a causal relationship has been established between adduct formation and mutation⁹.

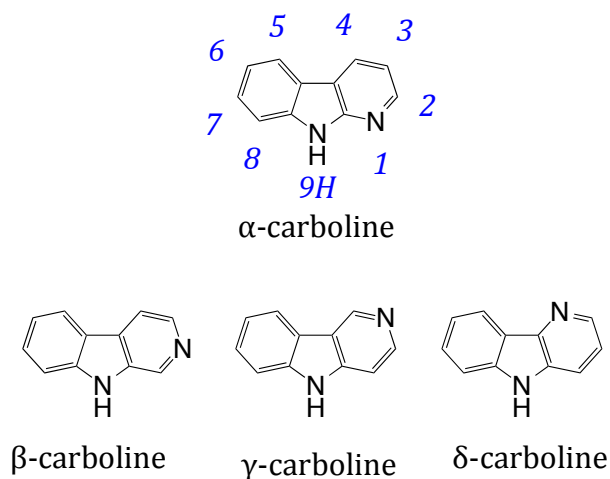


Figure 6: General structure and numbering scheme of carbolines.

4-Aminobiphenyl (4-ABP, figure 2) is a confirmed human bladder carcinogen present in cigarette smoke at concentrations ranging from 0.1 - 4.3 ng/cigarette¹⁸. Highly reactive electrophiles resulting from the metabolic activation of 4-ABP as outlined in figure 5 help to explain the increased incidence of bladder cancer among cigarette smokers. However, the increased incidence of gastrointestinal tract and liver cancers is largely unexplained.

Uridine 5'-diphospho-glucuronosyltransferase (UGT) is a phase II metabolic liver enzyme that catalyzes a glucuronidation reaction marking the metabolite for excretion. 2-A α C undergoes secondary metabolism in the liver by UGT and produces metabolites that are significantly *more* reactive towards the formation of DNA adducts than the activated species of 4-ABP²⁰(figure 7).

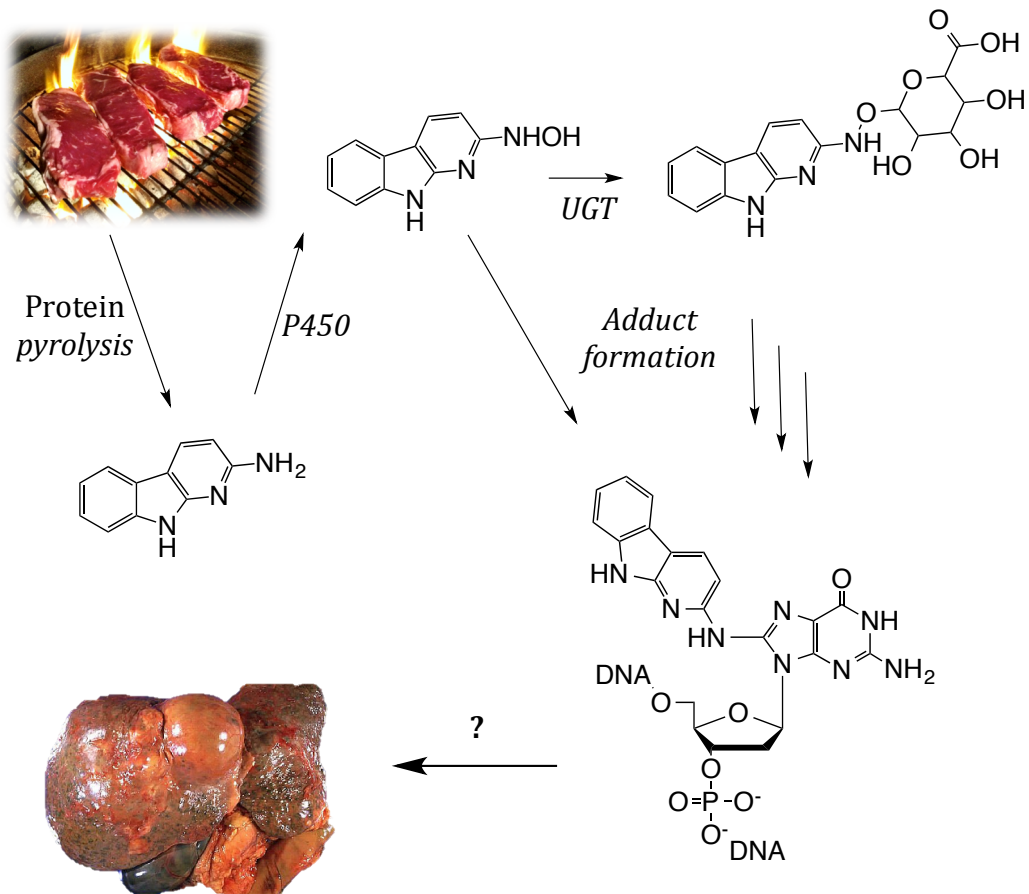


Figure 7: Metabolism of 2-AαC. 2-AαC is a pyrolysis product of protein and can be found when protein is exposed to heat, including grilled meat. It also undergoes UGT secondary metabolism where the bulky leaving group increases reactivity.

Furthermore, 2-AαC is present in cigarette smoke at a concentration ranging from 60 – 258 ng/cigarette, 1000 times greater than 4-ABP¹⁸. There is also a positive correlation between smoking and 2-AαC concentration in urine²¹.

Taken together, this provides a probable explanation for the increased incidence of GI tract and liver cancer in smokers.

Despite reports implicating 2-AαC in various human cancers, there are no studies available describing the structural, thermodynamic or kinetic properties of 2-AαC adducts. The value of this data is significant in drug development.¹² Currently, there is not an efficient synthetic protocol for 2-AαC and its corresponding C8-guanosine adduct described in literature. This is probably due to its relatively recent implication in human cancers.

DNA replication and repair is dependent on molecular recognition, the principles of which are based on structural and thermodynamic parameters within the system. The conformation of a DNA adduct will impact any biochemical process in which the adduct is involved, such as replication and repair¹⁴. Data that describes the nature and magnitude of structural and conformational changes induced by aromatic amines will provide insight as to how those parameters influence replication and repair proteins.

Bulky adducts of environmental aromatic amines, including HAAs, are known to exist in two major conformations: S- and B-conformers (figure 8)⁷. The S conformer disrupts Watson Crick base pairing between the modified nucleoside and its complementary base, placing the carcinogen inside the duplex where it slip-stacks with the neighboring bases. The B conformer maintains Watson Crick base pairing with an *anti* glycosidic modified dG, placing the carcinogen in the spacious major groove. As stacking ability of the carcinogen increases, the enthalpic contribution of the Watson Crick base pair

is reduced relative to the enthalpic considerations of stacking and Van der Waals interactions of the S conformer. Stacking ability will increase with planarity and favorable electronic distribution relative to the stacking partner^{22,23}. Electron distribution of aromatic compounds can be altered by substituents and cyclic heteroatoms^{24,25}. Whether or not a change in electron distribution increases stacking ability depends on the characteristics and orientation of the partner in the stacking interaction. As stacking ability of the aromatic amine increases within a given sequence context, the conformational equilibrium shifts toward the S conformer^{13,26}.

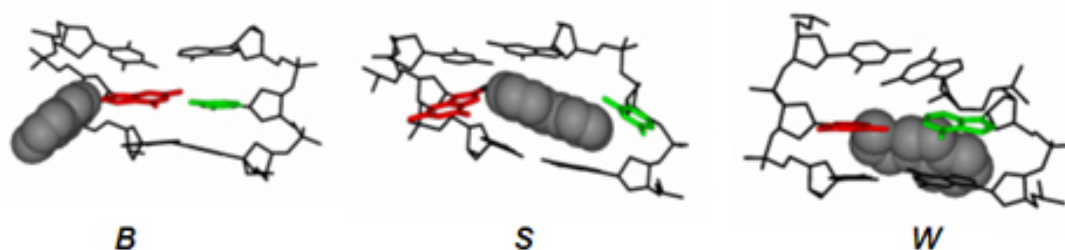


Figure 8: (B conformer) Carcinogen is placed in the major groove, Watson-Crick base pair is maintained. (S conformer) Carcinogen is “stacked” inside the duplex and disrupts Watson-Crick base pairing. (W conformer) Minor % population, places carcinogen in minor groove.

Properties of the individual carcinogen and neighboring sequence context of the duplex are known to affect the ratios of conformational heterogeneity, which may have disparate biological outcomes. The two effects are thought to be related, but aside from a general trend in stacking ability of the carcinogen, little is known about the relationship and their mutational and repair outcomes⁷.

2-Aminofluorene (2-AF) is a potent animal carcinogen with the same structure as 2-A α C, except 2-AF does not have endocyclic amines at position 1 and 9 (figure 9). 2-acetylaminofluorene (2-AAF) is identical to 2-AF with the addition of an acetyl group on the exocyclic amine. According to the stacking trend one would expect to see similar B/S-type ratios between 2-AAF and 2-AF, yet this was not observed^{7,14}. A structure activity relationship (SAR) between 2-AF and 2-AAF reveals an approximate 1:1 B/S conformational heterogeneity in 2-AF, while 2-AAF exists mostly in the S- and W-conformation in the same sequence context despite their similar ring structure. The difference between these conformational population ratios is due to the steric hindrance of the N-acetyl group of 2-AAF, restricting rotation around the central nitrogen linking base and the carcinogen as well as the glycosidic bond⁷.

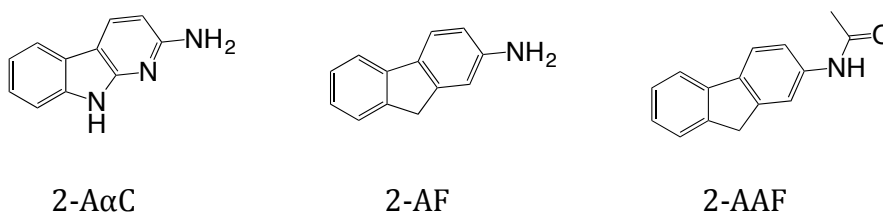


Figure 9: Structural comparison of 2-A α C, 2-AF, and 2-AAF. An existing SAR of 2-AF and 2-AAF indicate the acetyl group of 2-AAF “locks” the adduct in the anti-position of the glycosidic bond. This results in disparate bioactivity. An SAR of 2-A α C and 2-AF provide an opportunity to understand the effect of disparate electronic configurations in otherwise identical structures.

2-A α C provides a unique opportunity for a SAR when compared to 2-AF. Structural and thermodynamic differences will arise exclusively from the variations in the electronic configuration of the compounds. In addition to the

traditional value structural data on suspected human carcinogens provides, a comparison of 2-A α C and 2-AF may help clarify the relationship between sequence-dependent and adduct-dependent conformational heterogeneity, particularly if this relationship has a dependence on stacking ability.

In principle, thermodynamically favorable stacking positions of aromatic heterocycles can be predicted when accounting for the electronic distribution of bases and the carcinogen²⁷. This cannot be applied in large systems like DNA due to enormous structural and thermodynamic considerations of the non-stacking polymeric backbone. However, if sequence context has a different impact on adducts that differ *only* in electronic configuration of the carcinogen, this would support the idea that sequence effects may also arise because of differences in stacking interactions of the bases.

There is currently no published data regarding the structural or thermodynamic properties of 2-A α C DNA adducts. Given its implications in cancer, these types of studies are not only warranted, but overdue^{19,20,28}.

Biophysical analyses of normal and modified DNA duplexes yield valuable information used in drug development. Depending on the nature of the problem being addressed, different analogs of the modifying compound will be required. For example, ¹⁹F NMR is a powerful tool for assessing the

conformational heterogeneity of a modified DNA duplex^{29,30}. To perform this type of analysis, a fluorinated analog of the lesion is required³¹.

The lesion is one of many factors that impact the biophysical properties of DNA adducts. When investigating the effect of sequence context on biophysical properties, certain methods for adduct synthesis may limit the scope of the investigation as will be discussed. There are two major pathways for the synthesis of DNA adducts. The first mimics *in vivo* bioactivation and is aptly named biomimetic synthesis (figure 10) and the second is total synthesis (figures 11 and 12).

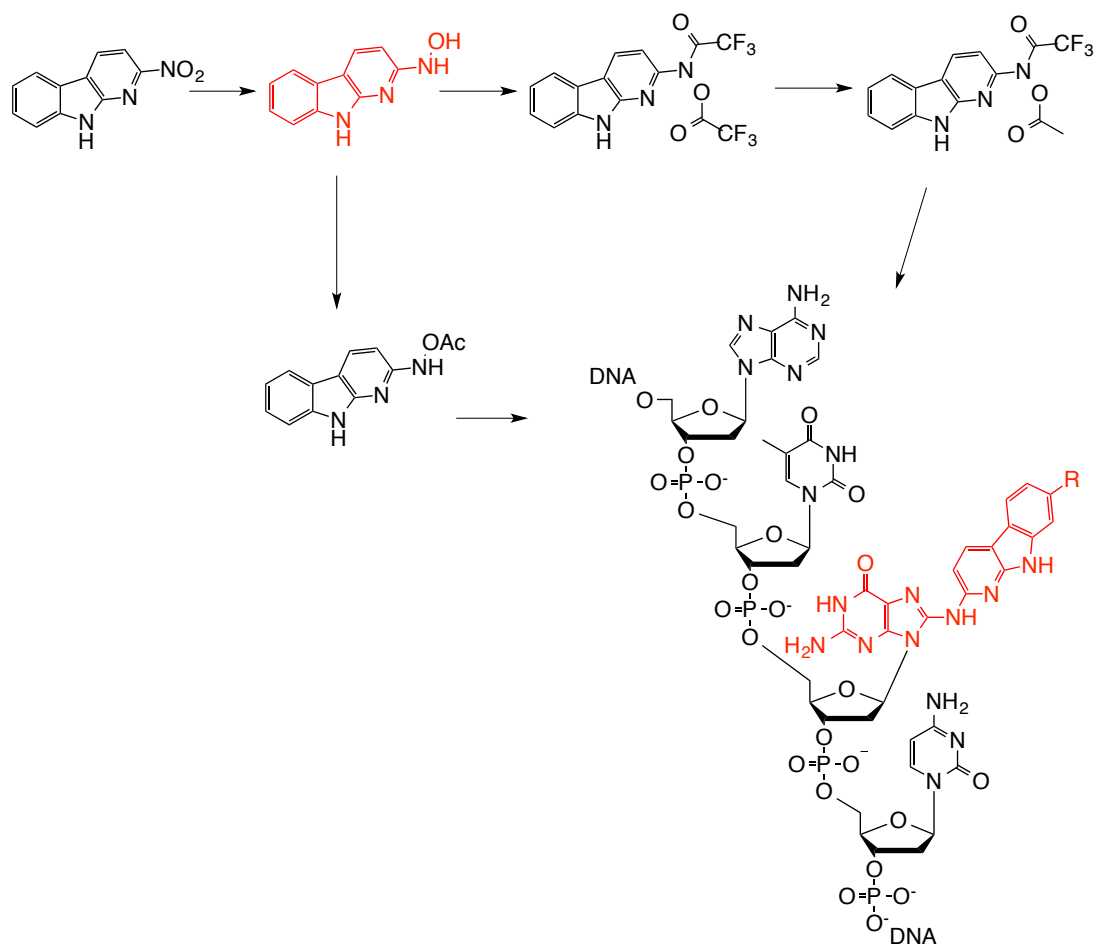


Figure 10: Biomimetic synthesis mimics *in vivo* bioactivation by creating a reactive N-hydroxyl electrophile and incorporating effective leaving groups. It is then reacted directly with ssDNA.

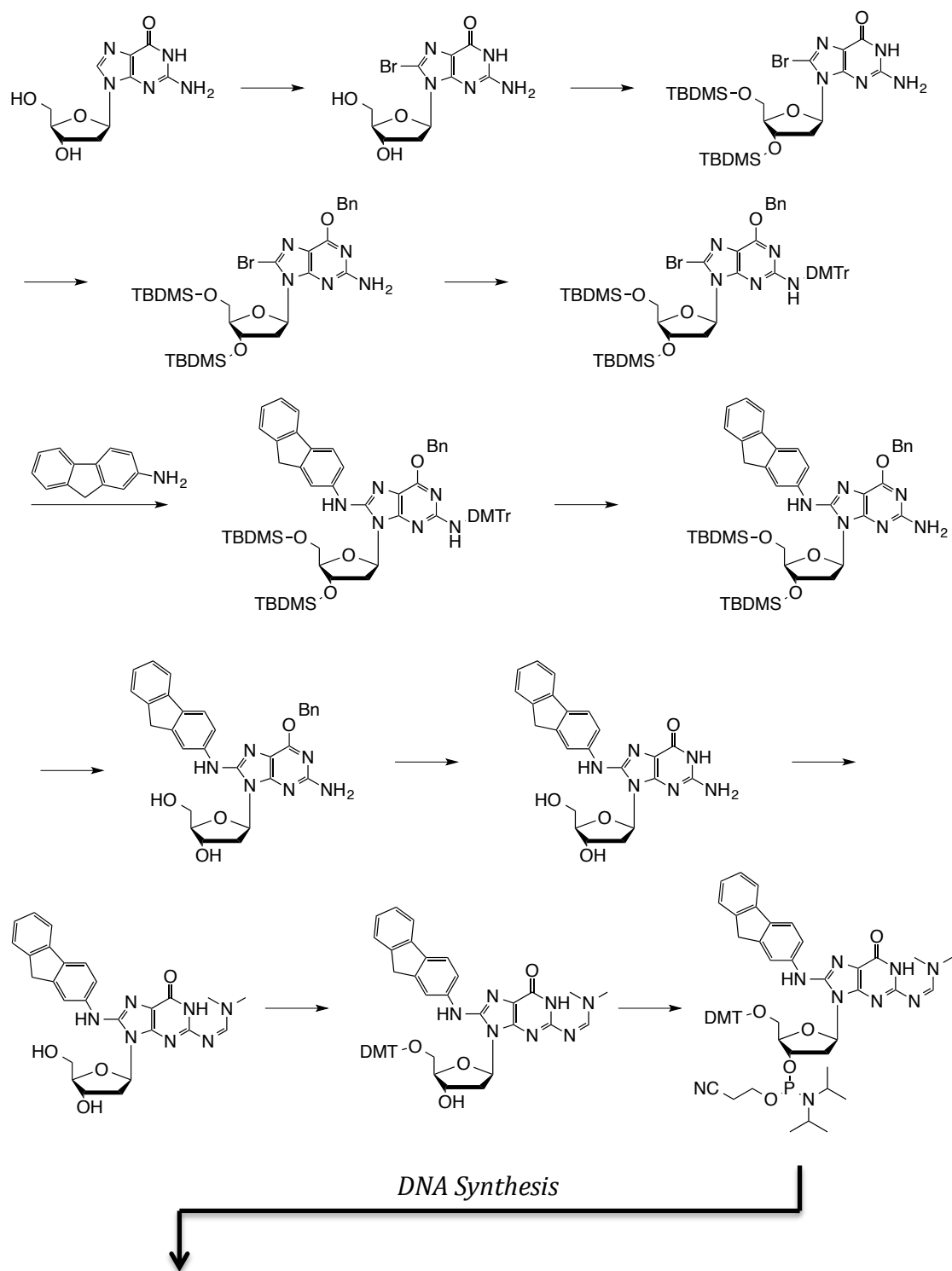


Figure 11: Synthesis of a guanosine phosphoramidite modified by 2-aminofluorene (2-AF) at the C8 position in preparation for automated total oligonucleotide synthesis as reported by Gillet Scharer, 2002³².

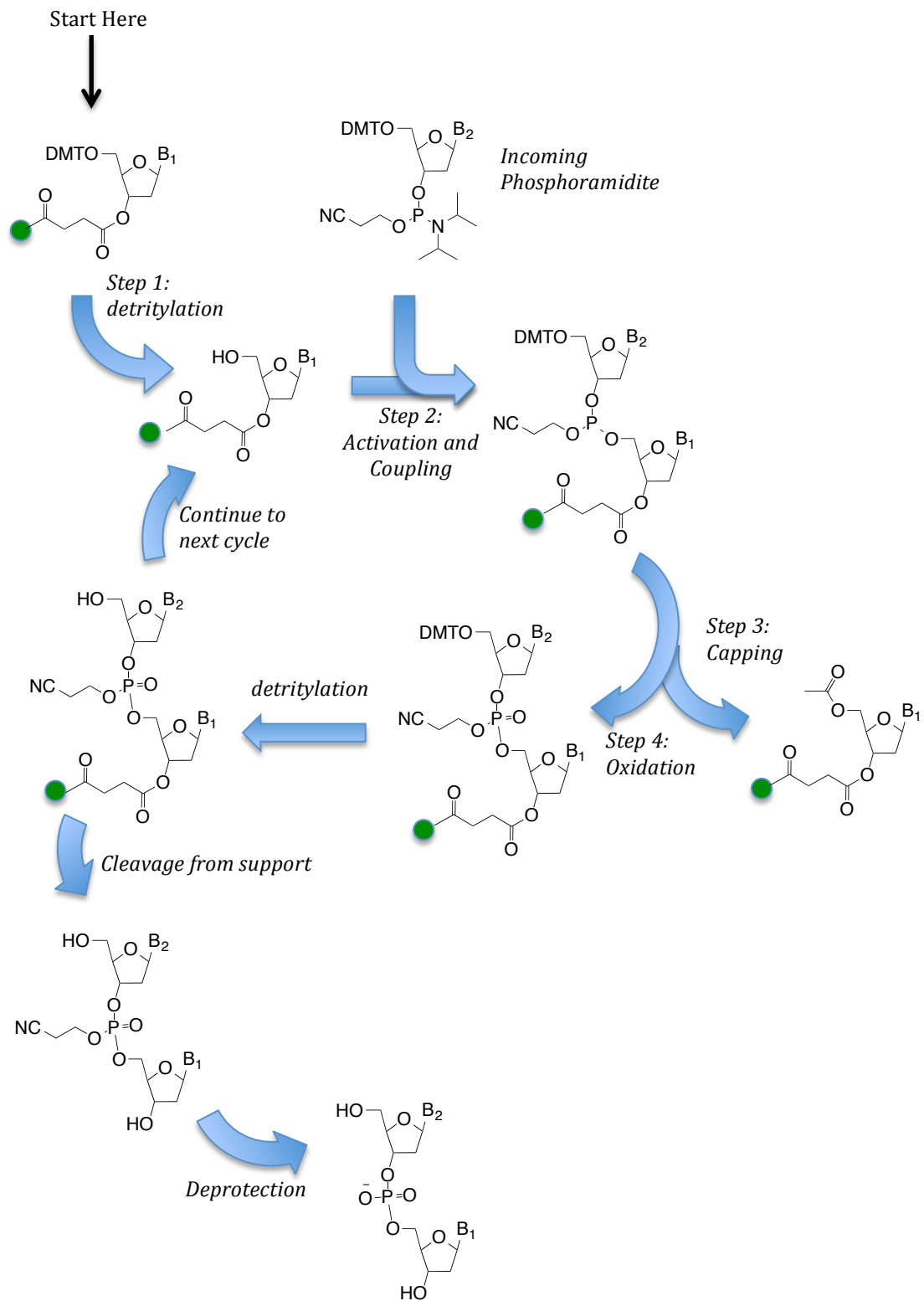


Figure 12: Total synthesis of an oligonucleotide using phosphoramidite nucleosides.

The biomimetic pathway is quicker and requires fewer synthetic steps than total synthesis but restricts the sequence context of the investigation. In biomimetic synthesis, the carcinogen is reacted directly with the ssDNA as shown previously in figure 10. The electrophile will react with the nucleophilic C8 position of guanine. However, if there is more than one nucleophilic site, the reaction will be nonspecific and provide a mixture of products (figure 13).

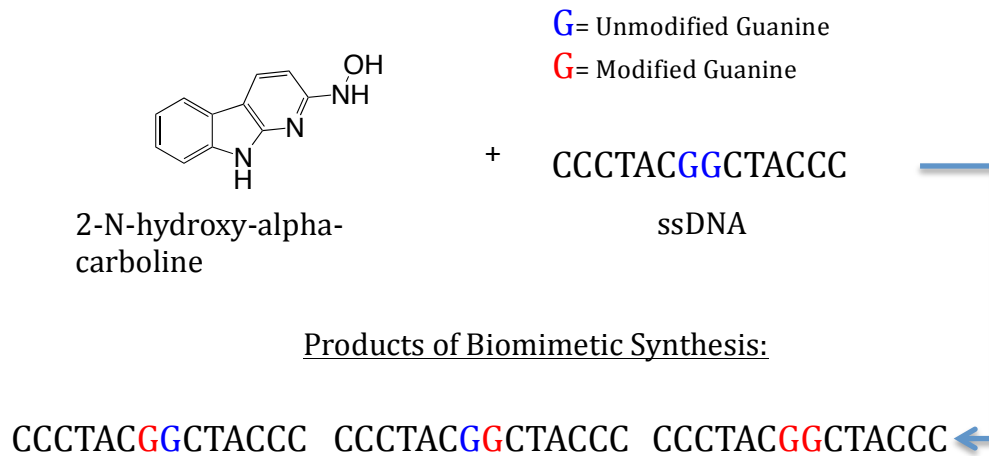


Figure 13: Electrophile in biomimetic synthesis reacts at the C8 position of guanine. If multiple guanines are present, purification of products is cumbersome.

The total synthetic pathway involves more steps, however the modification is incorporated during synthesis of the ssDNA, allowing for any sequence context to be investigated. Both pathways have appropriate applications, so establishing the viability of both routes would best facilitate a comprehensive investigation of 2-A α C-dG adducts in the future. The starting material for each route differs by the functional group at the 2-position as shown in figure 14.

Synthesis of starting material for one route can facilitate production of the other through established oxidation/ reduction reactions. For example, 2-AαC can be oxidized to 2-NαC using dimethyldioxirane, while 2-NαC can likely be reduced to 2-AαC using hydrazine or other reducing agents¹⁷.

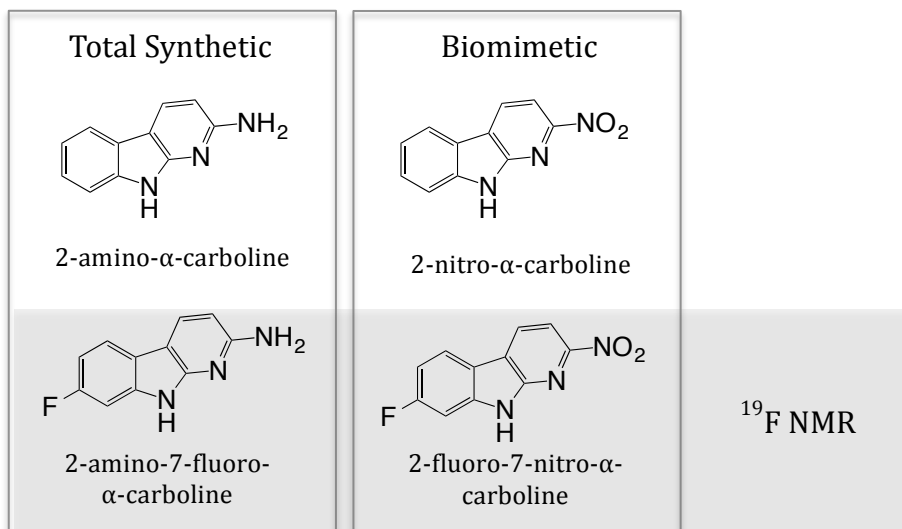


Figure 14: Starting material necessary for 2-AαC-dG adducts by route of synthesis (biomimetic or total synthetic). Analyses such as ¹⁹F NMR require specific analogs.

There is great interest in 2-AαC but the lack of efficient synthetic protocols for its production is a major issue to research labs. This project will outline a more efficient synthesis of 2-AαC as well as necessary analogs for future investigations. Additionally, it will describe attempts to improve the versatility and ease of the synthesis of C8- (2-AαC)-guanine adducts.

2. Synthesis of 2-Amino- α -Carboline and Relevant Analogs

Synthetic strategies yielding carboline analogs, including 2-A α C, have existed in literature for decades^{33,34}. However, these syntheses are inefficient and low yielding. Over the last decade the fluorescent, medicinal, and carcinogenic properties of these compounds have generated interest in carboline research³⁵⁻³⁷. As a result, the development of more efficient synthetic routes have presented in literature³⁷⁻³⁹.

Given the wide range of interesting properties carbolines present, highly specific analogs containing functionalities necessary to investigate the characteristics of 2-A α C lesions may easily have been overlooked. New synthetic strategies for indole-like compounds often consist of a Pd-catalyzed cross coupling reaction followed by a Pd-catalyzed intramolecular cyclization, or a Cadagan reductive cyclization³⁷⁻⁴².

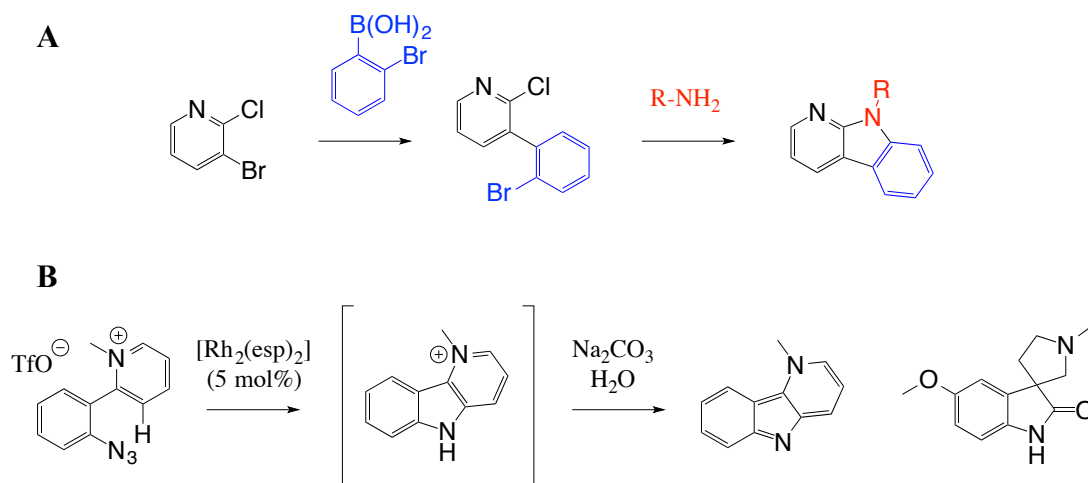


Figure 15: Recent synthesis of carbolines. (A) Suzuki coupling followed by a Pd-Catalyzed intramolecular coupling with incorporation of an amine. (B) Intramolecular cross-coupling.

A major goal of modern organic chemistry is to streamline chemical synthesis and maximize the utility of new reactions. Therefore, when a new strategy is reported, it is often accompanied by several examples with many functionalities and conditions to demonstrate robustness.

Examples of synthetic strategies for carbolines containing the individual functional groups necessary for this project are present in literature but their combination and position present complications. Furthermore, modern syntheses of alpha carbolines with common functionalities often require complex conditions that are not particularly robust compared to other indole-like compounds^{37,38,40}.

Early carboline syntheses took advantage of the cyclization reactions of triazoles and azaindoles^{43–45}. These reactions often occur under simple conditions and are compatible with primary amines but those reported thus far require several steps and exhibit low yields.

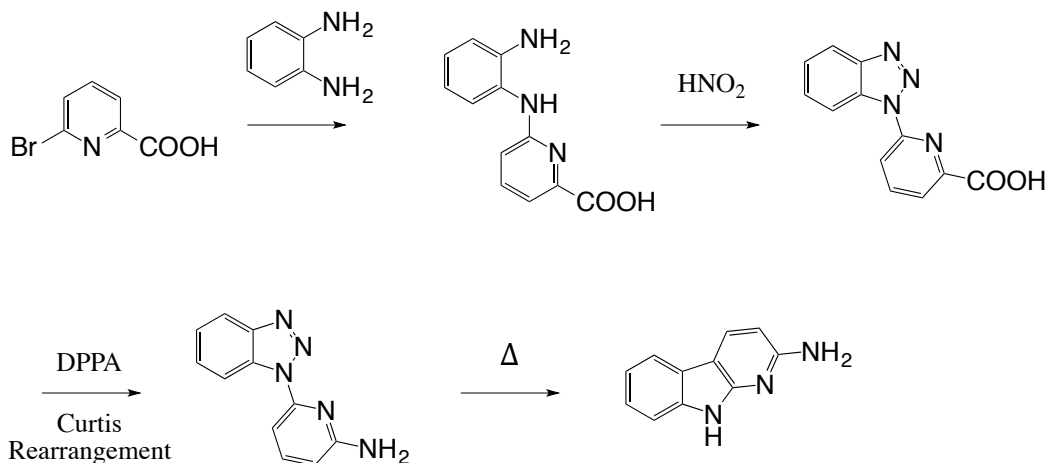


Figure 16: Abbreviated scheme for 2-AcC synthesis by Matsumoto *et al.*, 1979 utilizes cyclization of triazole³⁴.

New higher yielding synthetic strategies have complex conditions and high sensitivity to the presence of amines^{38,39,41,42}. In the scope of this project, low yields are acceptable, but simplifying conditions and minimizing the number of steps is highly desirable. For this project, two routes for the synthesis of 2-AcC were investigated simultaneously.

The first proposed route seeks to take advantage of high yielding cross-coupling reactions to obtain 2-AcC in two steps from commercially available starting material (figure 17). The second proposed route utilizes the Graebe-

Ullman cyclization of triazole, the final step of an existing synthesis for 2-A α C³⁴ (figure 30). The latter is based on a reasonable assumption that the 2-A α C precursor in the reported synthesis can be obtained from commercially available starting material using a number of coupling strategies that have been developed since the initial report, thus reducing the total number of steps from five to two.

2.1 Suzuki Coupling Followed by Reductive Cyclization

A thorough literature search was performed in order to determine which cross-coupling and cyclization reactions to utilize. Factors taken into consideration include functional group compatibility and availability of proposed starting material. Primary amines that are not part of the desired reaction often retard cross coupling via coordination with the metal catalyst, and/or through the production of by-products. This problem is often mitigated by the protection and de-protection of primary amines before and after cross coupling steps. Cross-coupling reactions that have demonstrated compatibility with unprotected primary amines were given preference in the interest of minimizing the total number of steps to maximize ease and accessibility of the product.

Following the cross coupling step, an intramolecular coupling or cyclization can be used to generate the carboline skeleton. This has been reported using intramolecular arylation, amination, and photo stimulated cyclization^{37,39,41}. These methods require complex reaction conditions and exhibit limited compatibility with desired functional groups, particularly primary amines. For this reason, these methods were not considered for the initial investigation but remain a possibility for the production of 2-AaC.

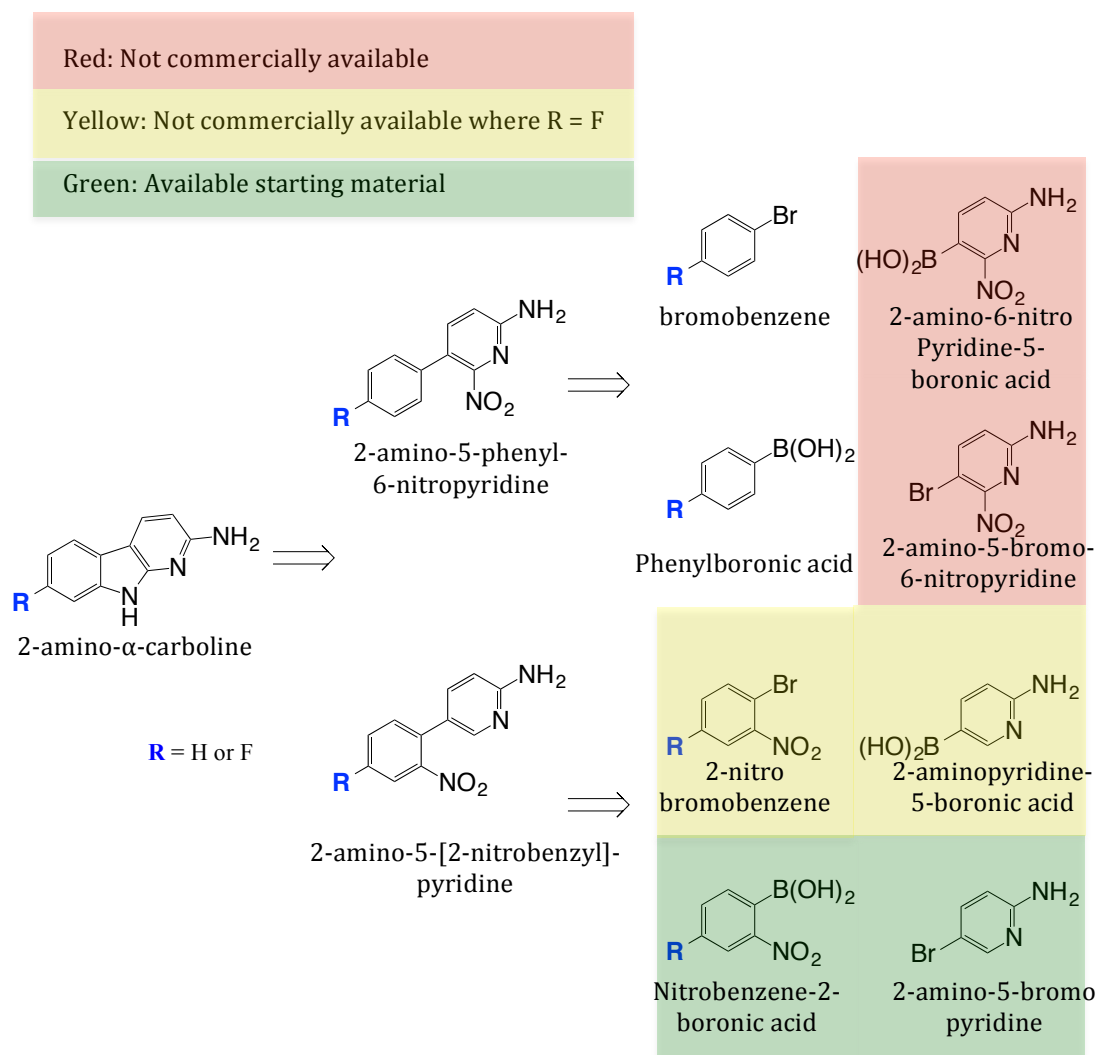


Figure 19: Retrosynthesis of Suzuki coupling/ Cadogan reductive cyclization reveals several combinations of possible starting material. Limitations are based on immediate commercial availability and cost.

The commercial availability of possible starting material causes a notable concern during reductive cyclization. Placement of the nitro group on the phenyl ring rather than the pyridine raises the possibility of two carboline products as a result of the freedom of rotation around the bond connecting the two rings. The possible products are the desired 2-A α C (1-4a), and an undesired 2-A γ C (1-6) assuming no side reactions (figure 20).

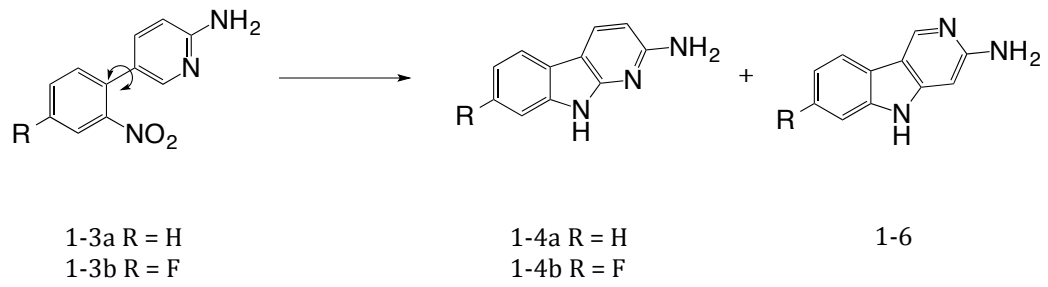


Figure 20: Free rotation around single bond on product of Suzuki coupling using starting material from figure 19 may result in 2 final products: 2-A α C (1-4a) and 2-A γ C (1-6).

2.1.1 Early Attempts:

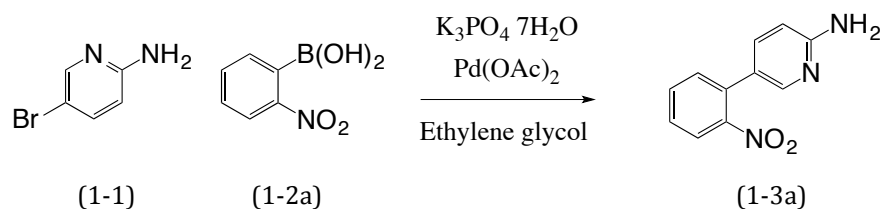


Figure 21: Step 1, Suzuki Coupling.

The coupling of 2-amino-5-bromopyridine (1-1) with phenylboronic acid (1-7) in ethylene glycol without the use of ligands or protecting groups has been reported⁴⁶. This system was used as a control to investigate initial conditions for the proposed reaction (figure 22).

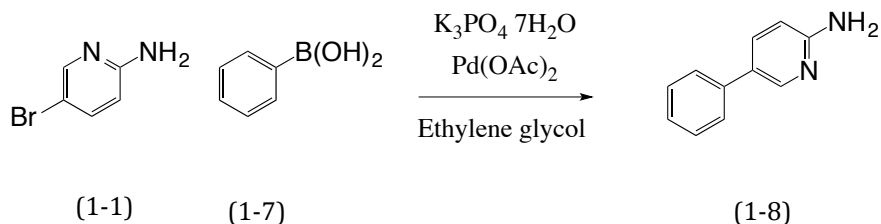


Figure 22: Coupling of 2-amino-5-bromopyridine (1-1) and phenylboronic acid (1-7) as reported by González *et al.*, 2005 was used as a control.

The report cites coordination between the primary amine and the bidentate ethylene glycol as a possible explanation for primary amine compatibility. The control reaction was performed simultaneously with the experimental reaction of 2-amino-5-bromopyridine (1-1) and 2-nitrophenylboronic acid (1-2a) under the reported conditions. Traditional Suzuki Coupling solvents were also used

for good measure. As expected, the control reaction was successful in producing 1-8, but 1-3a was not produced in the desired reaction.

The presence of a 2-nitro group on the 2-nitrophenylboronic acid (1-2a) is the only deviation from the control conditions in the experimental reaction. This indicates the nitro group of 2-nitrophenylboronic acid (1-2a) is causing undesired results. The root cause can be a function of several properties of the 2-nitro group. For example, steric hindrance caused by the position of a 2-nitro moiety may physically hinder transmetalation. The strong electron withdrawing properties of nitro groups may also inhibit this step. Furthermore, coordination of the nitro functionality with the catalyst may hinder the formation of an appropriate Pd-complex⁴⁷.

However, when using 2-nitrophenylboronic acid (1-2a) under the control conditions, ¹H NMR and MS results reveal nitrobenzene as a major product, suggesting that deboronation of the starting material is occurring (figure 23).

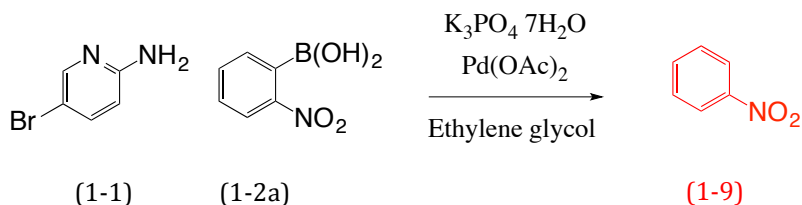


Figure 23: Deboronation of 1-2a during the desired Suzuki coupling.

Where ethanol and Na₂CO₃ are used as the solvent and base respectively, only 2-amino-5-bromopyridine (1-1) and nitrobenzene (1-9) are present after

work-up. Where the base is K_3PO_4 or K_2CO_3 and the solvent is propylene glycol or ethylene glycol, two additional products are present. One of those products is possibly the result of homocoupling between 2-amino-5-bromopyridine (1-1) as suggested by the 1H NMR spectrum.

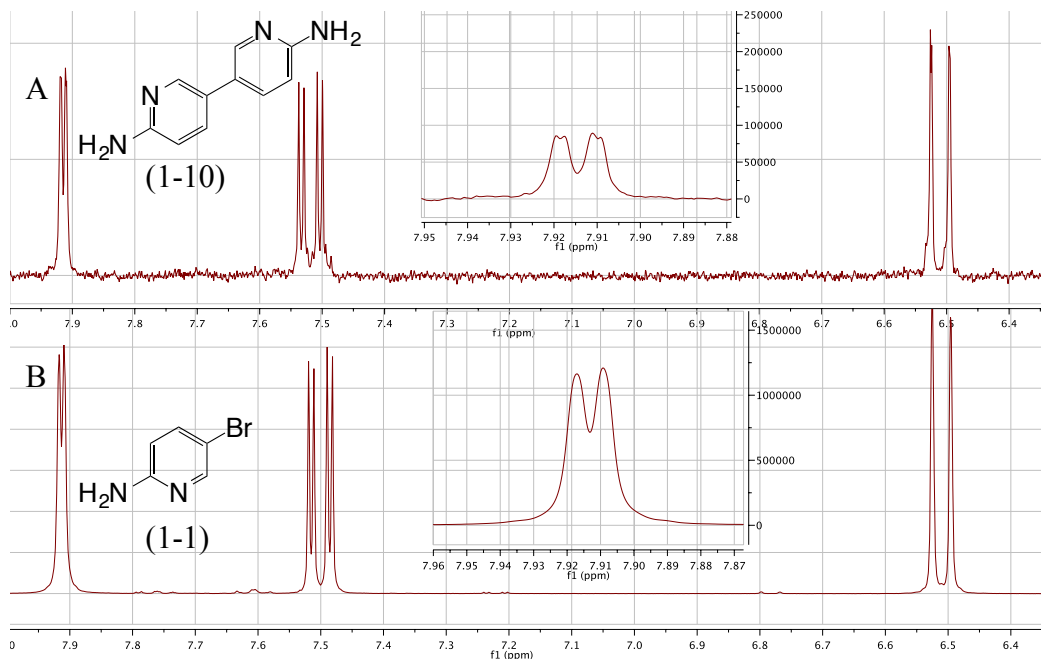
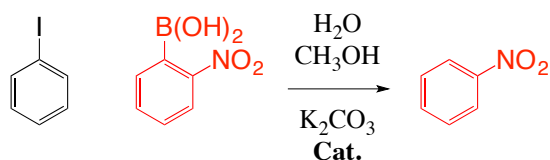


Figure 24: (A) Symmetry and peak splitting observed in 1H NMR in MeOD are consistent with product of homocoupling (1-10) but not confirmed. (B) 1H NMR of recovered 2-amino-5-bromopyridine (1-1)

If the rate of deboronation is faster than the rate of the catalytic cycle up to transmetalation, formation of the desired product will only occur in low yields, if at all. Deboronation, combined with the previously mentioned consideration of steric hindrance from the 2-nitro group further convolutes the probability of product formation via this route.

Figure 25 shows the effect temperature and Pd(OAc)₂ have on the deboronation of 2-nitrophenylboronic acid (1-2a) under Suzuki coupling conditions⁴⁸. While the reported solvent and base differ from the control reaction, the results indicate that for the proposed reaction to work, deboronation will need to be managed by altering certain conditions⁴⁸.



Cat.	T [°C]	t	Conv. Ph-I	Yield
Pd(OAc) ₂	20	15 min	0%	0%
	70	15 min	0%	31%
	100	30 min	0%	84%
-	70	15 min	0%	12%
	100	30 min	0%	19%
	150	24 h	0%	22%

Figure 25: Table and data from Gonzalez *et al.*, 2005 showing the effect of temperature and Pd(OAc)₂ on deboronation⁴⁸

2.1.2 Troubleshooting

An investigation was performed in order to determine what parameters can be changed in the control reaction while still undergoing the desired coupling. Given the lack of by-products in the control reaction (figure 22), the crude product could be assessed by ^1H NMR after work-up without further purification. Complete disappearance of the 2-amino-5-bromopyridine (1-1) starting material indicates 100% product formation on the relative scale used in this analysis and does not represent yield. The 6-H pyridine peaks for the starting material (1-1) and product (1-3a) in the crude product mixture were integrated and the ratios used to determine relative completion of the reaction for each parameter investigated.

To investigate the effect of temperature on the control reaction, the reaction was ran at a range of temperatures, and analyzed via ^1H NMR. The ratio of the 6-H pyridine singlet in the product (1-3a) was compared to the 6-H pyridine singlet in the starting material (1-1) and used to approximate completion of the reaction under the given conditions as shown in figures 26, and 27. As expected, the effect of temperature on the control reaction favored higher temperatures up to 80° C (higher temperatures were not tested in ethylene glycol).

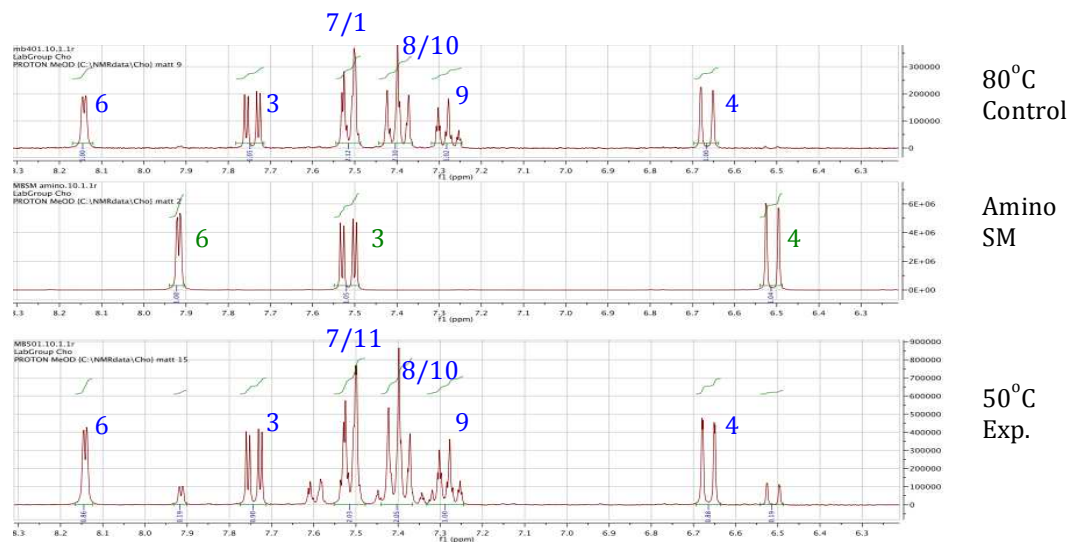
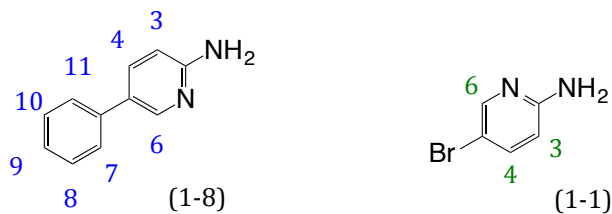


Figure 26: ^1H NMR of crude product in MeOD produced from Suzuki coupling at a range of temperatures. The relative percent ratio of the 6-H pyridine peaks at δ 7.95 (1-1) and δ 8.2 (1-8) were used to determine completion of reaction.

Temp (°C)	% Product	% SM
80	100.00	-
50	79.00	21.00
38	53.75	46.25
20	8.50	91.50

Figure 27: Relative percent ratio of product and starting material present after reaction at different temperatures. Percents were determined from the ^1H NMR ratio described in figure 26.

In addition to temperature, alternative Pd-catalysts, bases, and solvent systems were investigated. Results for Pd-catalysts are shown in figure 28.

Catalysts have different oxidation states and ligand groups. The most effective catalysts were Pd(OAc)₂ and PdCl₃, but all catalysts used produced the intended product (1-8). Selected results for other parameters investigated in the control reaction are shown in figure 29.

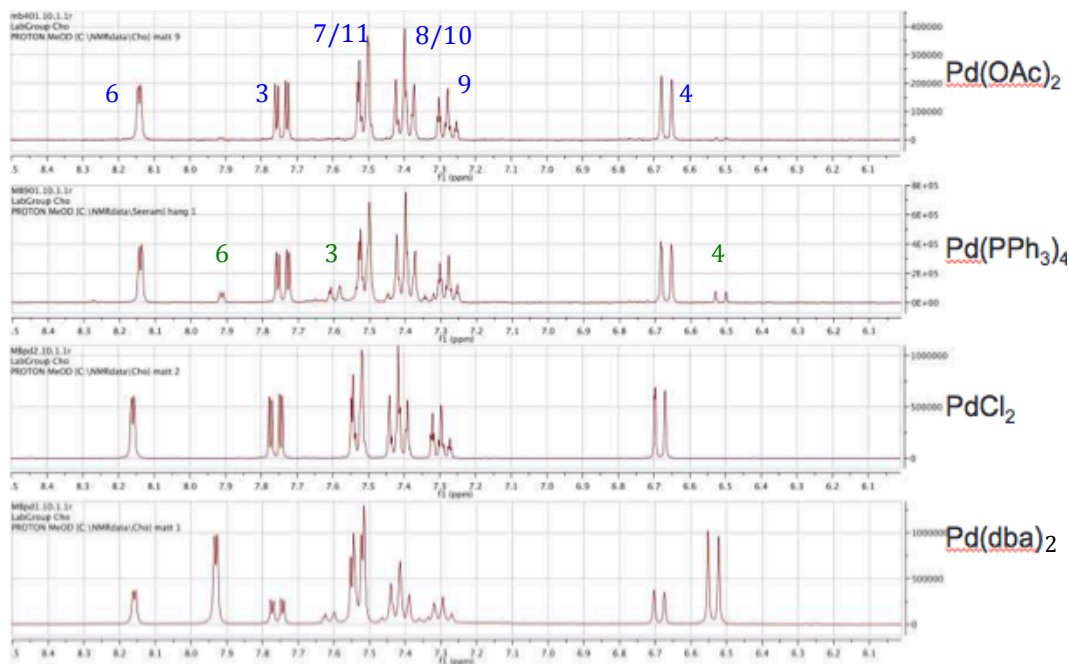
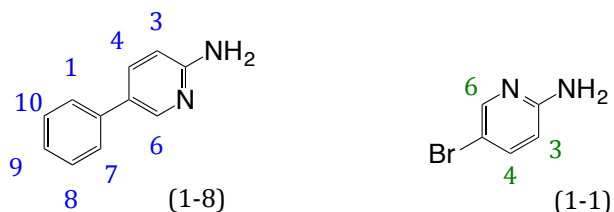


Figure 28: ¹H NMR of crude product in MeOD was used as described previously to determine the percent ratio of starting material (1-1) to product (1-8) in the reaction mixture for different catalysts.

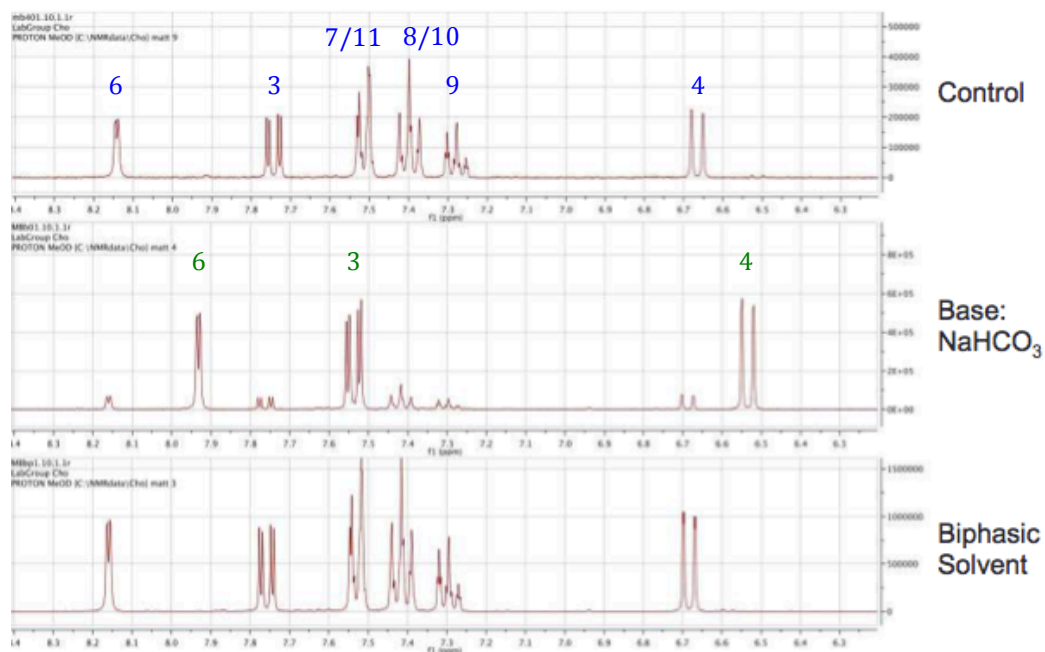
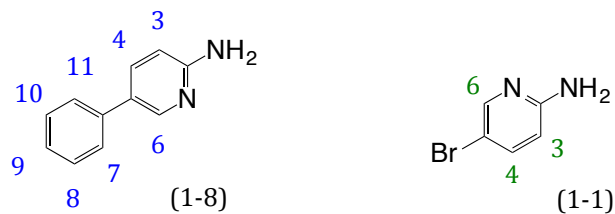


Figure 29: ¹H NMR of crude product in MeOD was used as described previously to determine the percent ratio of starting material (1-1) to product (1-8) in the reaction mixture for different variables. When NaHCO₃ is the base, the reaction does not progress to completion. Not all variables tested are shown.

Due to the success of a simultaneous investigation, time invested in the Suzuki Coupling/Cadagan Reductive Cyclization strategy was reduced and eventually eliminated.

2.2 Cu-Catalyzed Buchwald/Hartwig Coupling Followed by Graebe-Ullmann Cyclization of Triazole.

Synthesis of 2-A α C has been achieved using various strategies. Each reported route consists of many steps, often several that require chromatographic purification, resulting in low overall yields and high costs. Of particular interest was the 5-step reaction reported by Matsumoto *et. al.*, 1979³⁴. The precursor of the final product resembles a possible Buchwald-Hartwig Cu-Catalyzed coupling product of benzotriazole (2-2a) and 2-amino-6-bromopyridine (2-3) (figure 30)⁴⁹. Synthesis of the precursor in a single step from commercially available starting material opens the possibility of producing 2-A α C (1-4a) in only 2 steps.

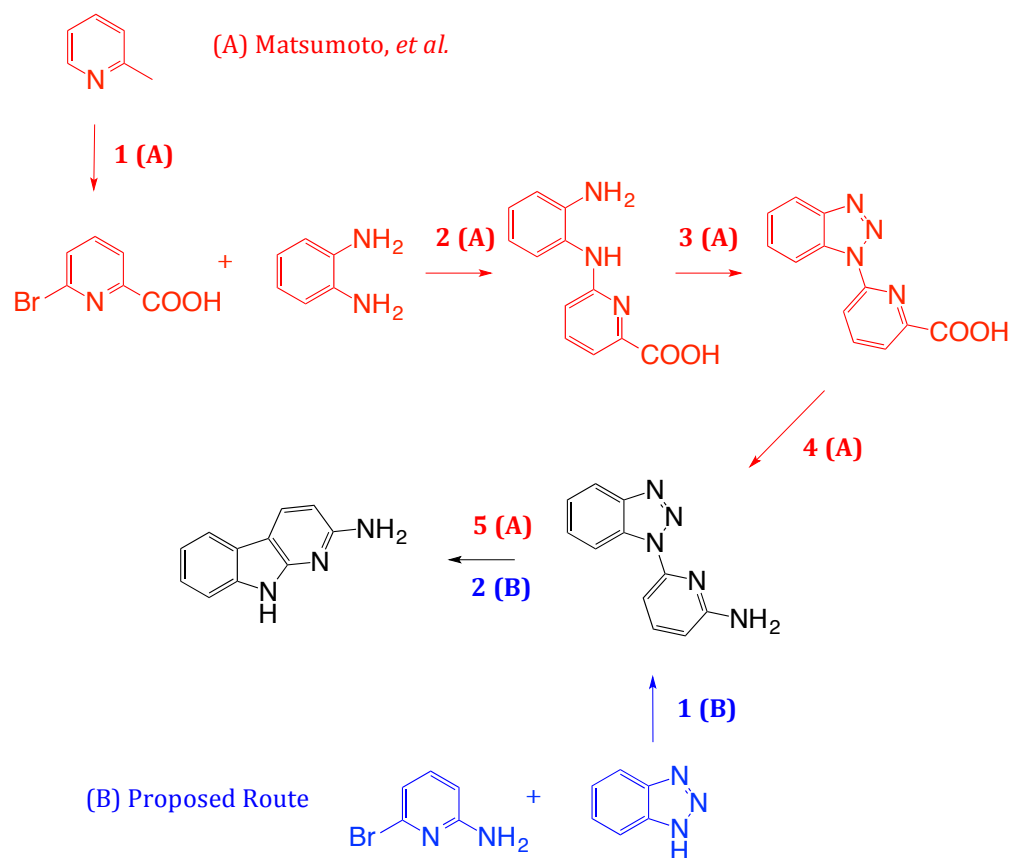


Figure 30: Comparison of previously existing scheme (red) vs proposed (blue) scheme. (A) Scheme by Matsumoto *et al.*, 1978 requires 5 steps to produce 2-AcC. (B) Step 1 of the proposed route, a Cu-catalyzed Buchwald-Hartwig coupling, produces the immediate precursor of 2-AcC from Matsumoto *et al.*, 1978, reducing the overall scheme from 5 to 2 steps^{34,49}.

In the proposed scheme, commercially available starting material can account for all analogs necessary for dG-2-AcC adduct synthesis and ¹⁹F NMR analysis via the proposed route as seen in figure 31.

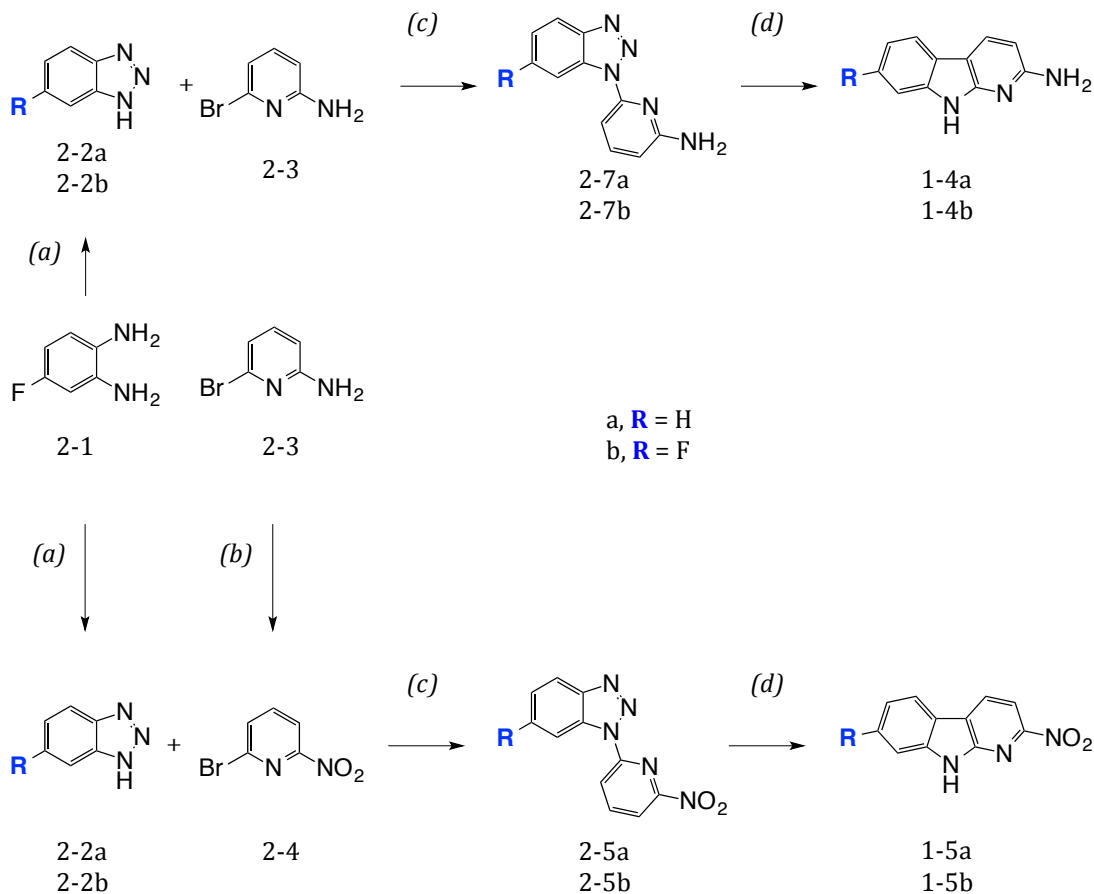


Figure 31: Production of 2-AxC (1-4a), 2-NxC (1-5a), and fluorinated analogs. (a) NaNO₂, AcOH, H₂O, RT, 20-30 min. (b) H₂SO₄, H₂O₂, H₂O, RT, 24-48 h. (c) CuI (5 mol%), K₃PO₄, N,N'-dimethylethylenediamine (DMEDA), DMF, 110°C, 24-48 h. (d) Polyphosphoric acid (PPA), 180°C, 30 min.

There are possible concerns regarding synthesis of the fluorinated analogs by this route due to the possibility of tautomerization of the 6-fluorobenzotriazole (2-2b). This will be discussed in detail later (figure 46). For now, it is not of great concern because ¹⁹F NMR experiments can be performed with fluorine in the 7 or 6 position.

2.2.1 Step 1: Cu-Catalyzed Coupling of Nitro Stating Material to Produce 6-(1H-benzotriazol-1-yl)-2-nitropyridine (2-5a)

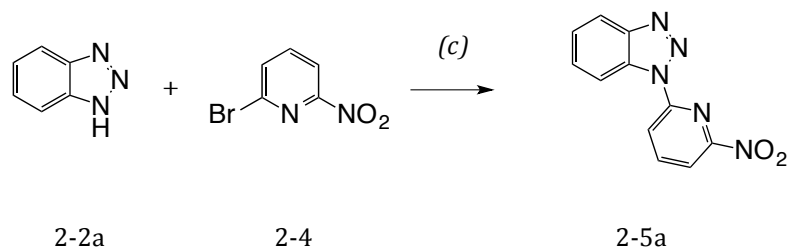


Figure 32: (a) Step 1, CuI (5 mol%), K₃PO₄, DMEDA, DMF, 110° C, 24hrs.

An oven-dried 50 mL round bottom flask with a small stir-bar was charged with 300 mg of benzotriazole (2.51 mmol), 614 mg of 2-bromo-6-nitropyridine (3.01 mmol), 24 mg CuI (0.13 mmol, 5 mol%), and 1.11g K₃PO₄ (5.27 mmol). The round bottom was sealed using a rubber septum, air was removed using a vacuum, replaced with N₂, and repeated three times. An N₂ balloon connected to a syringe was left in the septum. 27 µL of N,N'-dimethylethylenediamine (22 mg, 0.25 mmol) and 2 mL of DMF were mixed, taken up into an airtight syringe, and injected into the reaction flask. The round bottom was placed into an oil bath at 90° C and stirred for 24 hours.

The crude product results in 2 major spots and 1 minor spot on an aluminum-backed silica TLC plate with an absorbance indicator at 254 nm. The least polar spot represents the product with an R_f value of 0.63 in a mobile phase of 20% EtOAc in hexane. The crude product was purified by column chromatography in a glass column using silica stationary phase and a step-

wise gradient of the EtOAc/hexane mobile phase. The gradient started at 0% EtOAc and increased in increments of 5% ethyl acetate until each spot eluted. The progress of the separation was monitored by TLC (figure 33). After confirming the presence of the desired product, a Medium Pressure Liquid Chromatography (MPLC) method was developed on CombiFlash to better facilitate scaling up (figure 33).

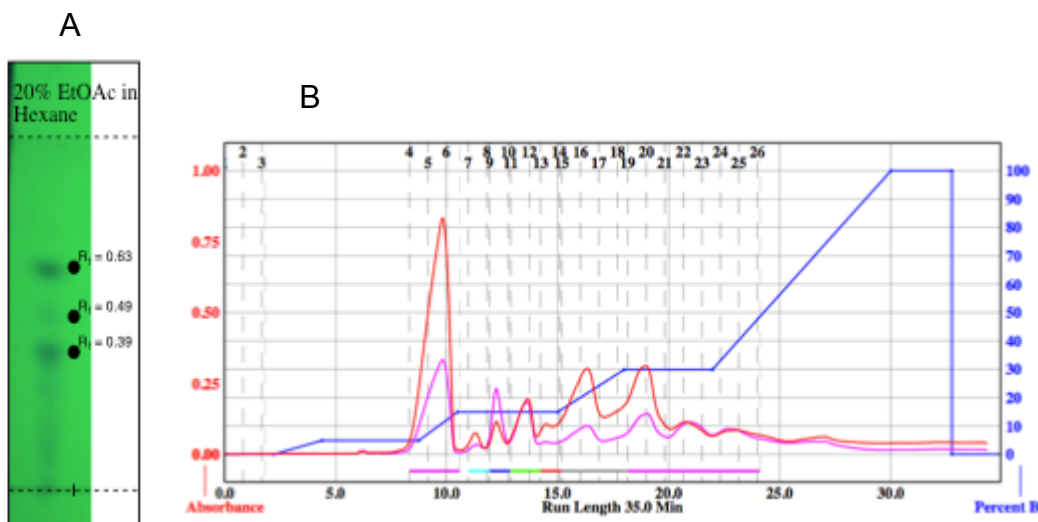
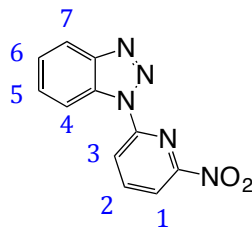


Figure 33: (A) TLC 20% EtOAc/hexane, product $R_f = 0.63$. (B) Normal phase MPLC chromatogram for reaction c. Gradient (percent EtOAc in hexane) = blue line. Red line = absorption at 260 nm. Purple line = absorption at 260 nm. The desired product (2-5a) is the major peak and elutes from 9-10 min.

The eluent containing the spot with R_f 0.63 was evaporated leaving behind 280 mg of a yellow crystalline solid. A portion of the solid was dissolved in DMSO- d_6 and analyzed by 1H NMR revealing a spectrum consistent with the desired product (Figure 34).



MB2301s.10.1.1rLabGroup Cho
 PROTON DMSO {C:\NMRdata\Cho} matt 20

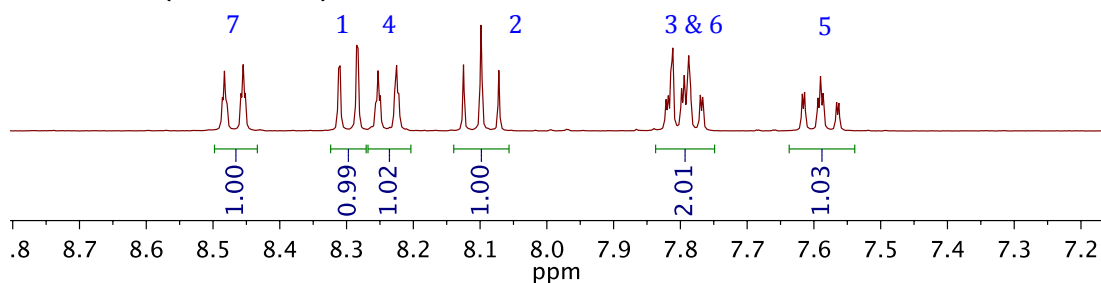


Figure 34: ^1H NMR in DMSO-d_6 for 6-(1*H*-benzotriazol-1-yl)-2-nitropyridine (2-5a) after column chromatography.

The spin systems are consistent with the 2-AaC precursor in figure 30, but in this case there is a nitro group in place of the amine. The triazole cyclization to produce the carboline product has not been reported with the nitro compound. Given the simplicity of the reaction, the fastest way to investigate compatibility is to attempt the desired reaction.

2.2.2 Step 2: Triazole Cyclization to produce 2-nitro-9H-pyrido[2,3-b]indole, (2-nitro- α -carboline, 2-N α C, 2-6a)

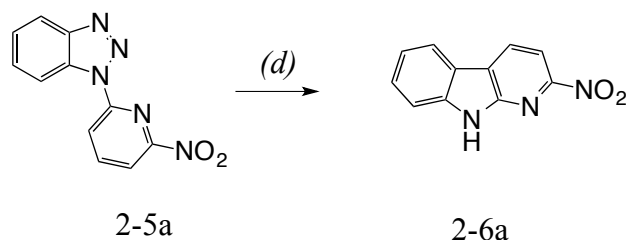


Figure 35: (d) Step 2, Polyphosphoric acid (PPA), 30 minutes, 180° C

A 50 mL round bottom flask was charged with 50 mg of product (1) from figure 31. Approximately 700 mg of polyphosphoric acid (PPA) was transferred to the round-bottom using a glass stir rod. The flask was transferred to an oil bath that was pre-heated to 180° C. After 10 minutes, the PPA turned a light brown/caramel color. Small bubbles can be observed, presumably from the release of N₂. After approximately 30 minutes, bubbles are no longer visible in the PPA. If there is SM stuck to the sides of the flask, it can be rotated and dissolved in PPA at which point small bubbles can again be observed until the reaction is complete (this can be performed as soon as the PPA is viscous enough to move around the flask; there is no need to wait until completion). The flask is then cooled at room temperature and diluted with water. For the purpose of solubility, it is best to dilute with water before the PPA reaches room temperature. The mixture is then neutralized with NaOH solution to a pH of 7 and extracted several times with ether. Evaporating the ether yields 30 mg of crude product as a light yellow powder.

One major and two minor products are visible by TLC (254 nm). The minor products are only visible at high concentrations. The crude product was purified by column chromatography in a glass column with a neutral alumina stationary phase and an isocratic mobile phase of 15% EtOAc/ hexane. The separation was monitored by TLC and yielded 22 mg of the major product at R_f 0.62.

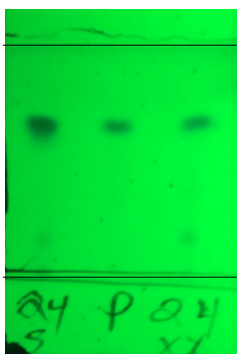


Figure 36: TLC for reaction (d) in 20% EtOAc/hexane. Desired product (2-5a) R_f = 0.62. Lane 1 & 3 = crude product from reaction (d), lane 2 = 2-5a after column chromatography.

The major product was dissolved in DMSO- d_6 and analyzed by 1H NMR. 1-D 1H NMR showed convincing coupling patterns consistent with the desired product. Different NMR solvents were used in order to obtain spectra without overlapping peaks to facilitate a more simple interpretation of 2-D NMR data. Acetone- d_6 is the aprotic solvent of that provides a spectrum without overlapping peaks (figures 37-40).

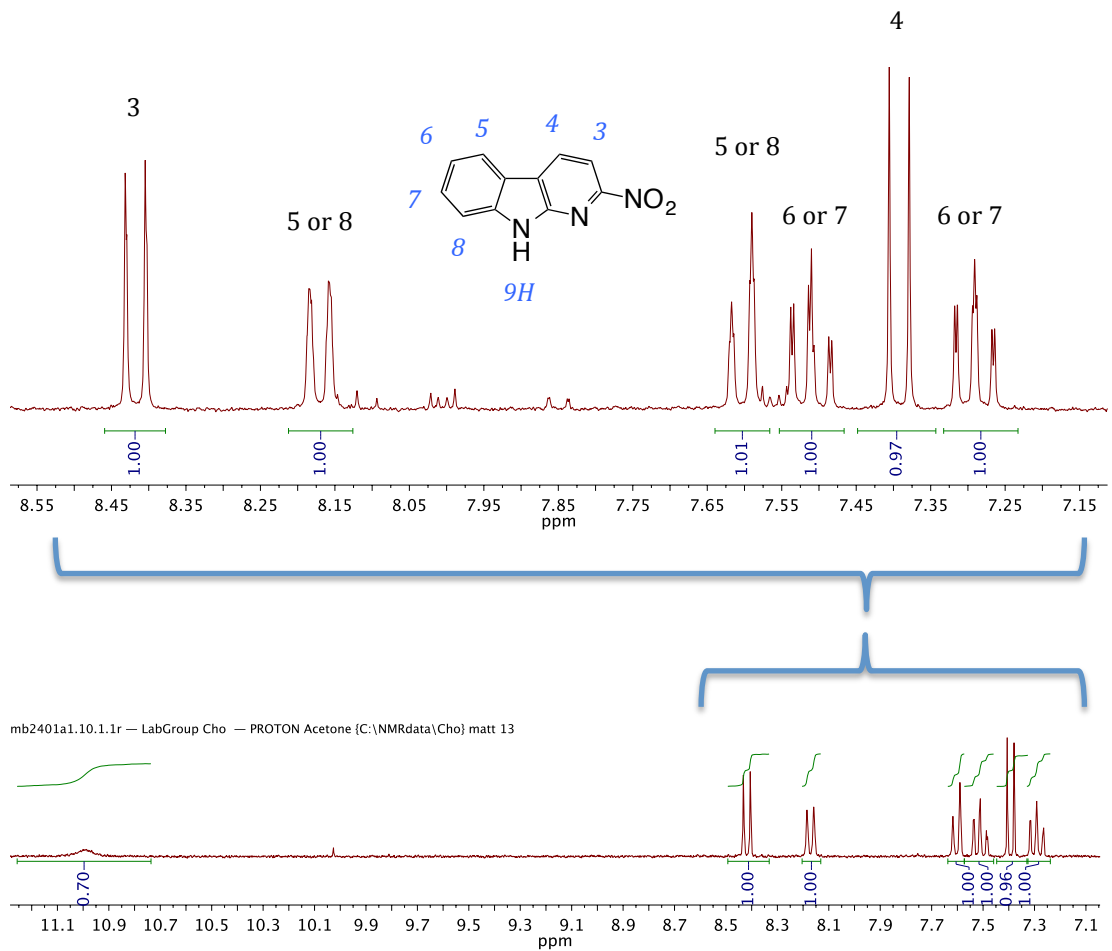


Figure 37: ¹H NMR for 2-6a in acetone-d₆ after chromatographic purification. 9H proton at δ 11.0, close-up shown for δ 7.15- 8.55. See experimental section for ¹H NMR spectrum of higher purity in CDCl₃. The above sample was used to confirm spin systems through COSY ¹H NMR. Acetone-d₆ was used as the solvent due to lack of overlap between peaks.

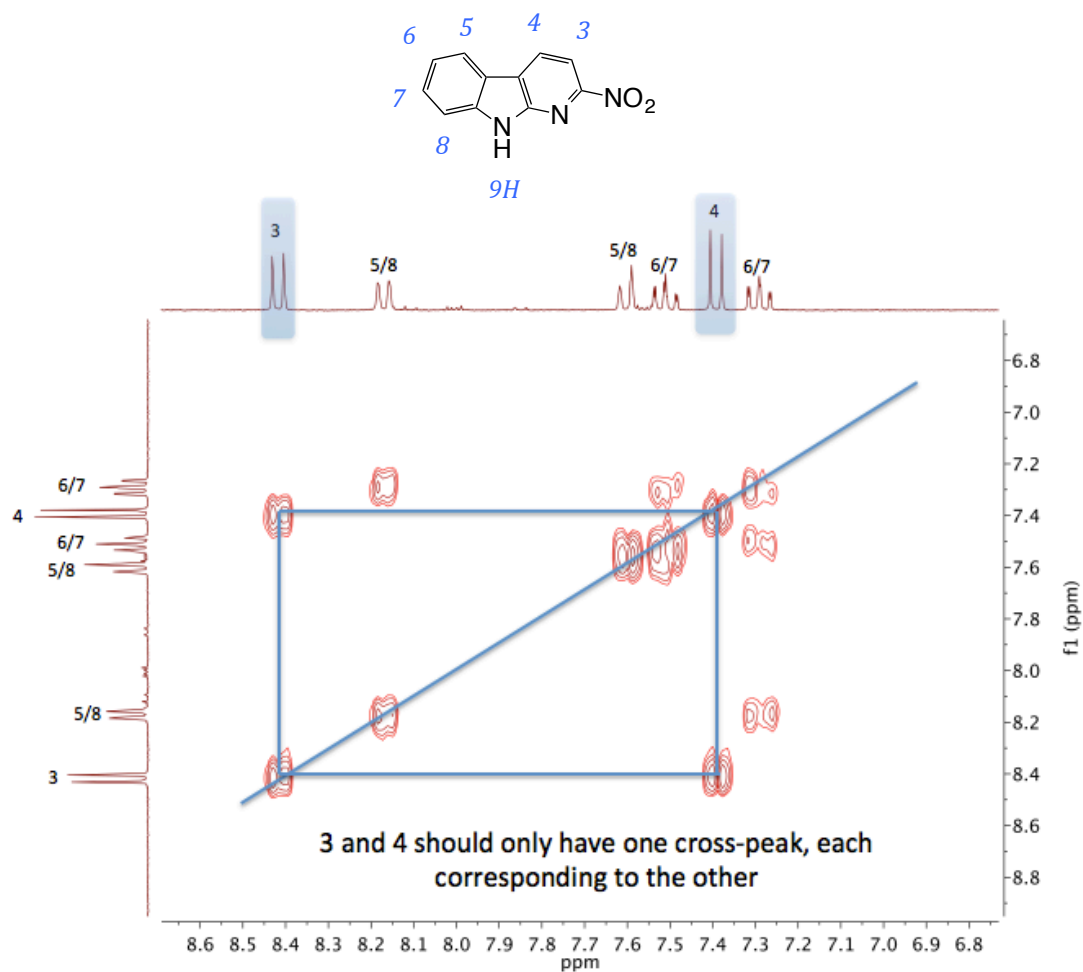


Figure 38: 2D ¹H NMR COSY for 2-6a in acetone-d₆. Peak 3 & 4 make up expected spin system and are assigned based on chemical shift. Proton nearest the nitro group (3) will be most deshielded as is observed by the chemical shift.

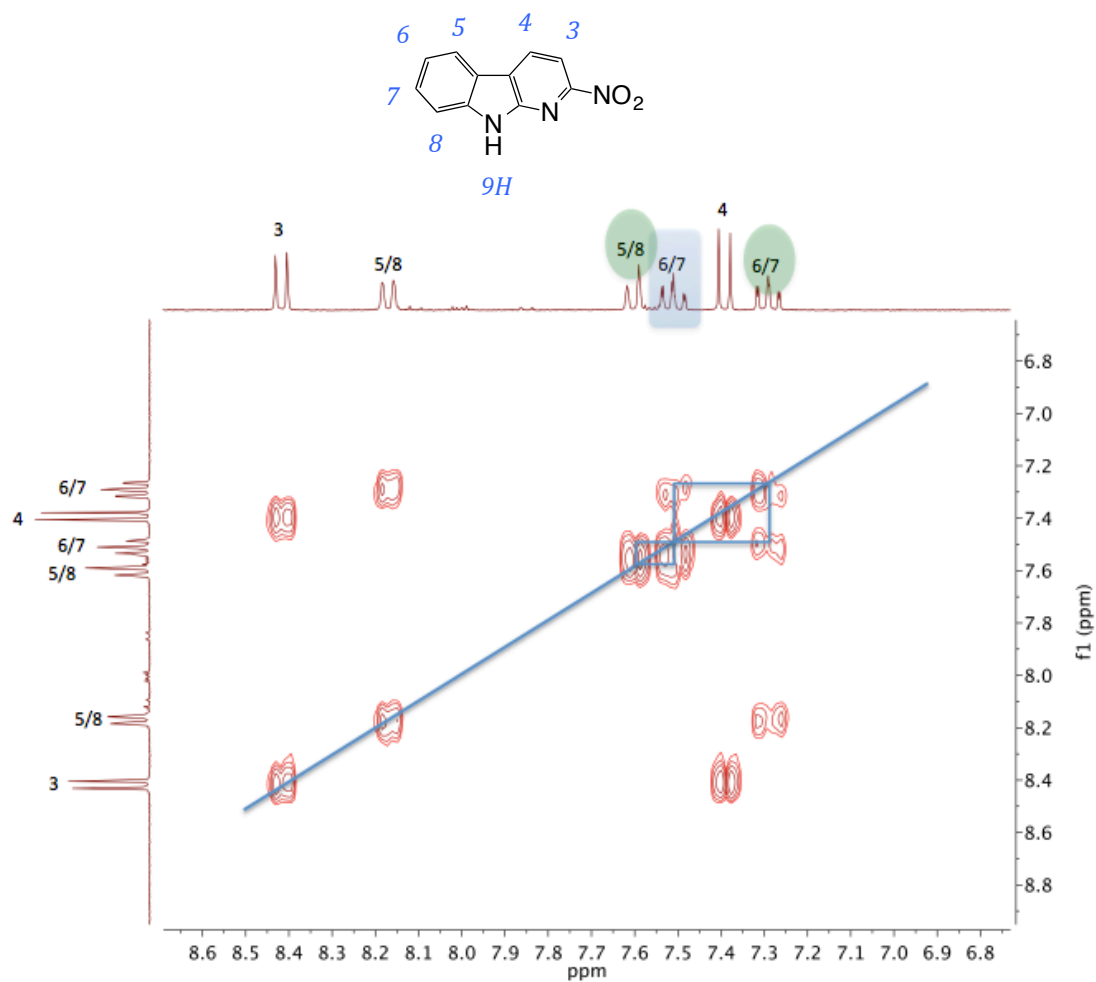


Figure 39: 2D ¹H NMR COSY 2-6a in acetone-d₆. Triplets of 6/7 and doublets of 5/8 make up the expected spin system. Individual assignment cannot be made with ¹H NMR COSY alone. Heteronuclear correlation would be required. ¹H NMR COSY does reveal the relative connectivity of the protons to each other.

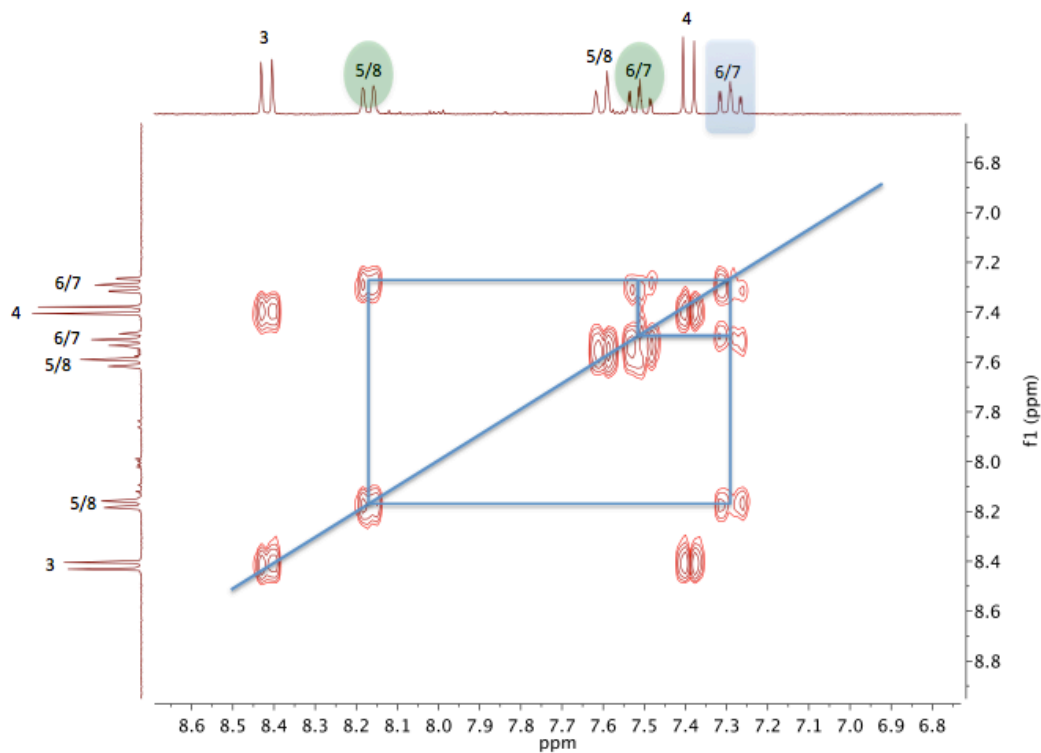
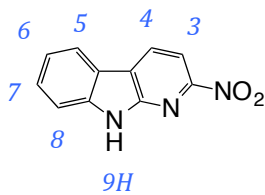


Figure 40: 2D ^1H NMR COSY of 2-6a in acetone- d_6 . Triplets 6/7 and doublets 5/8 make up the expected spin system. Individual assignment cannot be made with COSY. Heteronuclear correlation would be required.

The data indicates synthesis of 2-nitro- α -carboline (2-NaC) was successfully achieved in two steps. The synthesis of 2-NaC has previously only been reported via oxidation of 2-AaC making this the first report directly producing 2-NaC without the 2-AaC intermediate^{17,33}.

2.2.3 Step 1: Cu-Catalyzed Coupling of Amine Starting Material (2-3) to

Produce 2-amino-9H-pyrido[2,3-b]indole, (2-amino- α -carboline, 2-A α C, 2-7a)

With small-scale production of 2-N α C (1-5a) confirmed, 2-A α C (1-4a) and the fluorinated analogs of each need to be produced (1-4b, 1-5b). Given the available scheme, 2-A α C can be obtained from the reduction of 2-N α C using hydrazine. Reduction of Ar-NO₂ with hydrazine is the most common technique used for the partial reduction in biomimetic synthesis as described in section 4.2. If the reaction conditions are not controlled, the nitro group will be fully reduced to the amine. Alternatively, 2-amino-6-bromopyridine may be used in place of 2-bromo-6-nitropyridine in the established reaction assuming the primary amine does not complicate or prevent the Cu-Catalyzed coupling.

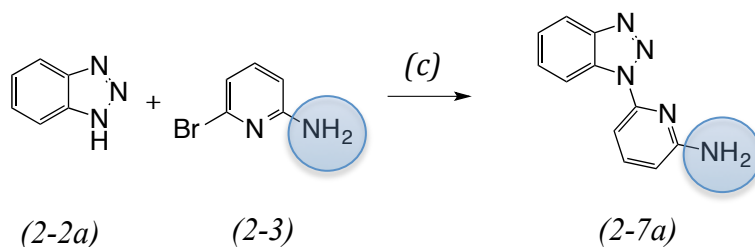


Figure 41: Step 1, reaction c with amine functionality (2-3). (c) CuI (5 mol%), K₃PO₄, DMEDA, DMF, 110°C, 48 hrs.

Step one was repeated using 100 mg of 2-amino-6-bromopyridine (0.83 mmol) and the scaled stoichiometric ratios of the corresponding reagents (figure 31). Set-up, work-up, and purification procedures were the same as the nitro analog, except where noted. Care was taken to maintain an inert atmosphere

during the reaction. After 24 hours, the TLC (254 nm) revealed 3 major spots and several minor spots. The least polar spot was the most intense and only varied in R_f from the next spot by 0.03 (figure 42).

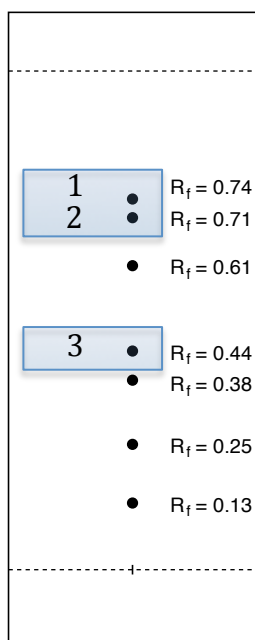


Figure 42: Reconstructed TLC of crude product from reaction c in 40% EtOAc/hexane. Desired product, 2-amino-9H-pyrido[2,3-b]indole, (2-amino- α -carboline, 2-A α C, 2-7a) is spot 1 and represents the major product $R_f = 74$. Spots 2 and 3 represent other major products, remainder of spots are minor by-products. Reaction with the amine starting material results in more byproducts than the product of the nitro starting material.

During workup, the silica plug was substituted for a neutral alumina plug as a precaution for the primary amine. Similarly, a neutral alumina column was substituted for a silica column during purification.

Isolated spots were analyzed by HNMR in CDCl₃. Spot 1 was the most intense spot on the TLC plate and corresponded to 2-amino-6-bromopyridine (2-3).

Spot 2 corresponded to the desired product (2-7a) as seen in figure 43.

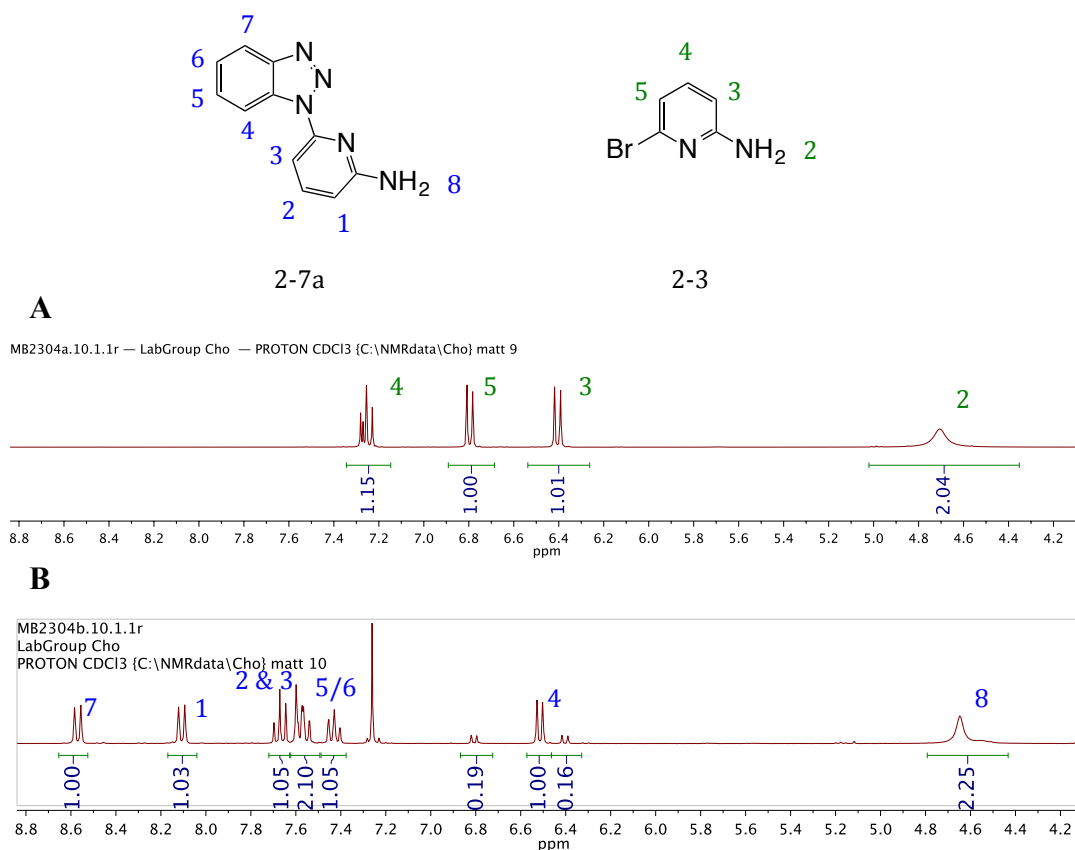


Figure 43: (A) ¹H NMR of 2-amino-6-bromopyridine (2-3) in CDCl₃ recovered after purification of product mixture. (B) ¹H NMR of desired product, 2-7a, in CDCl₃.

The amount of pure product (2-7a) recovered was 11 mg while approximately 55 mg of 2-amino-6-bromopyridine (2-3) was recovered. This confirms the desired product can be formed using this strategy but indicates the reaction proceeds more slowly when using the amine starting material (2-3). The coupling of 2-amino-6 bromopyridine (2-3) therefore requires a longer reaction

time, or a higher temperature. It also has lower yields and more byproducts as evident by TLC.

The reaction was repeated and allowed to run for 48 hours. While the spot corresponding to the SM was still present, the product spot was now the most intense on the TLC and purification yielded 38 mg recovered. In both instances, purification was difficult due to the similarity in R_f values of the starting material and the product resulting in eluent that contained both spots. Originally, this eluent was not further purified and any product it contained was not part of the reported recovery making the yield appear lower than reality. One of the ways to address this issue during scale-up was to use 2-amino-6-bromopyridine (2-3) as the limiting reagent. After 48 hours the SM was not visible by TLC and 52 mg of the desired product was recovered.

During scale-up an MPLC method was developed for CombiFlash on a neutral alumina column. A representative chromatogram is shown in figure 44.

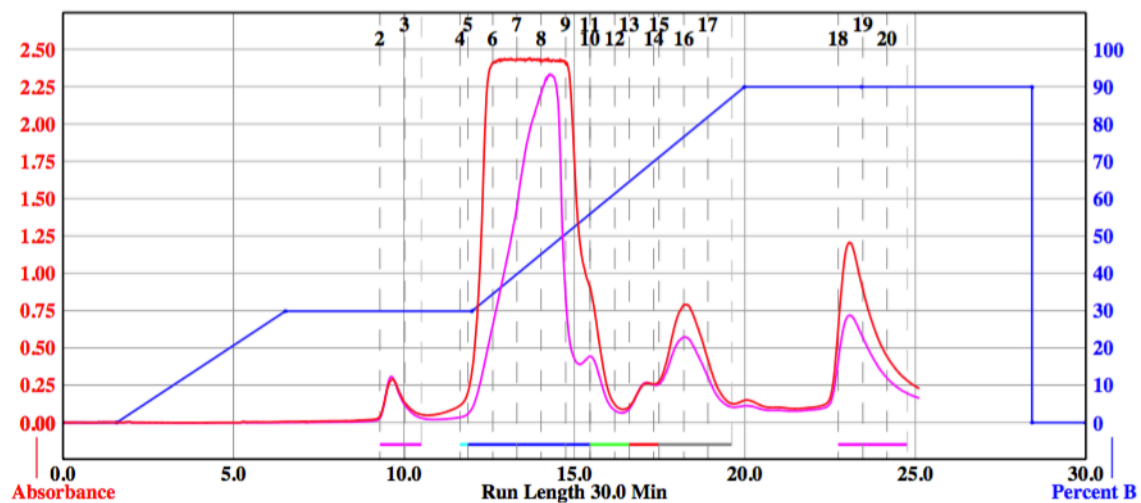


Figure 44: MPLC chromatogram from CombiFlash alumina column. EtOAc/hexane, EtOAc = solvent B. Dry pack. Amine starting material is present in small amount (≈ 10 min). Product elutes from ≈ 11 -15.5 min.

2.2.4 Step 2: Triazole Cyclization to produce 2-amino-9H-pyrido[2,3-b]indole, (2-amino- α -carboline, 2-A α C, 1-4a)

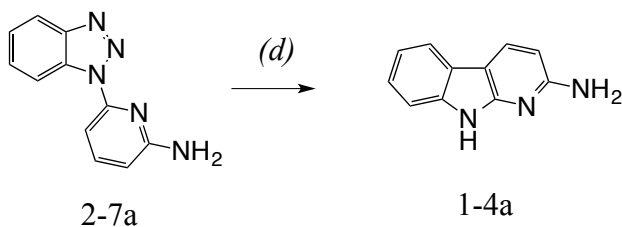


Figure 45: (d) Step 2, Polyphosphoric acid (PPA), 30 minutes, 180° C

Since 2-7a is the 2-A α C precursor from figure 30, the next step of the reaction is already established. Following the same procedure as reported for 1-5a, and that by Matsumoto *et al.*, 2-7a was reacted in PPA as previously described. The Turesky group at the University of Minnesota Cancer Center provided a reliable 2-A α C standard for analysis. TLC was performed at various proportions of EtOAc/ Hexane in comparison with the product and standard. R_f values and co-spot tests support production of the desired product.

2.2.5 Fluorine Analogs

Having demonstrated the capacity to synthesize both 2-AcC (1-4a) and 2-NaC (1-5a) in a two-step reaction, synthesis of the 7-fluorinated analogs (1-4b, 1-5b) needs to be established for potential ^{19}F NMR experiments. Since there is not a known method to selectively fluorinate the 7-position of carbolines, fluorine must be present at the start of the reaction as shown in step *b* of figure 31. This raises the concern that tautomerization of the 6-fluorobenzotriazole during step *d* will result in an isomeric mixture. If the reaction proceeds there are 2 possibilities as described in figure 46.

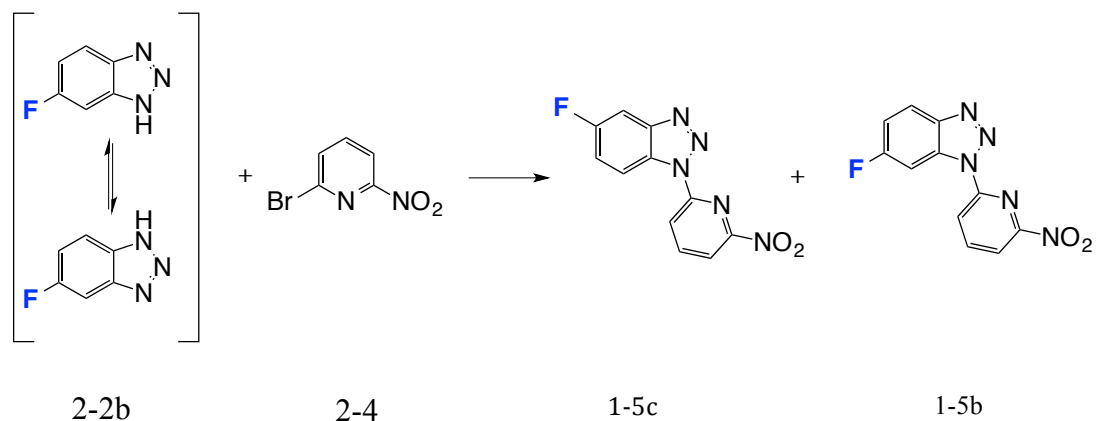


Figure 46: Tautomerization of 6-fluorobenzotriazole (2-2b) can result in an isomeric mixture. 1-5b and 1-5c represent the isomers.

Since ^{19}F NMR can be performed with the 7-fluoro or 6-fluoro isomer of 1-5 and 1-4, the only remaining concern is purification, a topic that will be

discussed later. A procedure reported by Wasik *et al.*, 2010 was used to produce 6-fluorobenzotriazole 2-2b⁵⁰.

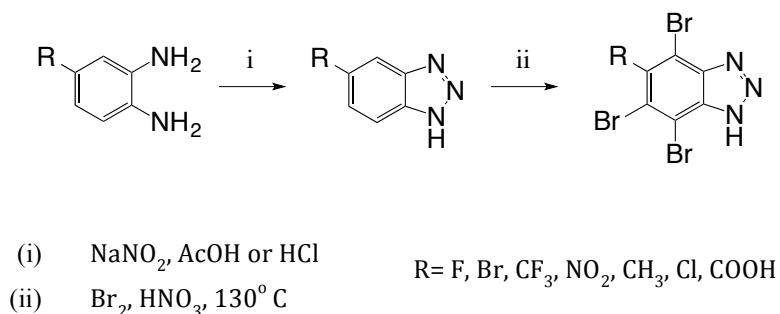


Figure 47: Synthesis of 2-2b as reported by Wasik *et al.*, 2010⁵⁰ Note the product in their scheme is the undesired tautomer. However, the product results in the desired tautomer as measured in NMR solvents on an NMR time scale.

Initially 100 mg starting material 2-1 was used, but the reaction was scaled to 1 g. Because of the nature of their investigation, the authors do not follow the conventional heterocyclic numbering format, referring to this product as 5-fluorobenzotriazole. Tautomerization makes this point relevant upon identification of the product's subsequent coupling with 2-amino-6-bromopyridine (2-3) and 2-bromo-6-nitropyridine (2-4) as shown in figure 46. The production of 6-fluorobenzotriazole (2-2b) was confirmed by ^1H NMR in DMSO-d_6 (figure 48). The spectrum is consistent with the desired product and matches that of the reported procedure.

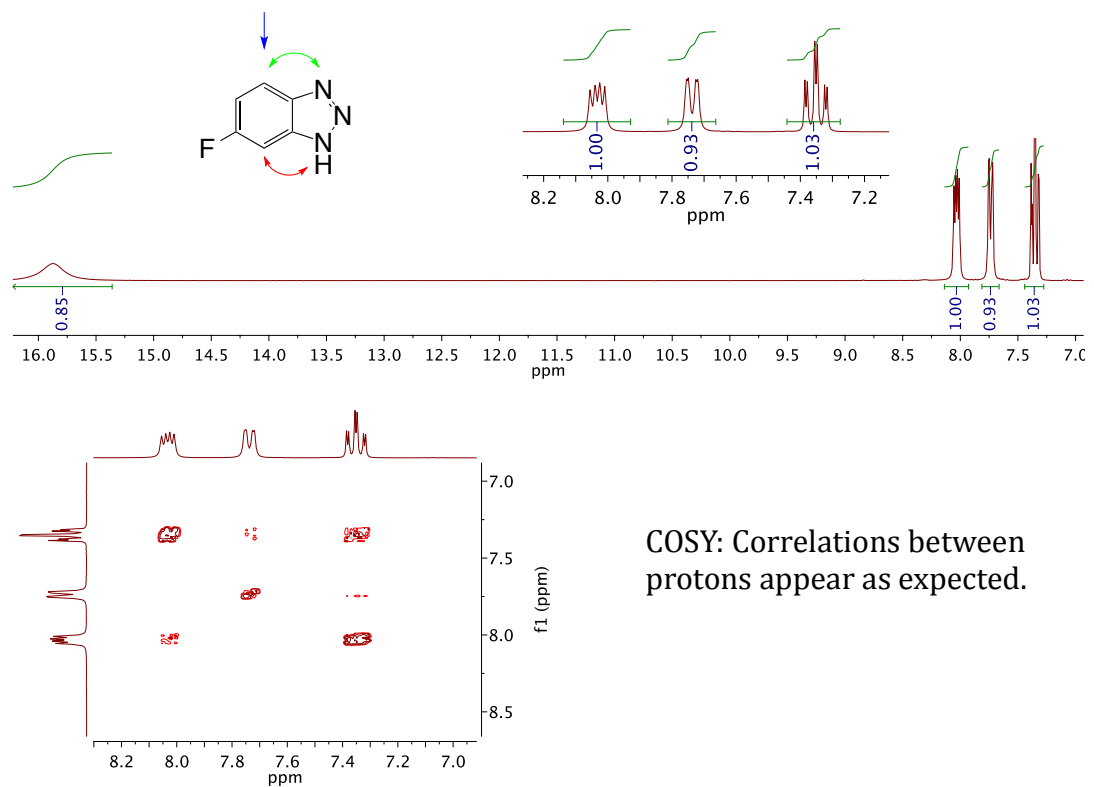


Figure 48: ^1H NMR (*II-F*) Acetone D_6 .

6-fluorobenzotriazole 2-2b was subsequently used in reaction a under the same conditions as 2-2a, producing an isomeric mixture. 4 spots are clear on the TLC, however the isomeric mixture represents only one of those spots unless TLC conditions are optimized (figure 49).

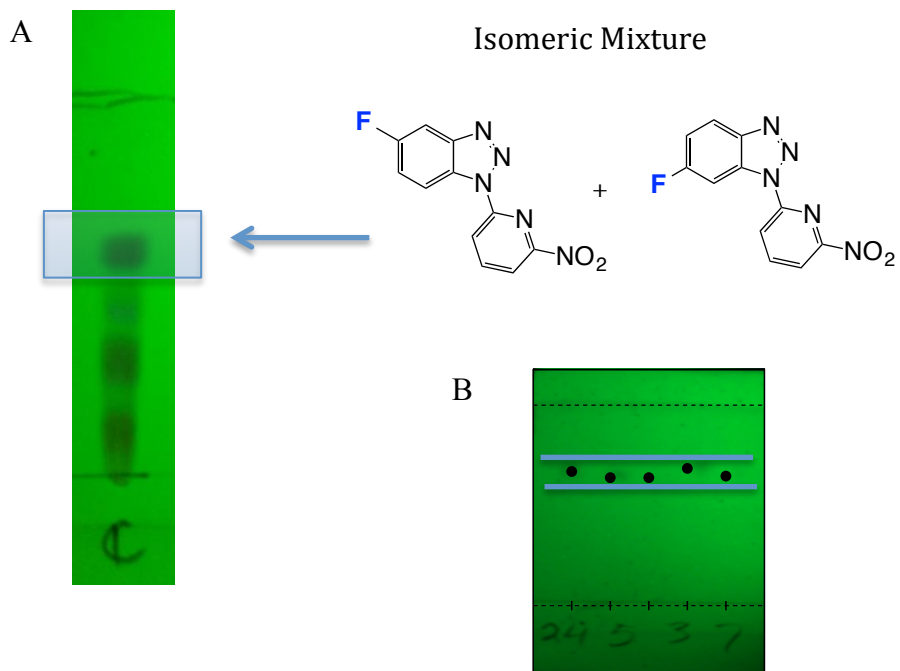


Figure 49: TLC (1-F) Least polar spot in (A) represents 2 products as seen after 2nd purification in TLC (B).

Initially, the isomeric mixture was isolated as a single spot. The fact that it was a mixture became evident after ¹H NMR (figure 50).

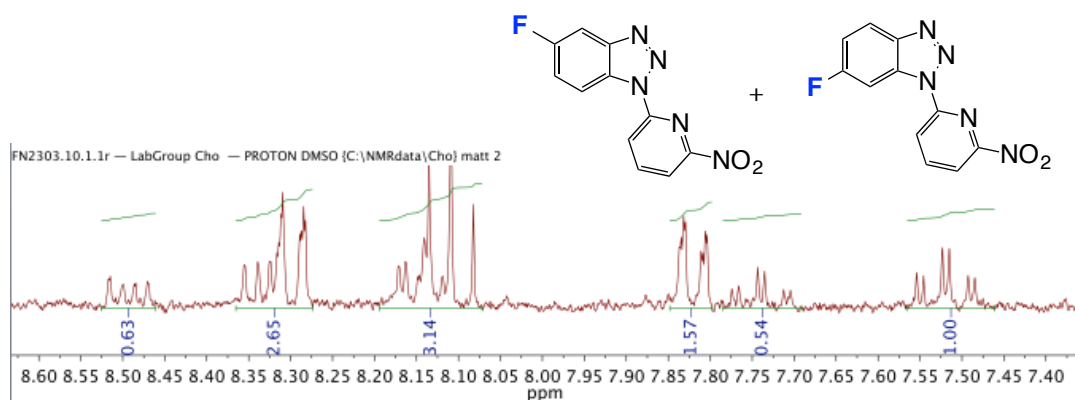


Figure 50: ¹H NMR in DMSO-d₆ 1-5b, 1-5c Isomeric mixture.

Purification of each isomer was done by column chromatography on a glass column with a silica stationary phase and very gradual stepwise gradient of EtOAc and hexane starting at 0% EtOAc. A larger than average column width to height ratio, as well as a larger amount of stationary phase is desirable for this purification. Due to similar polarities, purification by column chromatography takes several hours. ¹H NMR was used to identify the isomers shown in figure 51.

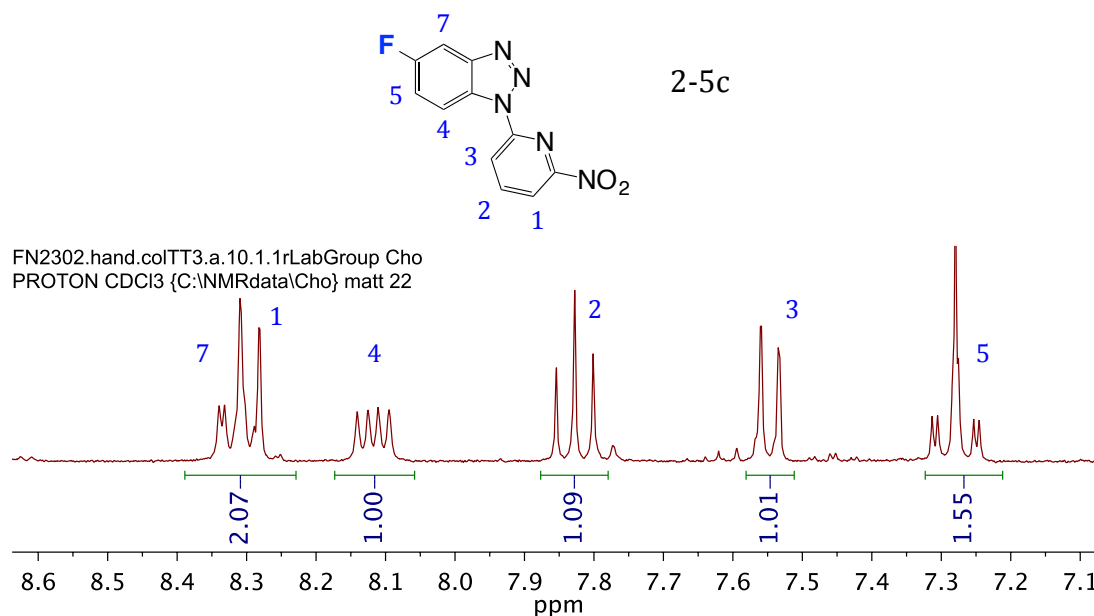
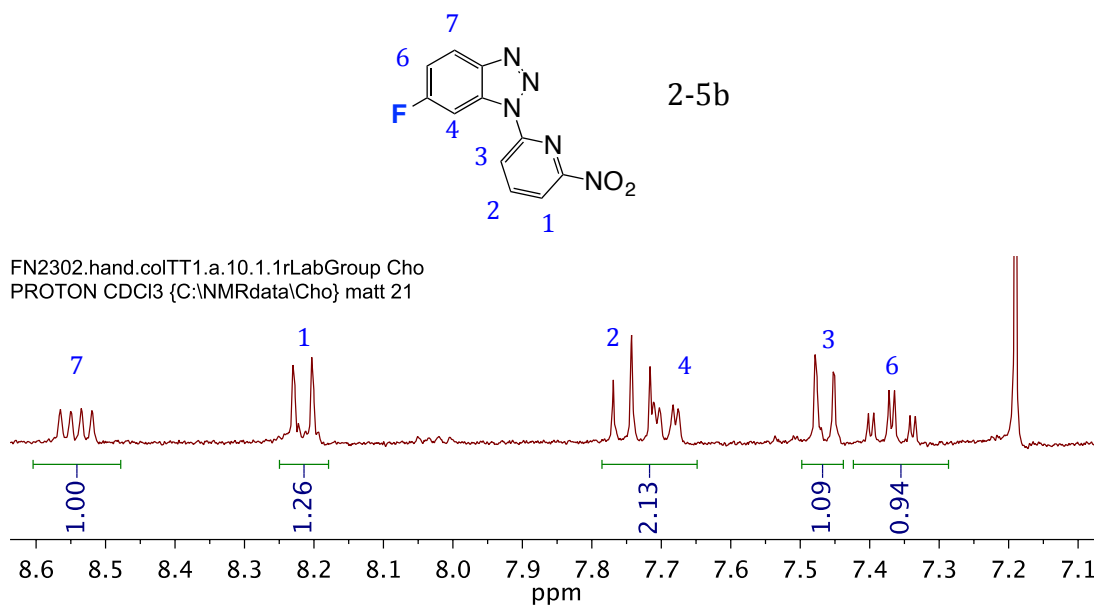
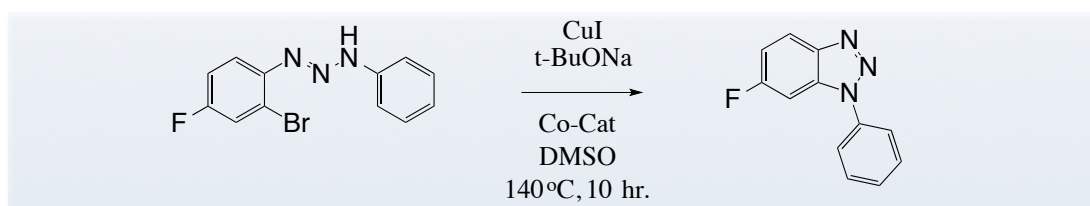


Figure 51: ^1H NMR in CDCl_3 . Pure isomers as shown in TLC figure 49.

Identification of the isomers in figure 51 can be done by performing ^1H - ^{15}N -HMBC, or NOESY. However, due to limitations on time, precedent in literature (figure 52), and the fact that ^{19}F NMR experiments can be performed with

either pure isomer, time was not allocated to increasing the certainty of identification. Figure 52 explains how the identity of each isomer was determined using meta coupling constants from literature precedent and a chemical shift argument.



6-Fluoro-1-phenyl-1H-benzotriazole (2i). Pale yellow solid (43 mg, 40%). M.p. 102–104°. IR: 3103, 1625, 1506, 1487, 1450, 1249, 1148, 1112, 762, 694. $^1\text{H-NMR}$: 8.11 (*dd*, $J = 9.04, 4.66$, 1 H); 7.75 (*d*, $J = 7.93$, 2 H); 7.63 (*t*, $J = 7.81$, 2 H); 7.53 (*t*, $J = 7.38$, 1 H); 7.40 (*dd*, $J = 8.11, 2.14$, 1 H); 7.22 (*dt*, $J = 9.03, 2.16$, 1 H). $^{13}\text{C-NMR}$: 163.9; 161.5; 143.2; 136.5; 132.7; 132.5; 129.9; 128.8; 122.6; 121.7; 121.6; 114.4; 114.1; 96.3; 96.0. HR-MS: 213.0702 (M^+ , $\text{C}_{12}\text{H}_8\text{FN}_3$; calc. 213.0702).

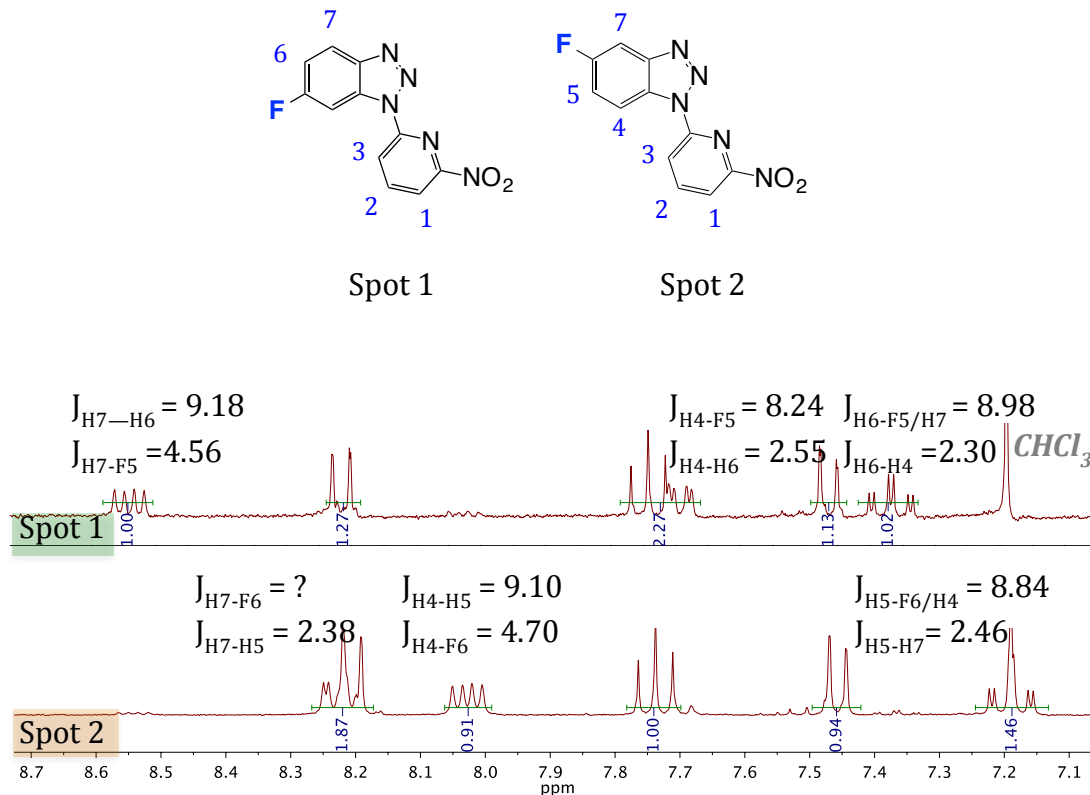


Figure 52: Justification for $^1\text{H-NMR}$ assignment of isomers. Reaction reported by Liu *et al.*, 2010 does not permit formation of isomeric mixture⁵¹. Coupling constants of relevant peaks are highlighted and consistent with isomer assignments.

3. Adduct synthesis

As mentioned previously, the two major pathways for the synthesis of DNA adducts are 1) the biomimetic route and 2) the total synthetic route.

Biomimetic synthesis is a classic approach used to covalently attach bulky aromatic electrophiles to the C-8 position of guanine in single-stranded oligonucleotides. This strategy mimics the biochemical mechanism of adduct formation via reactive N-hydroxyl intermediates (see figures 5 & 10). *In vivo*, amines are partially oxidized to N-hydroxyls by an enzymatic reaction with various CYP isoforms (figure 5). During *in vitro* biomimetic synthesis, amines are oxidized to nitro groups, partially reduced to N-hydroxyls, and reacted with the nucleophilic sites of DNA as in nature (figure 10).

The biomimetic approach is effective only when there is a single guanine present in the oligonucleotide because it can react with any guanine present. Therefore an oligonucleotide with just two guanines will produce three products via the biomimetic route (figure 13). The problem at this point becomes purification of the desired product. Given the size of an oligonucleotide, even bulky modifications make purification a cumbersome effort.

The total synthetic approach is significantly less restrictive but requires more time, equipment, and other resources. In total synthesis, the nucleoside is

modified before incorporation into the oligonucleotide typically requiring several protecting/ deprotecting steps. After the modification is incorporated, the nucleoside needs to be protected for automated solid phase oligonucleotide synthesis (figure 12). While this approach may require as many as 10-15 steps prior to automation, the reactions are quick, robust, and high yielding. Production of the 2-A α C-dG adduct, and its compatibility with the conditions of solid phase DNA synthesis are the major concerns of this route.

The total synthetic route provides greater utility for biophysical analysis. Therefore, establishing a total synthesis for 2-A α C-dG lesions is important for future investigations of this adduct. Furthermore, a biomimetic route has been established previously to produce 2-A α C-dG adducts in low yields and small scales^{17,33}. Authors have reported difficulties in ease of synthesis, reproducibility, and scaling-up. Since biomimetic routes involve fewer steps and less resources than total synthesis, it would best facilitate future investigations of 2-A α C-dG adducts if both routes were viable, thus biomimetic synthesis is included in this project.

3.1 Total Synthetic Route

Solid-phase DNA synthesis is currently the most efficient way to synthesize natural or modified oligonucleotides of any sequence⁵². This technique utilizes nucleosides with both acid and base sensitive protecting groups in order to facilitate selective removal at the appropriate step (Figure 53). As such, choosing the appropriate protecting groups during synthesis of the modified nucleoside may reduce the total number of steps.

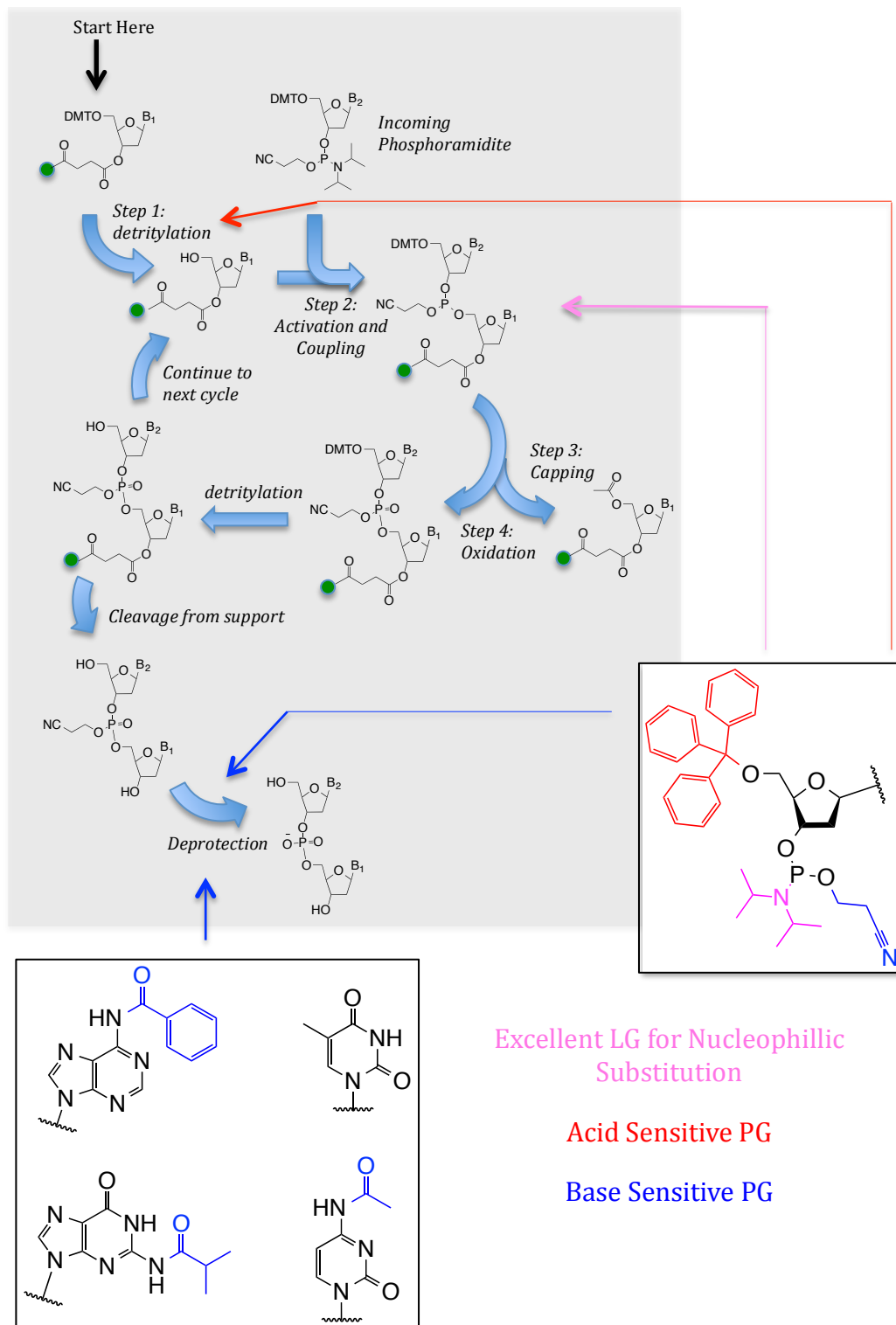


Figure 53: Automated DNA synthesis showing essential functional groups and their role in solid support polymerization.

Nucleoside phosphoramidites have superior yield in automated solid-phase DNA synthesis and have become the standard. Unfortunately, the sensitivity of phosphoramidites to water and air limit the compatibility of the automation step with the conditions necessary for certain nucleoside modifications, thus it is not common to see the same protecting groups in the modification step and the automation step^{48,52}. This creates additional protecting and deprotecting steps to synthesize the modified nucleoside phosphoramidite. Since nucleoside phosphoramidites are the standard in DNA synthesis, many schemes have been developed to covalently attach various aromatic amines at the C8 position of guanosine resulting in desired modified nucleoside phosphoramidite.

The most common strategy is to protect the reactive functional groups on the nucleoside and use a metal-catalyzed coupling technique to attach the bulky modification. The protecting groups are then removed and the new protecting groups for DNA synthesis are added.

Pd-catalyzed Buchwald-Hartwig (BH) reactions between the PAH or HAA and C8-brominated guanosine are often used for the coupling step^{32,53}. Under these conditions, the nucleophilic sites of guanosine must be protected. If possible, one would want to use the same protecting groups used in DNA synthesis, however, the basic conditions of BH coupling are not compatible⁵². Therefore, different protecting groups must be chosen resulting in lengthy

synthetic schemes. Given that these reactions are well established, it is reasonable to test the compatibility of this strategy with 2-A α C.

3.1.1 Preparing dG for Buchwald-Hartwig Coupling

The scheme reported by Gillet and Scharer, 2002 for C8 modification of dG by various aromatic amines was attempted using 2-AαC³². The C8 position of guanosine was brominated and the nucleophilic sites were protected following the general procedure for coupling PAH's or HAA's with guanosine. 2-AF was used as a control reaction. ¹H NMR in DMSO-d₆ was performed on purified products and the spectrum compared to that reported by Gillet and Scharer, 2002³².

Step 5 (figure 54) was not compatible with 2-AαC. Figure 55 shows the ¹H NMR results of the control reaction and matches that of the literature report, confirming technique is adequate. Section 4.1.2 discusses troubleshooting methods used for 2-AαC.

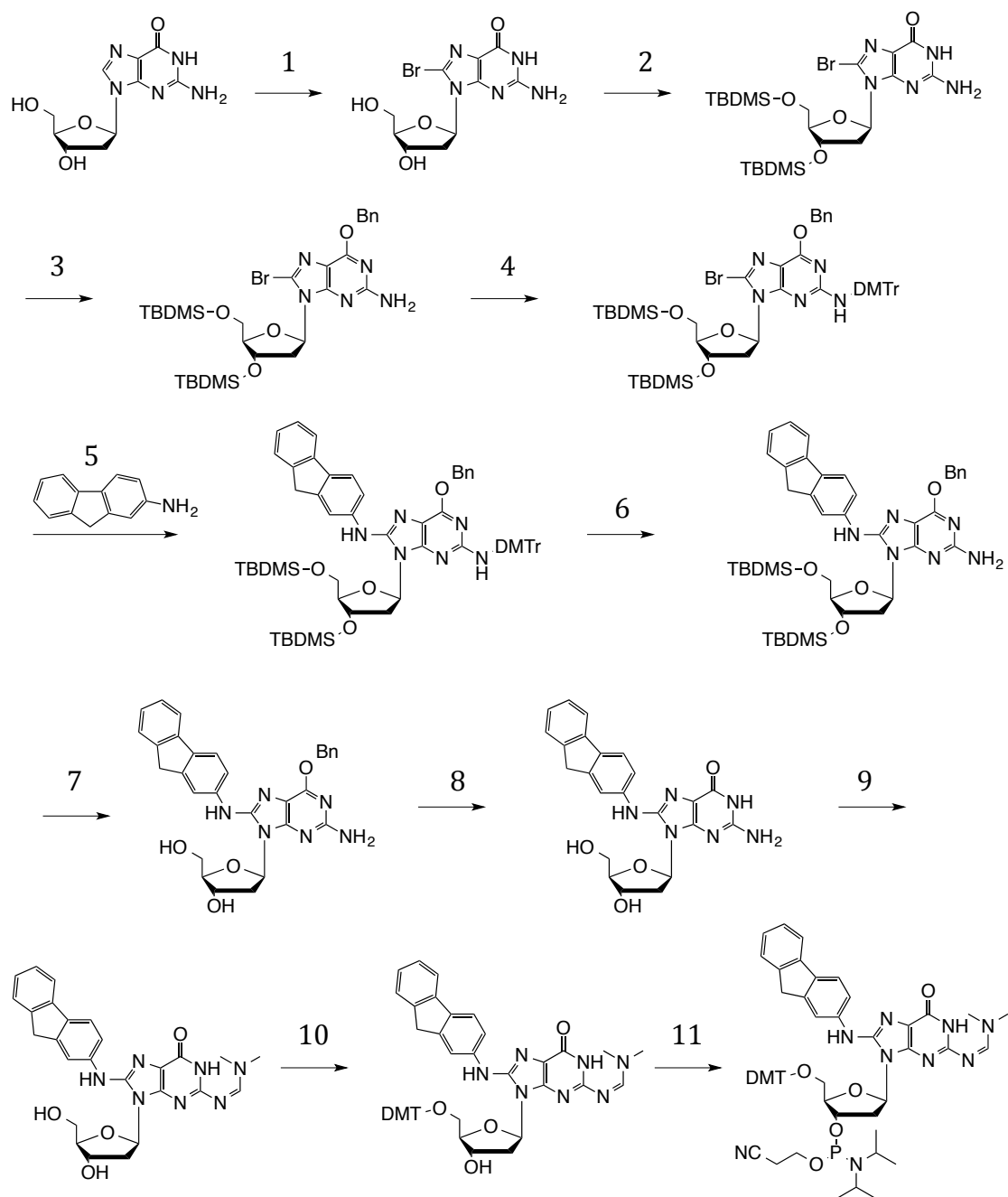
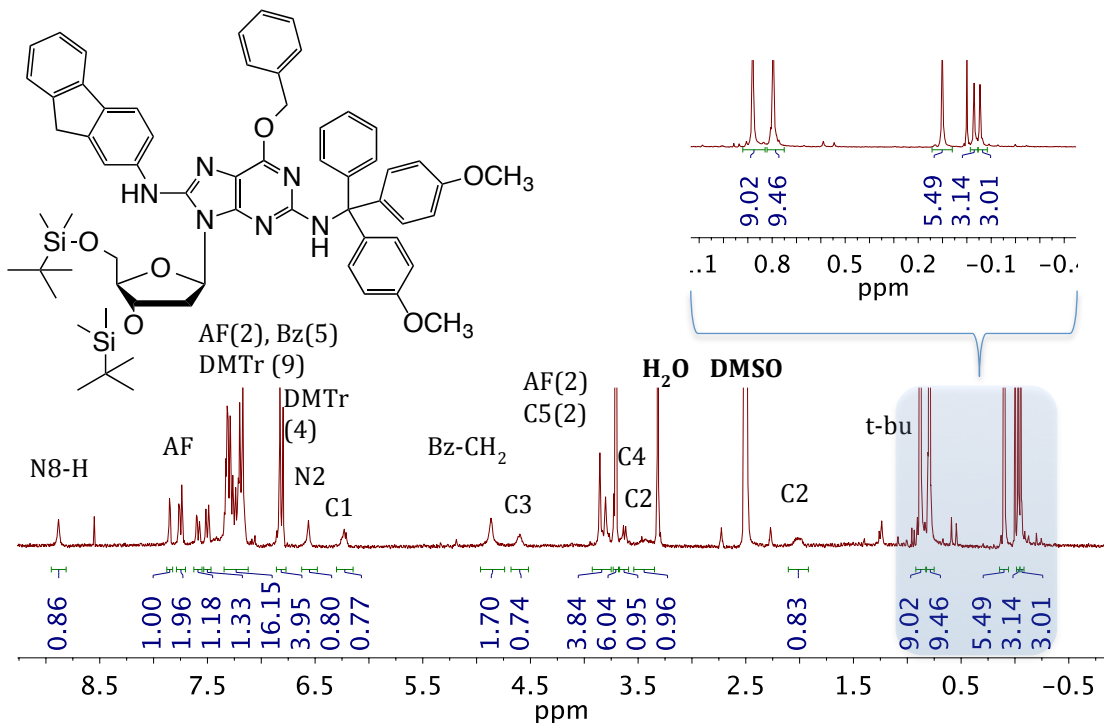
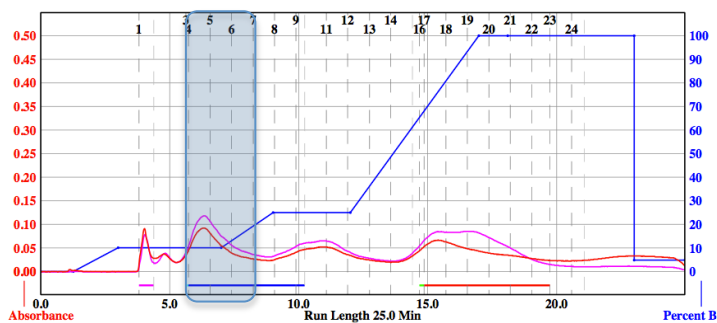
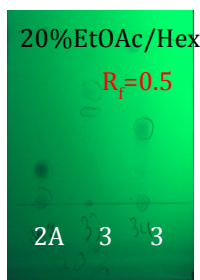
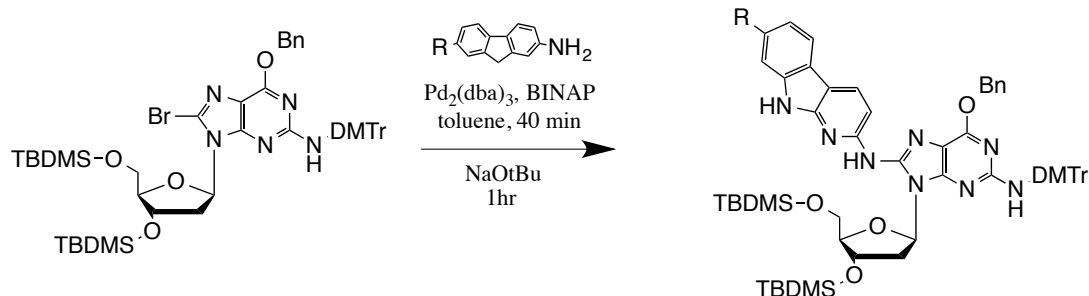


Figure 54: Synthesis of a nucleoside phosphoramidite modified by 2-AF. 1-5 followed the procedure reported by Gillet and Schärer, 2002 for the 2-AF control. Troubleshooting techniques for step 5 using 2-A α C are outlined in section 3.1.2. 6-11 are for illustrative purposes only and represent the complete scheme reported by Gillet and Schärer, 2002³².



¹H NMR (DMSO-d₆) (ppm) 8.85 (s, 1H, N8-H), 7.85 (m, 1H, AF-C1-H), 7.72-7.77 (m, 2H, AF-H2), 7.59 (m, 1H, AF-H), 7.50 (m, 1H, AF-H), 7.12-7.35 (m, 16H, AF-H2+Bz-H5+DMTr-H9), 6.81 (m, 4H, DMTr-H4), 6.53 (s, 1H, N2-H), 6.22 (dd, J=6.7, 6.7, 1H, C1'-H), 4.88 (br s, 2H, Bz-CH₂), 4.60 (m, 1H, C3'-H), 3.76-3.88 (m, 4H, AF-C9-H2+ C5'-H2), 3.71 (s, 6H, 2"OMe), 3.64 (m, 1H, C4'-H), 3.42 (m, 1H, C2'-H), 2.02 (m, 1H, C2'-H), 0.88 (s, 9H, tBu-H), 0.80 (s, 9H, tBu-H), 0.10 (s, 6H, 2"CH₃), -0.03 (s, 3H, CH₃), -0.05 (s, 3H, CH₃)

Figure 55: (A) Purification and (B) Identification by ¹H NMR: dG-C8-2-AF matches that reported by Gillet and Schärer, 2002³².

3.1.2 Troubleshooting the Buchwald-Hartwig Coupling

Coupling of 2-A α C with the protected dG-Br under the reported conditions (step 5) was not successful. The success of the 2-AF control reaction under identical conditions indicates the problem is specific to the 2-A α C starting material. Variables such as solvent, base, co-catalyst ligand, temperature, and length of time were systematically changed to see if the reaction of 2-A α C would proceed.

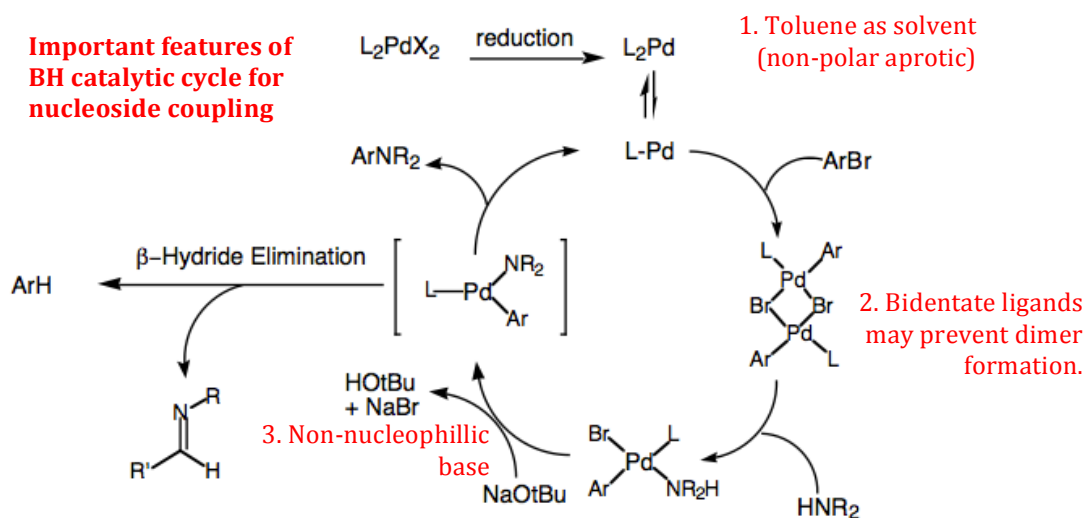


Figure 56: Buchwald Hartwig catalytic cycle with relevant elements for nucleoside synthesis highlighted in red.

Heterocycles often require higher temperatures and longer reaction times during BH coupling due to the retarding effect of undesired Pd-coordination with non-reacting heteroatoms. Being the simplest variable to change, higher

temperatures and longer reaction times were unsuccessfully attempted. As expected, this did not have an impact on product formation, however, degradation of the protected bromoguanosine was observed after 48 hours.

NatBuO⁻ is a strong base and may result in undesired 9H deprotonation of 2-A α C. The predicted pKa of 2-A α C in aqueous solution is approximately 14.5 while the predicted pKa of tBuOH (the conjugate acid of NatBuO⁻) in aqueous solution using the same prediction software is 15.4. Since relative acidity determined from pKa values cannot be compared across solvents, this data does not provide a definitive conclusion regarding 2-A α C ionization under the experimental conditions. ¹H NMR of 2-A α C and NatBuO⁻ in toluene with could reveal the degree of ionization, however, this experiment was not performed.

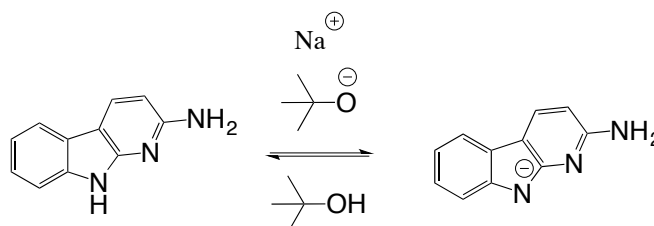


Figure 57: Possible ionization equilibrium of 2-A α C under Buchwald-Hartwig conditions

There are several examples in literature of mildly acidic heterocycles successfully undergoing coupling in these conditions, however, it cannot be known from the available information if ionization is occurring⁵⁴. In the provided literature examples, ¹H NMR experiments were not performed to

determine the extent of ionization in the reaction solvent. Furthermore the effect of ionization on the catalytic cycle is not well understood. Ionization itself may actually have little impact on the catalytic cycle and may be more dependent on the overall electronic configuration.

Since the impact of ionization on the catalytic cycle is not well understood, a wide range of bases was used, all providing the same negative result. Organic bases such as DIPEA and DBU provided low yields of the 2-AF control, and did not produce the product when 2-A α C was used. All experimental reactions were allowed to run for several days with no product formation observed by HPLC. Degradation of the nucleoside SM was observed.

Traditionally, BH coupling of nucleosides is performed in toluene, however, other common aprotic solvents were also screened, including THF and DMF^{32,53,55}. Changing the solvents had no effect on the outcome.

Arguably, the most important variable that can be altered in a BH system is the co-catalyst ligand. The correct choice of ligand is tedious since it is highly specific to the starting material, whereas the previous conditions, while easy to screen, are general.

BINAP is a ligand that has become standard for Pd-catalyzed coupling of nucleosides partly due to its bidentate coordination^{32,53}. This is useful for

heterocyclic coupling since heteroatoms are known to interfere with the Pd-complex and form dimers that disrupt the catalytic cycle (figure 56). The affinity of the heteroatom for the Pd complex, and the stability of the dimer are important factors in the overall impact dimer formation will have on the catalytic cycle. Bidentate ligands are commonly used to sterically hinder access to the Pd center and reduce or eliminate dimer formation.^{54,56}

Given the negative results using BINAP as a co-catalyst and the high chemoselectivity of ligands for the coupling partner, ligands outside the normal scope of BH Pd-catalyzed nucleoside coupling were investigated.

Structural and electronic configurations similar to that of 2-aminopyridine have poor success rates in metal catalyzed coupling. This is likely because they present an extreme example of undesired heteroatom coordination due to the proximity of the heteroatom to the Pd complex. The configuration of 2-A α C presents the same challenge. It is interesting to note that heterocycles with two nitrogen atoms adjacent to the reacting functional group (either the primary amine or the halide) do not have this problem. One could speculate that the coordinating strength of these heteroatoms is reduced as a result of their competing electronegativity, resulting in an even electronic distribution relative to heterocycles with a single heteroatom.

Successful coupling of 2-amino-pyridine like compounds has been reported with BINAP, XantPhos (bidentate ligands), and tBuXPhos (monodentate ligand)⁵⁴. In each attempt, these ligands were unsuccessful at coupling 2-A α C but the control, 2-AF, successfully coupled with its nucleoside partner in various yields.

Changes to the solvent, base, co-catalyst ligand, temperature, and length of time did not produce the desired product. The structural and electronic configuration of 2-A α C is the likely culprit due to various complications it presents. As was already discussed, the proximity of the aromatic heteroatom relative to the reactive amine results in an increased possibility of undesired Pd-coordination. This essentially causes it to act as a bidentate ligand with high affinity for the Pd complex.

Furthermore, the electronic properties that result from the secondary amine in the 9-position and a tertiary aromatic amine in the 2-position raises the possibility of tautomerization that would be unfavorable for BH conditions. The BH ligands that have been tested thus far are used for coupling primary amines, whereas the tautomer is a secondary amine. While the HNMR for 2-A α C does not indicate the presence of the tautomer in question, one cannot be certain the reaction conditions do not alter the thermodynamic stability of the tautomer.

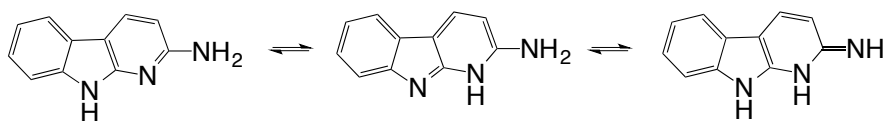


Figure 58: Possible tautomerization of 2-A α C. Secondary amine formation is unfavorable for the BH conditions being utilized.

As was already discussed, deprotonation/ ionization at the 9H position may be responsible for difficulty coupling 2-A α C (figure 57). This is a less likely cause relative to the effects of the electronic and structural configuration because of the range of bases that were tested, and the numerous coupling examples in literature that use starting material with similar acidity to 2-A α C. There is no doubt the problem arises from properties of the secondary amine in the 9-position since the otherwise structurally identical 2-AF is capable of coupling with the nucleoside under many of the conditions that were explored.

3.1.3 *Alternative Plans*

There are many reasonable strategies to further troubleshoot this reaction and total synthesis. Given time constraints and uncertainties associated with further investigating this reaction, we turned our attention to the biomimetic synthesis. Below are alternative plans that were discussed in order to achieve total synthesis if time were to be allocated.

A protecting group may reduce or eliminate effects the 9H proton has on the catalytic cycle. As was already discussed, deprotonation/ ionization itself is not likely a major concern. However, a protecting group could have several effects. First off, the deprotonation at the 9H position increases the possibility of unfavorable 2-A α C tautomers. Furthermore, a bulky protecting group in the 9-position may sterically hinder the 1-position and reduce coordination of the aromatic amine with the Pd complex. Using a bulky protecting group could potentially address several concerns at once. The downside of this approach is the addition of a protecting and deprotecting step to an already lengthy protocol. Ideally, the protecting group could be removed during the same step as another protecting group on the nucleoside.

3.2 Biomimetic Synthesis

It has been shown *in vitro* and *in vivo* that 2aAc is metabolized by CYP isoforms to the N-hydroxyl, converting the amine into a reactive electrophilic intermediate that reacts with the nucleophilic C8 position of guanine^{17,18,21}. Additionally, it undergoes UGT N-glucorination in the liver and is *more* reactive towards the C8 position of guanine than the N-hydroxy intermediate. This biological process can be mimicked to yield the desired C8-2aAc guanine oligonucleotide.

Biomimetic synthesis has been used for decades^{17,33}. It takes advantage of the reactivity of metabolites like the N-hydroxyl intermediate. Similar to the UGT N-glucorination, bulky leaving groups can be added that will increase reactivity and selectivity of the N-hydroxyl. Over time, these leaving groups have been established resulting in successful strategies for biomimetic synthesis summarized in figure 10. Path 2 is the highest yielding and most efficient option for aromatic amines.

3.2.1 Control reaction with 2-fluoro-6-nitro-fluorene

A 100 ml round bottom flask was charged with 300 mg of 2-fluoro-6-nitro-fluorene and a stir bar. The solid was dissolved in 10 mL THF and allowed to stir on ice. To the solution, 200 mg of 5% Pd/C were added. At 0° C, hydrazine was added in 50 μ L increments every 15-20 minutes. After each addition, 100 μ L of the solution was removed and diluted to 1 mL with MeOH and centrifuged for 2 minutes. The sample was analyzed by HPLC on a photodiode array. The reaction was stopped after approximately a 90% reduction in the UV signal of the nitro starting material.

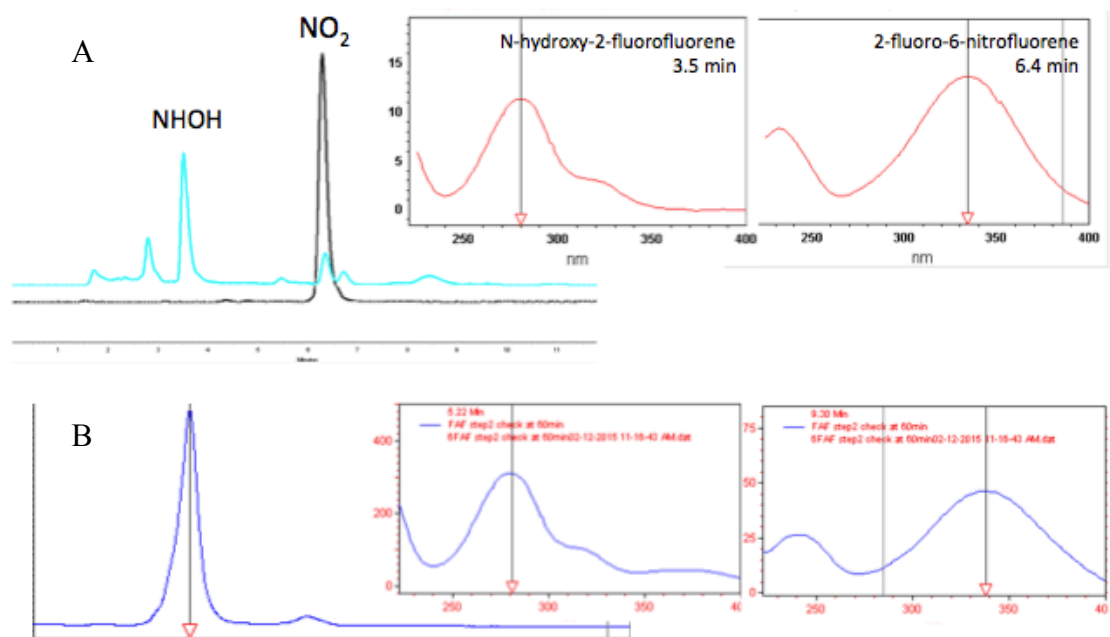


Figure 59: HPLC chromatogram, 70% MeOH in H₂O, isocratic. (A) Partial reduction of 2-FAF to N-hydroxyl-2-fluorofluorene. (B) Comparison of confirmed UV spectra indicate success of the control reaction.

The UV spectra matched previous runs that had been confirmed in the Cho lab (figure 59). Following the established procedure, the N-hydroxyl product was used in the next step of biomimetic synthesis. Figure 60 shows PDA results for each step of the reaction with a comparison to previously confirmed spectra.

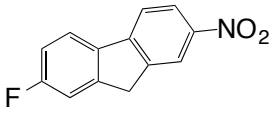
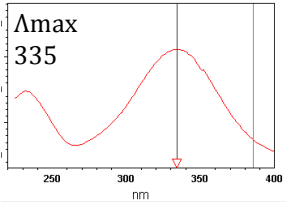
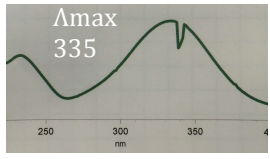
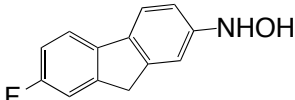
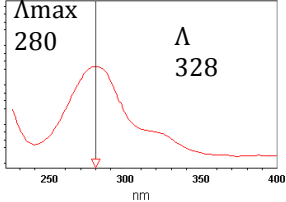
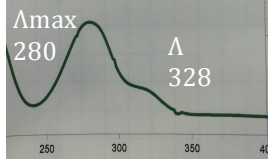
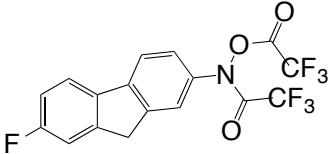
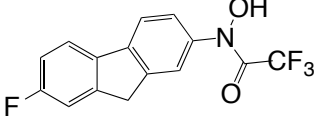
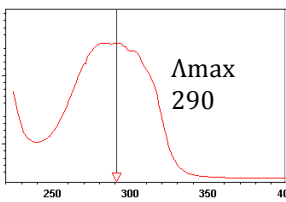
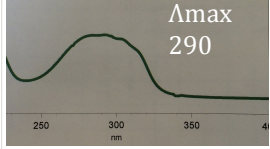
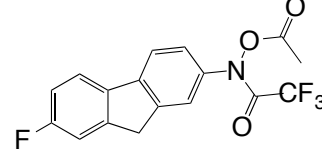
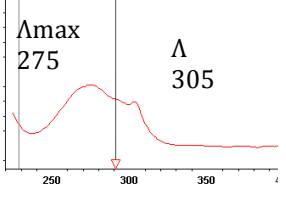
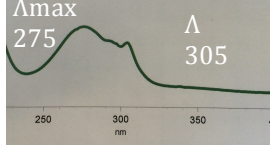
Compound	Retention Time	Measured UV Spectrum	Historical UV Spectrum
 2-fluoro-6-nitrofluorene	6.3 min		
 N-hydroxy-2-fluorofluorene	3.1 min		
 N,N-trifluoroacetyl-2-fluorofluorene		No spectra measured	
 N-trifluoroacetyl-N-hydroxy-2-fluorofluorene	5.7 min		
 N-acetoxy-N-trifluoroacetyl-2-fluorofluorene	8.1 min		

Figure 60: Biomimetic control reaction. Scheme from figure 10, route 2 was executed for 2-AF. PDA UV spectrum was compared to confirmed spectra. According to this data all 2-AF control reactions were successful. Due to the established protocols and UV spectra in the Cho lab, this was the only means of identification.

3.2.2 Results Using 2-AaC

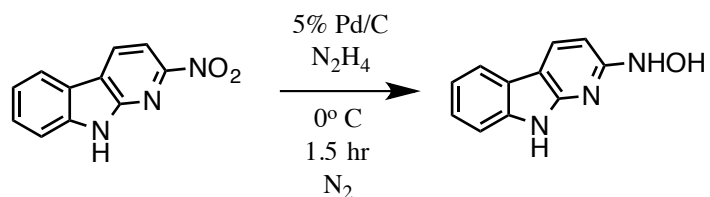


Figure 61: Partial reduction of 2-AaC under identical conditions to the control 2-FAF.

Having demonstrated proper technique for the partial reduction, attempts were made using 2-NaC. The established conditions for 2-fluoro-6-nitro-fluorene were not compatible with 2-NaC as shown by the representative HPLC chromatogram in figure 62.

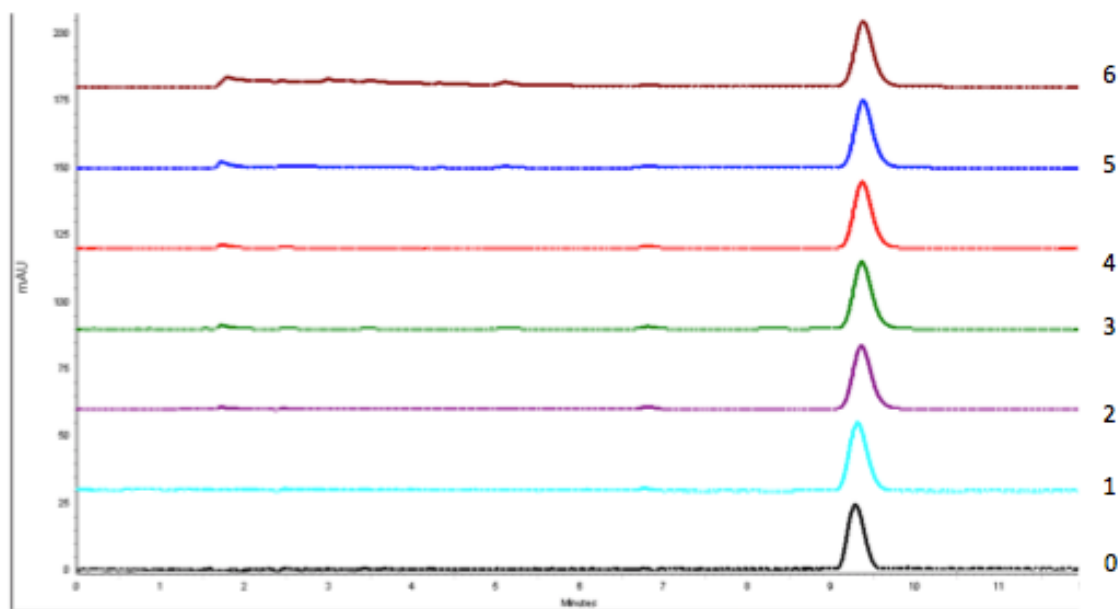


Figure 62: Chromatogram from partial reduction of 2-AaC. No product formation. Time point 0, before addition of hydrazine. Time point (1-4) 15 minute intervals. Time point 5 +2 hours, time point 6, +24 hours at RT. Excess hydrazine added.

Novak *et al.* reported the partial reduction of 2-AxC and noted sensitivity to air, moisture, and peroxides that are not as pervasive in the fluorene model³³. The conditions were modified to accommodate more sensitive reagents.

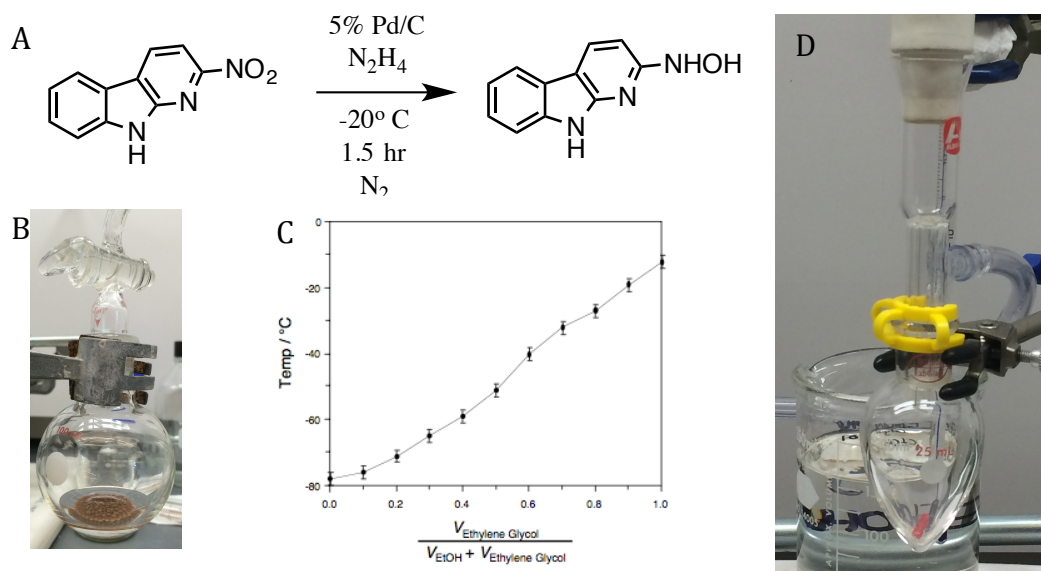


Figure 63: Adjustments made based on Novak's model. Explanations in text.

Fresh, commercially available, anhydrous THF was degassed and treated with heat-activated 4Å molecular sieves under N₂ for 2.5 hours (figure 63 B). An ethylene glycol/EtOH bath was used in combination with dry ice to manipulate the temperature from -20° C to 0° C during the reaction (figure 63 C). 2-NaC was added to a 25 mL pear bottom and fitted with an adaptor and septum as shown in figure 63 D. The system was vacuumed and backfilled with N₂ three times. THF was added through a syringe and 2-NaC was dissolved. The pear bottom was placed in the ethylene glycol/EtOH dry ice bath and the temperature was monitored to -20° C. The septum was removed under a

steady stream of N₂, 5% Pd/C was added to the flask, and the septum was immediately replaced. Hydrazine was added as a mixture with THF, and a sample was removed for HPLC analysis by a glass syringe with an 8-inch needle. After 5 hours no change occurred.

Despite the structural similarities of 2-AF and 2-AαC, 2-fluoro-6-nitro-fluorene undergoes the partial reduction and subsequent biomimetic reactions, whereas 2-NαC does not. The endocyclic amines of 2-NαC drastically alter the electronic configuration within the structure compared to 2-fluoro-6-nitro-fluorene and can effect redox reactions. Ionization of the 9H proton and tautomerization of 2-NαC are also potential obstacles for the reduction in hydrazine. Coordination with Pd/C is also a possibility given the position of the 1-N relative to the 2-NO₂ site being reduced to the N-hydroxyl.

4. Experimental

In Section 2, new compounds were created, and shorter routes to synthesize old compounds were established. Figure 31 outlines the synthetic plan and provides an overview of the scheme. Execution of the plan was described in the text, however, figure 64 summarizes what compounds were successfully synthesized and what compounds are new. This section will provide further experimental details on compounds that are new or were synthesized using a new strategy.

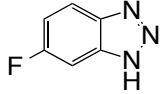
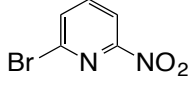
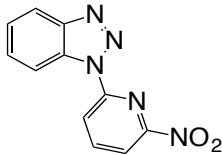
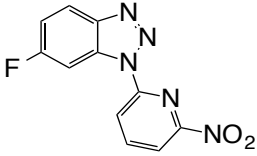
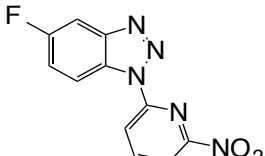
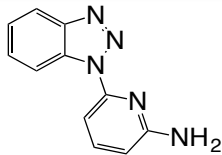
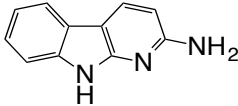
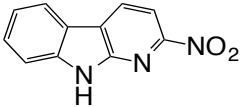
Compound	Name	New Compound
	6-fluorobenzotriazole	N/A
	2-bromo-6-nitropyridine	N/A
	6-(1 <i>H</i> -benzotriazol-1-yl)-2-nitropyridine	New
	6-(6-fluoro-1 <i>H</i> -benzotriazol-1-yl)-2-nitropyridine	New
	6-(5-fluoro-1 <i>H</i> -benzotriazol-1-yl)-2-nitropyridine	New
	6-(1 <i>H</i> -benzotriazol-1-yl)-2-aminopyridine	N/A ^a
	2-amino-9 <i>H</i> -pyrido[2,3- <i>b</i>]indole (2-AαC)	N/A ^b
	2-nitro-9 <i>H</i> -pyrido[2,3- <i>b</i>]indole (2-NαC)	N/A ^c

Figure 64: Compounds synthesized in the triazole route. New compounds are indicated as such. (a, b) First report for synthesis of 2-7a and 1-4a via proposed route. . (c) First known report of 1-5a *not* via oxidation of 1-4a.

6-(1*H*-benzotriazol-1-yl)-2-nitropyridine

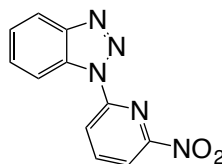


Figure 65: (2-5a)

An oven-dried 50 mL round bottom flask with a small stir-bar was charged with 300 mg of benzotriazole (2.51 mmol), 614 mg of 2-bromo-6-nitropyridine (3.01 mmol), 24 mg CuI (0.13 mmol, 5 mol%), and 1.11g K₃PO₄ (5.27 mmol). The round bottom was sealed using a rubber septum. Air was removed using a vacuum syringe and replaced with N₂ (repeated three times). A balloon filled with N₂ connected to a syringe was left in the septum. 27 μ L of N,N'-dimethylethylenediamine (22 mg, 0.25 mmol) and 2 mL of DMF were mixed in a small Erlenmeyer flask, taken up into an airtight syringe, and injected into the reaction flask. The round bottom was placed in a pre-heated oil bath at 90°C and stirred for 24 hours.

R_f 0.63 in 20% EtOAc/hexane. The crude product was purified by column chromatography on a silica stationary phase and a step-wise gradient of EtOAc/hexane. The gradient started at 0% EtOAc and increased in increments of 5% EtOAc until each spot eluted. Separation was monitored by TLC (figure 33). The mobile phase containing the purified product was evaporated and the

product transferred to an oven-dried 50 mL round bottom flask. Approximately 3-5 mg was taken for NMR and the round bottom was wrapped in aluminum foil (light protection) and left on a vacuum for 4 hours. 280 mg (1.16 mmol) of 2-5a was recovered, providing a 46% yield.

^1H NMR and ^{13}C NMR in CDCl_3 are consistent with desired product. To fully characterize this compound, MS is needed.

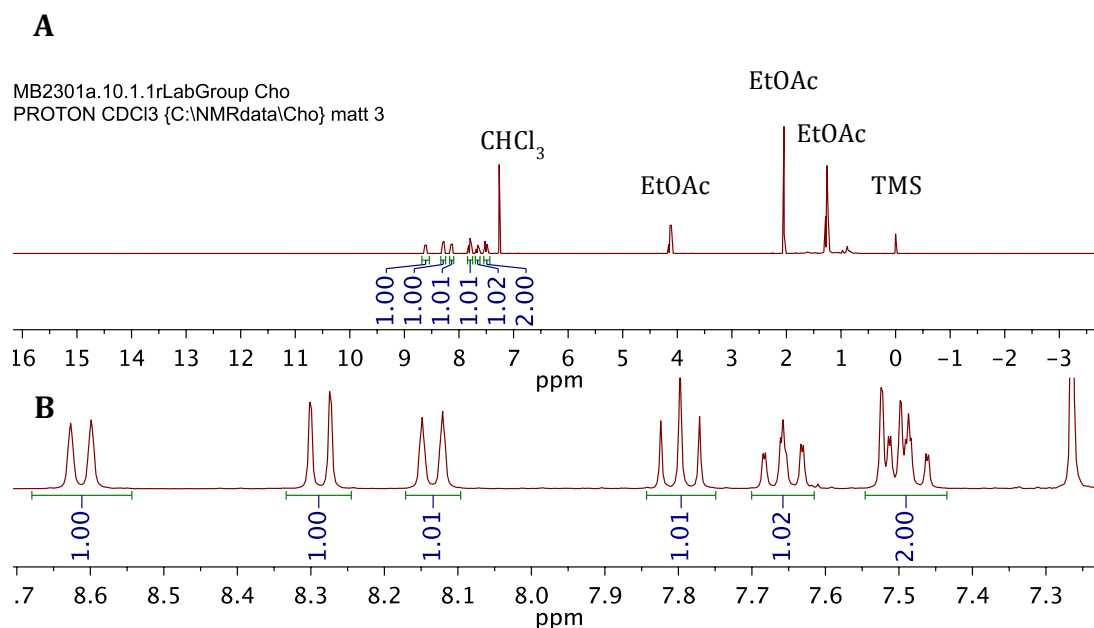


Figure 66: ^1H NMR in CDCl_3 δ (ppm), J (Hz) 8.61 (1H, d, J= 8.71), 8.29 (1H, d, J= 9.24), 8.13 (1H, d, J= 8.19), 7.79 (1H, t, J= 7.91), 7.66 (1H, td, J= 8.21, 1.14), 7.51 (1H, d, J= 7.91), 7.49 (1H, td, J= 8.15, 0.90). Ethyl Acetate (EtOAc) impurity, NMR solvent (CHCl_3), and TMS are identified in the spectrum.

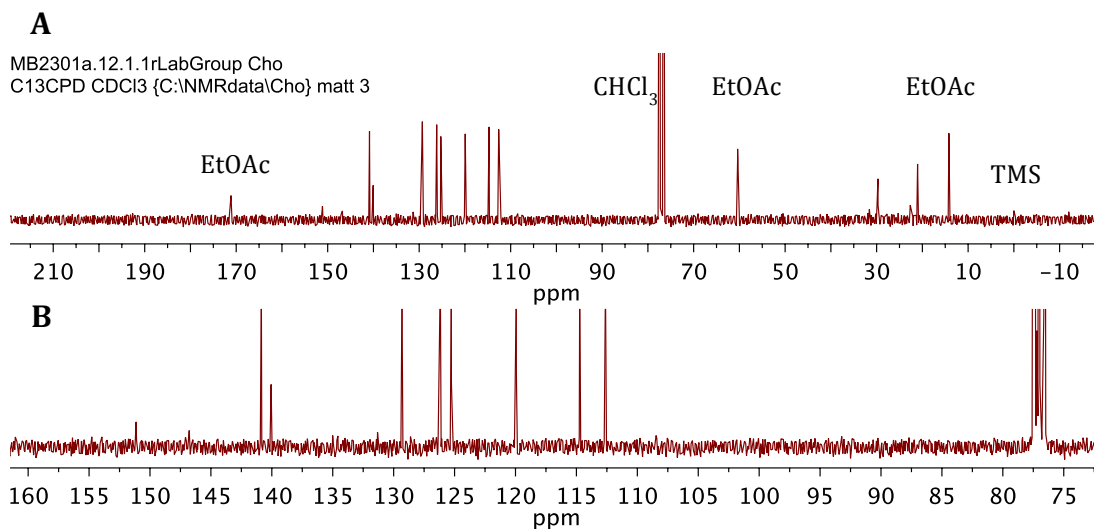


Figure 67: ¹³C NMR in CDCl₃ δ (ppm) 151.08 (1C), 146.73 (1C), 140.82 (1C), 139.98 (1C), 131.27 (1C), 129.28 (1C), 126.20 (1C), 125.22 (1C), 119.74 (1C), 114.66 (1C), 112.42 (1C). Ethyl Acetate (EtOAc) impurity, NMR solvent (CHCl₃), and TMS are identified in the spectrum.

A Medium Pressure Liquid Chromatography (MPLC) method was developed on CombiFlash to better facilitate scaling up (figure 33).

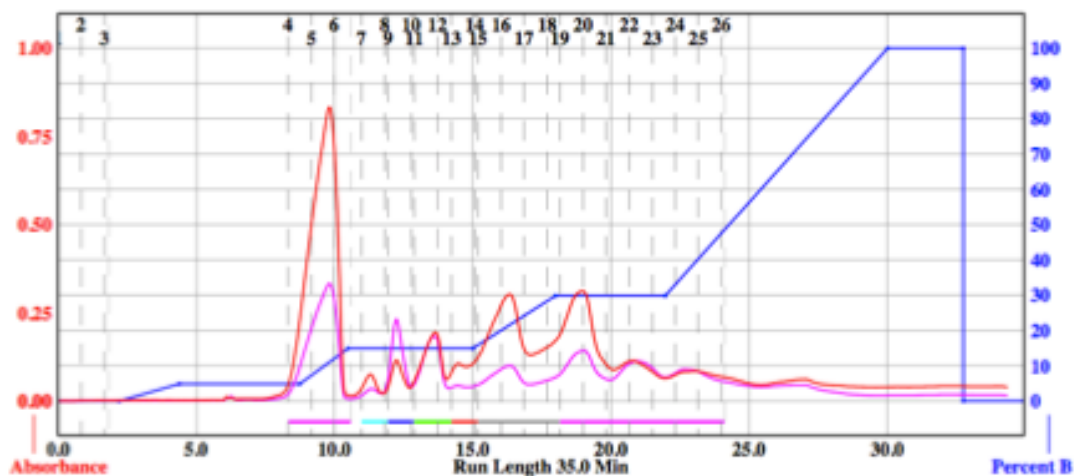


Figure 68: Normal phase MPLC chromatogram for reaction c. Gradient is EtOAc (%B) in hexane shown as a blue line. Red line = absorption at 260 nm. Purple line = absorption at 260 nm. The desired product (2-5a) is the major peak and elutes from 9-10 min

2-nitro-9H-pyrido[2,3-b]indole, (2-nitro- α -carboline, 2-N α C)

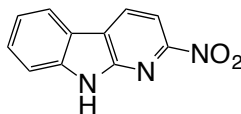


Figure 69: 1-5a

To the 50 mL round bottom flask containing 50 mg (0.207 mmol) of 2-(1*H*-benzotriazol-1-yl)-6-nitropyridine (2-5a) was added 700 mg of Polyphosphoric acid (PPA) using a glass stir rod. The round bottom flask was placed in a preheated oil bath at 180°C. The reaction mixture turns from transparent/colorless to light brown. Bubbles can be observed until the reaction is complete (approximately 30 minutes). If starting material is stuck to the sides of the round bottom flask, the flask can be rotated so the solid is dissolved in PPA. Bubbles can again be observed until the reaction is complete (this can be performed as soon as the PPA is viscous enough to move around the flask; there is no need to wait until completion).

The crude mixture was cooled at room temperature, diluted with water, and neutralized to pH 7 with 1M NaOH. For the purpose of solubility, water was added before the PPA reached room temperature. Product was extracted with ether several times until aqueous layer did not show absorbance on TLC plates with 254nm indicator. $R_f = 0.62$ in 20% EtOAc/Hexane on silica TLC plates. The crude product was purified by column chromatography in a glass

column with a neutral alumina stationary phase and an isocratic mobile phase of 15% EtOAc/ hexane. 22 mg (0.103 mmol) of product (1-5a) was recovered providing a 49.8% yield.

^1H NMR in Acetone- d_6 is consistent with desired product. To fully characterize this compound, MS and ^{13}C NMR are needed.

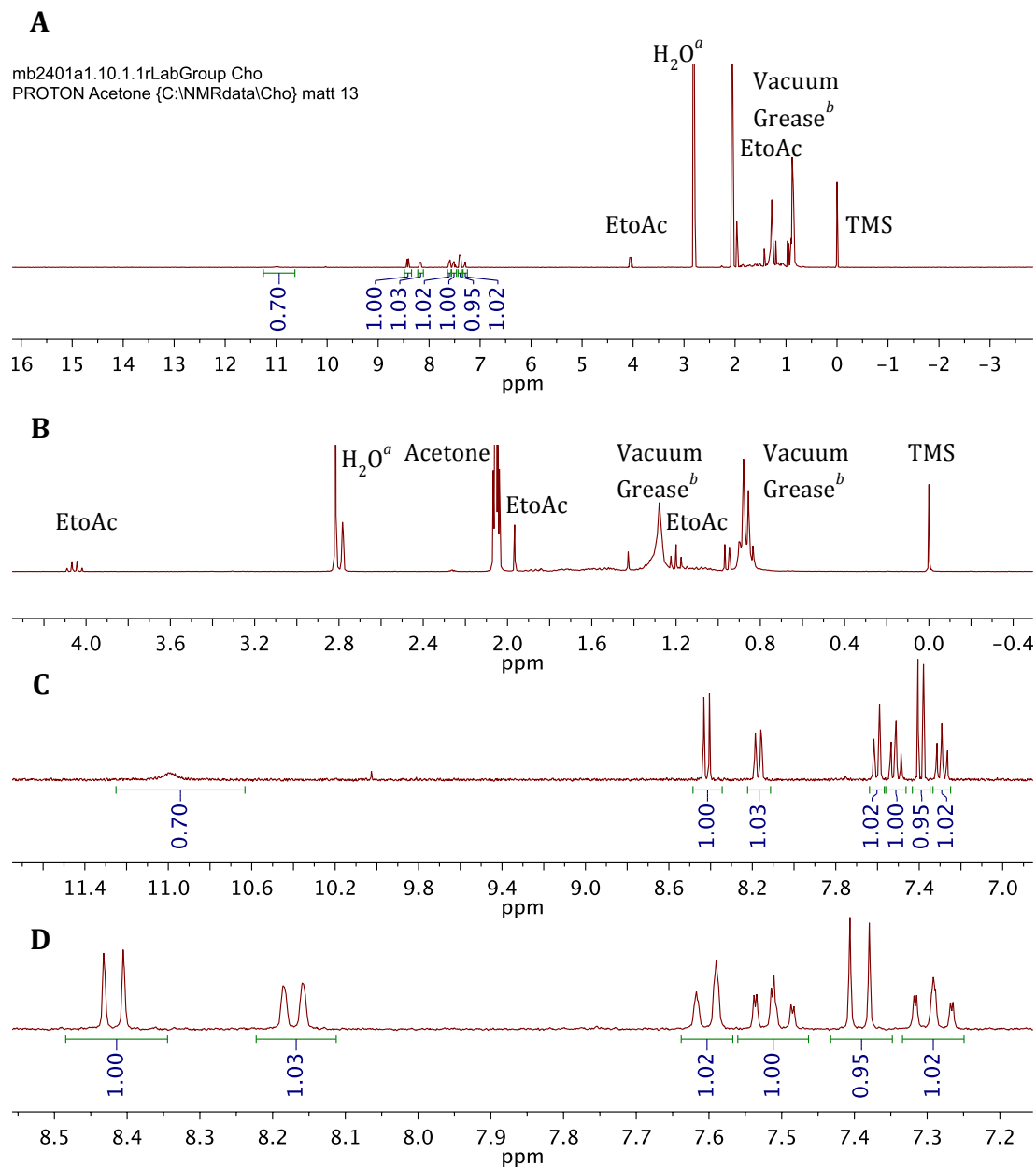


Figure 70: ^1H NMR in Acetone- d_6 δ (ppm), J (Hz) 8.42 (1H, d, J= 8.01), 8.17 (1H, d, J= 7.74), 7.60 (1H, d, J= 8.01), 7.51 (1H, td, J= 7.48, 1.21), 7.39 (1H, d, J= 8.01), 7.29 (1H, td, J=7.74, 1.06). Ethyl Acetate (EtOAc) impurity, NMR solvent (Acetone- d_6), vacuum grease, and TMS are identified in the spectrum.

6-(1H-benzotriazol-1-yl)-2-aminopyridine

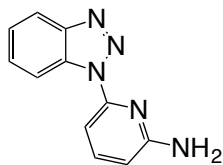


Figure 71: 2-7a

The same procedure was followed as for 2-(1*H*-benzotriazol-1-yl)-6-nitropyridine using appropriately scaled stoichiometric ratios except the reaction is ran for 48 hours due to the retarding effect the primary amine has on Cu coordination. The similarity in R_f values between 2-amino-6-bromopyridine and the desired product, 6-(1*H*-benzotriazol-1-yl)-2-aminopyridine, can make purification tedious. Changing 2-amino-6-bromopyridine to the limiting reagent (previously benzotriazole) simplifies purification. Coupling of 2-amino-6-bromopyridine (2-3) resulted in moderate yields (20%) compared to the nitro starting material (2-4), presumably due to complications caused by the primary amine.

^1H NMR in CDCl_3 is consistent with the desired product. To fully characterize this compound, MS and ^{13}C NMR are needed.

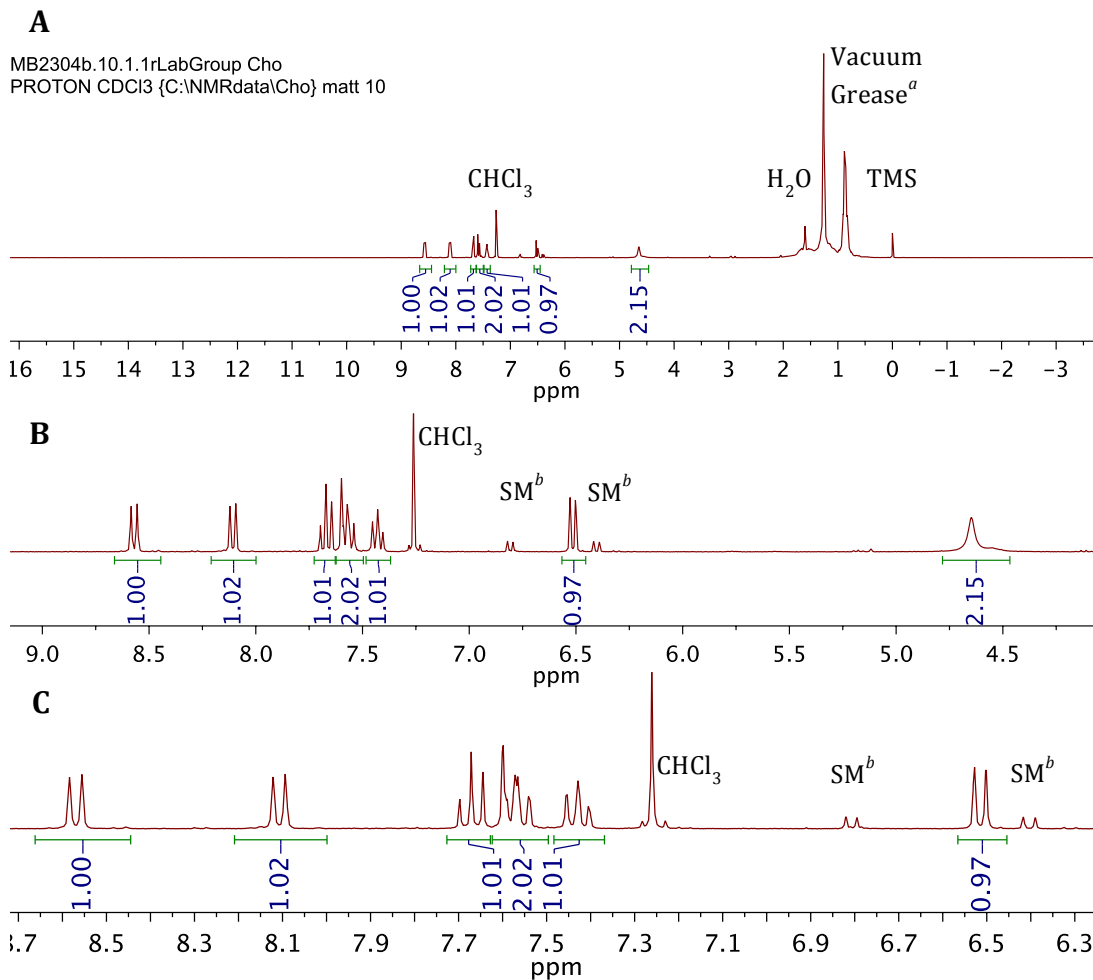


Figure 72 ¹H NMR in CDCl₃ δ (ppm), J (Hz) 8.57 (1H, d, J= 8.31), 8.11 (1H, d, J= 8.31), 7.66 (1H, t, J= 7.90), 7.58 (1H, d), 7.56 (1H, td, J= 8.75, 1.33), 7.42 (1H, td, J=7.40, 0.90) 6.52 (1H, d, J= 7.90), 4.67 (2H, s). NMR solvent (CDCl₃), vacuum grease, and TMS are identified in the spectrum.

An MPLC method was developed for CombiFlash on a neutral alumina column to facilitate scaling up. A representative chromatogram is shown in figure 44.

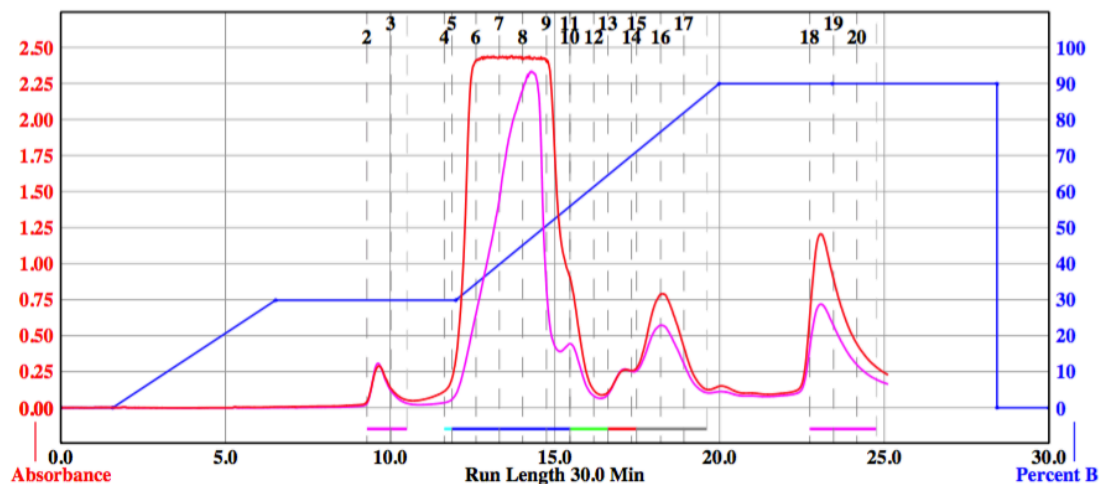


Figure 73: Normal phase MPLC chromatogram for reaction c to produce 2-7a. Gradient is EtOAc (%B) in hexane shown as a blue line. Red line = absorption at 260 nm. Purple line = absorption at 260 nm. The desired product (2-7a) is the major peak and elutes from 12-16 min.

2-amino-9H-pyrido[2,3-b]indole, (2-amino- α -carboline, 2-A α C)

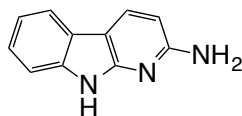


Figure 74: (1-4a)

The same procedure was followed as for 2-nitro-9H-pyrido[2,3-b]indole, (2-nitro- α -carboline, 2-N α C) using appropriately scaled ratios. The Turesky group at the University of Minnesota Cancer Center provided a reliable 2-A α C standard for analysis. TLC was performed at various proportions of EtOAc/Hexane in comparison with the product and standard. R_f values and co-spot tests support production of the desired product. Cyclization of 2-7a resulted in

moderate yields (15%) compared to the nitro starting material (2-5a), presumably due to complications caused by the primary amine.

6-(5-fluoro-1*H*-benzotriazol-1-yl)-2-nitropyridine

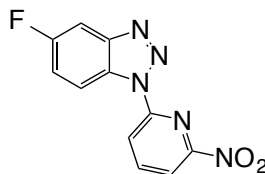


Figure 75: (2-5c)

The same procedure was followed as for 2-(1*H*-benzotriazol-1-yl)-6-nitropyridine using appropriately scaled stoichiometric ratios. Benzotriazole was replaced by 6-fluorobenzotriazole. The reaction produced an isomeric mixture of 6-(5-fluoro-1*H*-benzotriazol-1-yl)-2-aminopyridine and 6-(6-fluoro-1*H*-benzotriazol-1-yl)-2-aminopyridine. The isomers purified by column chromatography on silica gel in a stepwise gradient of EtOAc/Hexane starting at 0% EtOAc increasing in 5% increments. Separation was monitored by TLC. ¹H NMR was initially performed in DMSO-*d*₆. To fully characterize this compound, MS and ¹³C NMR are needed. Yield was not recorded for the fluorinated analogs.

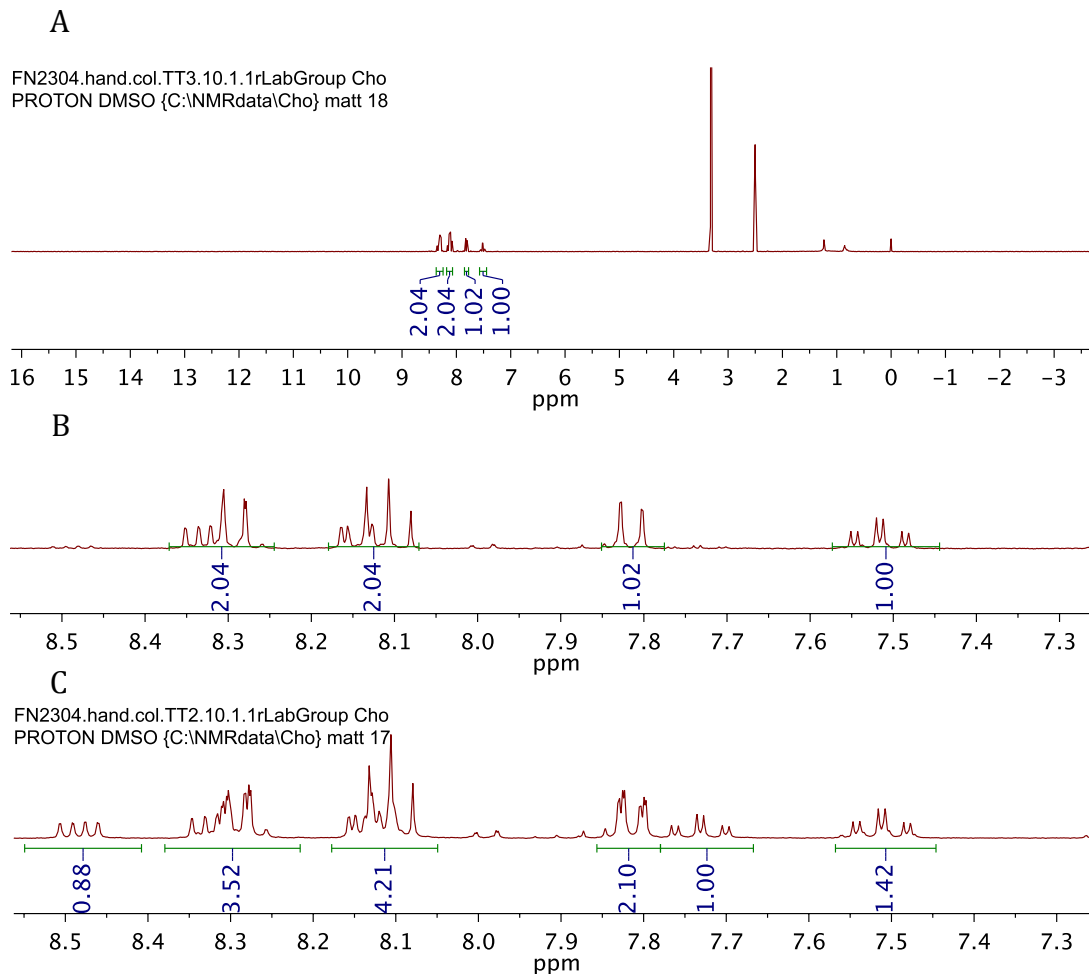


Figure 76: ^1H NMR in DMSO-d_6 δ (ppm) 8.34 (1H, m), 8.29 (1H, d), 8.15 (1H, dd), 8.10 (1H, t), 7.81 (1H, d), 7.51 (1H, dt). Coupling constants are measured in CDCl_3 and explained in section 2. H_2O , NMR solvent (DMSO-d_6), vacuum grease, and TMS are present in the spectrum. (A) Full spectrum, (B) aromatic region, (C) mixture of 2-5b and 2-5c

6-(6-fluoro-1H-benzotriazol-1-yl)-2-nitropyridine

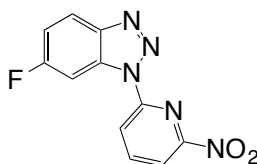
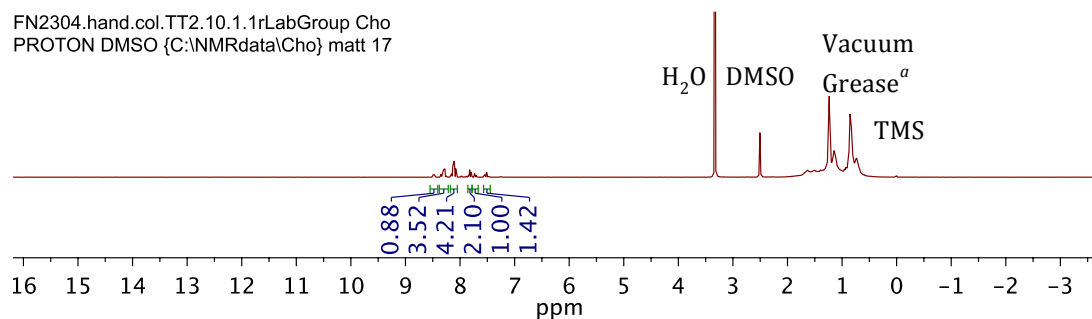


Figure 77: 2-5b

Created simultaneously with 6-(5-fluoro-1*H*-benzotriazol-1-yl)-2-nitropyridine and assessed in the same manner. To fully characterize this compound, MS and ¹³C NMR are needed. Yield was not recorded for the fluorinated analogs.

FN2304.hand.col.TT2.10.1.1rLabGroup Cho
PROTON DMSO {C:\NMRdata\Cho} matt 17



FN2304.hand.col.TT1.10.1.1rLabGroup Cho
PROTON DMSO {C:\NMRdata\Cho} matt 16

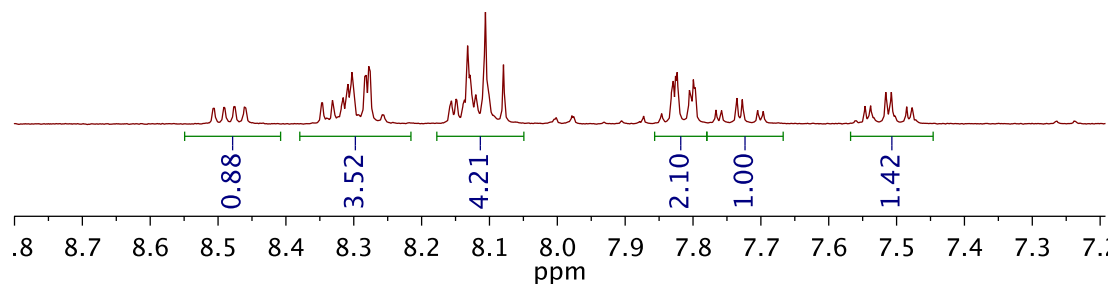
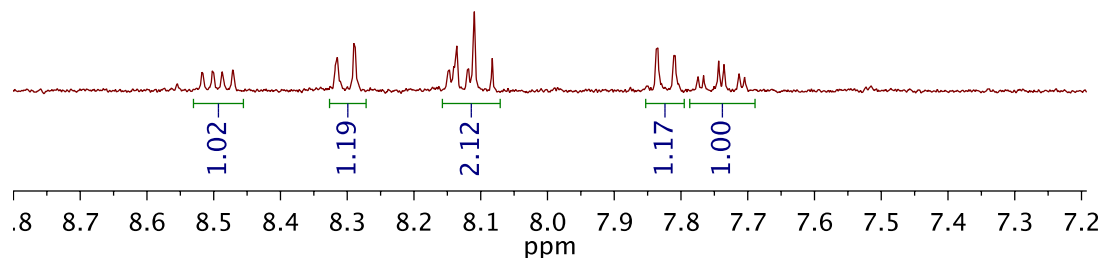
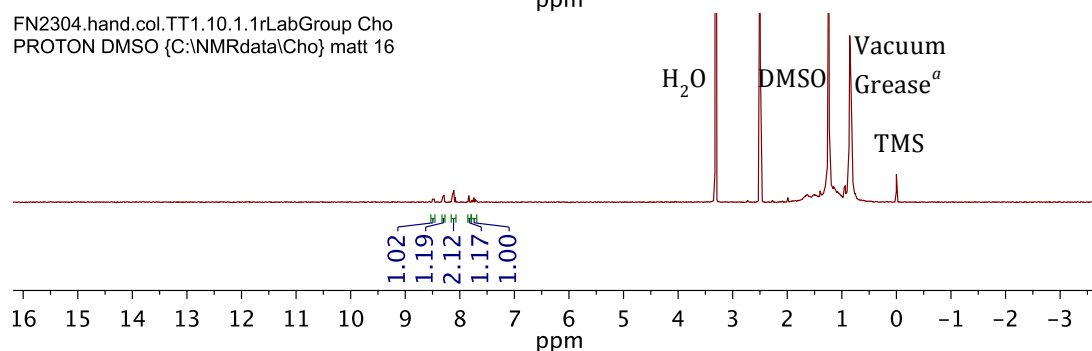


Figure 78: ^1H NMR in DMSO-d_6 δ (ppm) 8.50 (1-H, dd), 8.30 (1H, d), 8.12 (1H, d), 8.11 (1H, t), 7.82 (1H, d), 7.74 (1H td). Coupling constants are measured in CDCl_3 and explained in section 2. H_2O , NMR solvent (DMSO-d_6), vacuum grease, and TMS are present in the spectrum. Full spectrum, aromatic region, and an isomeric mixture of 2-5b and 2-5c are shown.

Bibliography

1. Carol Bernstein, Anil R. Prasad, Valentine Nfonsam, Harris Bernstein. DNA Damage, DNA Repair and Cancer. In: ; N1 43929 UR <http://www.intechopen.com/books/export/citation/ReferenceManager/new-research-directions-in-dna-repair/dna-damage-dna-repair-and-cancer>.
2. De Bont R, van Larebeke N. Endogenous DNA damage in humans: a review of quantitative data. *Mutagenesis* 2004;19(3):169-185.
3. Kelley MR. Chapter 1 - Introduction and Overview of DNA Repair Targets: From Bench to Clinic. In: Kelley MR, ed. *DNA Repair in Cancer Therapy*. San Diego: Academic Press; 2012:1-16.
4. Sancar A, Lindsey-Boltz LA, Ünsal-Kaçmaz K, Linn S. Molecular Mechanisms of Mammalian DNA Repair and the DNA Damage Checkpoints. *Annu. Rev. Biochem.* 2004;73(1):39-85.
5. Marteijn JA, Lans H, Vermeulen W, Hoeijmakers JHJ. Understanding nucleotide excision repair and its roles in cancer and ageing. *Nat Rev Mol Cell Biol* 2014;15(7):465-481.
6. Turchi JJ, Patrick SM. Chapter 6 - Targeting the Nucleotide Excision Repair Pathway for Therapeutic Applications. In: Kelley MR, ed. *DNA Repair in Cancer Therapy*. San Diego: Academic Press; 2012:109-117.
7. Cho BP. Dynamic conformational heterogeneities of carcinogen-DNA adducts and their mutagenic relevance. *J. Environ. Sci. Health, Part C: Environ. Carcinog. Ecotoxicol. Rev.* 2004:57-90.
8. Veglia F, Matullo G, Vineis P. Bulky DNA Adducts and Risk of Cancer A Meta-Analysis. *Cancer Epidemiology Biomarkers & Prevention* 2003;12(2):157-160.
9. Hemminki K. DNA adducts, mutations and cancer. *Carcinogenesis* 1993;14(10):2007-2012.
10. Benigni R, Bossa C. Mechanisms of chemical carcinogenicity and mutagenicity: a review with implications for predictive toxicology. *Chem. Rev* 2011; 111 (4): 2507-2536.
11. Nebert DW, Bigelow SW, Okey AB, Yahagi T, Mori Y, Nagao M, Sugimura T. Pyrolysis products from amino acids and protein: Highest mutagenicity requires cytochrome P1-450. *Proceedings of the National Academy of Sciences* 1979; 76 (11): 5929-5933.
12. Garbett NC, Chaires JB. Thermodynamic studies for drug design and screening. *Expert opinion on drug discovery* 2012;7(4):299-314.

13. Liang F, Meneni S, Cho BP. Induced circular dichroism characteristics as conformational probes for carcinogenic aminofluorene-DNA adducts. *Chemical research in toxicology* 2006;19(8):1040–1043.
14. Meneni S, Shell SM, Zou Y, Cho BP. Conformation-specific recognition of carcinogen-DNA adduct in Escherichia coli nucleotide excision repair. *Chemical research in toxicology* 2007;20(1):6–10.
15. Vaidyanathan VG, Liang F, Beard WA, Shock DD, Wilson SH, Cho BP. Insights into the Conformation of Aminofluorene-Deoxyguanine Adduct in a DNA Polymerase Active Site. *Journal of Biological Chemistry* 2013;288(32):23573–23585.
16. Liang F, Cho BP. Probing the thermodynamics of aminofluorene-induced translesion DNA synthesis by differential scanning calorimetry. *Journal of the American Chemical Society* 2007;129(40):12108–12109.
17. King RS, Teitel CH, Kadlubar FF. In vitro bioactivation of N-hydroxy-2-amino- α -carboline. *Carcinogenesis* 2000;21:1347-1354.
18. Nauwelaers G, Bessette EE, Gu D, Tang Y-J, Rageul J, Fessard V, Yuan J-M, Yu MC, Langouet S, Turesky RJ. DNA Adduct Formation of 4-Aminobiphenyl and Heterocyclic Aromatic Amines in Human Hepatocytes. *Chem. Res. Toxicol.* 2011;24:913-925.
19. Tang Y, Kassie F, Qian X, Ansha B, Turesky RJ. DNA Adduct Formation of 2-Amino-9H-pyrido[2,3-b]indole and 2-Amino-3,4-dimethylimidazo[4,5-f]quinoline in Mouse Liver and Extrahepatic Tissues During a Subchronic Feeding Study. *Toxicol. Sci.* 2013;133:248-258.
20. Tang Y, LeMaster DM, Nauwelaers G, Gu D, Langouet S, Turesky RJ. UDP-Glucuronosyltransferase-mediated Metabolic Activation of the Tobacco Carcinogen 2-Amino-9H-pyrido[2,3-b]indole. *J. Biol. Chem.* 2012;287:14960-14972.
21. Turesky RJ, Yuan J-M, Wang R, Peterson S, Yu MC. Tobacco smoking and urinary levels of 2-amino-9H-pyrido[2,3-b]indole in men of Shanghai, China. *Cancer Epidemiol., Biomarkers Prev.* 2007;16:1554-1560.
22. Luo R, Gilson HS, Potter MJ, Gilson MK. The physical basis of nucleic acid base stacking in water. *Biophysical journal* 2001;80(1):140–148.
23. Cockroft SL, Hunter CA, Lawson KR, Perkins J, Urch CJ. Electrostatic control of aromatic stacking interactions. *Journal of the American Chemical Society* 2005;127(24):8594–8595.

24. Cockroft SL, Perkins J, Zonta C, Adams H, Spey SE, Low CM, Vinter JG, Lawson KR, Urch CJ, Hunter CA. Substituent effects on aromatic stacking interactions. *Organic & biomolecular chemistry* 2007;5(7):1062–1080.
25. Guin M, Patwari GN, Karthikeyan S, Kim KS. Do N-heterocyclic aromatic rings prefer π -stacking? *Physical Chemistry Chemical Physics* 2011;13(13):5514–5525.
26. Meneni SR, D’Mello R, Norigian G, Baker G, Gao L, Chiarelli MP, Cho BP. Sequence effects of aminofluorene-modified DNA duplexes: thermodynamic and circular dichroism properties. *Nucleic acids research* 2006;34(2):755–763.
27. Li P, Zhao C, Smith MD, Shimizu KD. Comprehensive Experimental Study of N-Heterocyclic π -Stacking Interactions of Neutral and Cationic Pyridines. *The Journal of organic chemistry* 2013;78(11):5303–5313.
28. Nauwelaers G, Bessette EE, Gu D, Tang Y, Rageul J, Fessard V, Yuan J-M, Yu MC, Langouët S, Turesky RJ. DNA adduct formation of 4-aminobiphenyl and heterocyclic aromatic amines in human hepatocytes. *Chemical research in toxicology* 2011;24(6):913–925.
29. Cho B, Zhou L. Probing the conformational heterogeneity of the acetylaminofluorene-modified 2'-deoxyguanosine and DNA by 19F NMR spectroscopy. *Biochemistry* 1999;38(23):7572—7583.
30. Meneni SR, Shell SM, Gao L, Jurecka P, Wang L, Sponer J, Zou Y, Chiarelli MP, Cho BP. Spectroscopic and Theoretical Insights into Sequence Effects of Aminofluorene-Induced Conformational Heterogeneity and Nucleotide Excision Repair. *Biochemistry* 2007;46(40):11263-11278.
31. Yang T, Huang Y, Cho BP. Synthesis and characterization of enantiomeric anti-2-fluorobenzo [a] pyrene-7, 8-dihydrodiol-9, 10-epoxides and their 2'-deoxyguanosine and oligodeoxynucleotide adducts. *Chemical research in toxicology* 2006;19(2):242–254.
32. Gillet LC, Schärer OD. Preparation of C8-amine and acetylamine adducts of 2'-deoxyguanosine suitably protected for DNA synthesis. *Organic letters* 2002;4(24):4205–4208.
33. Kazerani S, Novak M. Synthesis and Characterization of the Food-Derived Carcinogens 2-(Hydroxylamino)- α -carboline and 2-(Hydroxylamino)-3-methyl- α -carboline. *The Journal of organic chemistry* 1998;63(3):895–897.
34. Matsumoto T, Yoshida D, Tomita H, Matsushita H. Synthesis of 2-Amino-9H-pyrido[2, 3-b]indole Isolated as a Mutagenic Principle from Pyrolytic Products of Protein. *Agricultural and Biological Chemistry* 1979;43(3):675-677.

35. Im Y, Lee JY. Effect of the position of nitrogen in pyridoindole on photophysical properties and device performances of α -, β -, γ -carboline based high triplet energy host materials for deep blue devices. *Chemical Communications* 2013;49(53):5948–5950.
36. Nafisi S, Bonsaii M, Maali P, Khalilzadeh MA, Manouchehri F. β -Carboline alkaloids bind DNA. *Journal of Photochemistry and Photobiology B: Biology* 2010;100(2):84–91.
37. Laha JK, Barolo SM, Rossi RA, Cuny GD. Synthesis of Carbolines by Photostimulated Cyclization of Anilinothalopyridines. *J. Org. Chem.* 2011;76(15):6421-6425.
38. Peng H, Chen X, Chen Y, He Q, Xie Y, Yang C. Solvent-free synthesis of δ -carbolines/carbazoles from 3-nitro-2-phenylpyridines/2-nitrobiphenyl derivatives using DPPE as a reducing agent. *Tetrahedron* 2011;67(32):5725-5731.
39. Laha JK, Petrou P, Cuny GD. One-Pot Synthesis of α -Carbolines via Sequential Palladium-Catalyzed Aryl Amination and Intramolecular Arylation. *J. Org. Chem.* 2009;74(8):3152-3155.
40. Freeman AW, Urvoy M, Criswell ME. Triphenylphosphine-mediated reductive cyclization of 2-nitrobiphenyls: a practical and convenient synthesis of carbazoles. *The Journal of organic chemistry* 2005;70(13):5014–5019.
41. Appukkuttan P, Van der Eycken E, Dehaen W. Microwave-enhanced Cadogan cyclization: an easy access to the 2-substituted carbazoles and other fused heterocyclic systems. *Synlett* 2005;(1):127-133.
42. Hung TQ, Dang TT, Janke J, Villinger A, Langer P. Efficient synthesis of α - and δ -carbolines by sequential Pd-catalyzed site-selective C–C and twofold C–N coupling reactions. *Organic & biomolecular chemistry* 2015;13(5):1375–1386.
43. Lopchuk JM. Chapter 4.2 - Five-Membered Ring Systems: Pyrroles and Benzo Analogs. In: Gordon W. Gribble and John A. Joule, ed. *Progress in Heterocyclic Chemistry*. Vol Volume 25. Elsevier; 2013:137-182.
44. Mérour J-Y, Joseph B. Synthesis and Reactivity of 7-Azaindoles (1H-Pyrrolo (2, 3-b) pyridine). *Current Organic Chemistry* 2001;5(5):471–506.
45. Thomae D, Jeanty M, Coste J, Guillaumet G, Suzenet F. Extending the Scope of the Aza-Fischer Synthesis of 4- and 6-Azaindoles. *European Journal of Organic Chemistry* 2013;2013(16):3328–3336.
46. Liu C, Han N, Song X, Qiu J. A General and Highly Efficient Method for the Construction of Aryl-Substituted N-Heteroarenes. *European Journal of Organic Chemistry* 2010;2010(29):5548–5551.

47. Yan G, Yang M. Recent advances in the synthesis of aromatic nitro compounds. *Organic & biomolecular chemistry* 2013;11(16):2554–2566.
48. González RR, Liguori L, Carrillo AM, Bjørsvik H-R. Synthesis of 2-Nitro- and 2,2'-Dinitrobiphenyls by Means of the Suzuki Cross-Coupling Reaction. *J. Org. Chem.* 2005;70(23):9591-9594.
49. Buchwald S, Klapars A, Kwong F, Streiter E, Zanon J. *Copper-catalyzed Formation of Carbon-heteroatom and Carbon-carbon Bonds*. Google Patents; 2004. Available at: <http://www.google.com/patents/US20040138468>.
50. Wasik R, Lebska M, Felczak K, Poznański J, Shugar D. Relative role of halogen bonds and hydrophobic interactions in inhibition of human protein kinase CK2 α by tetrabromobenzotriazole and some C (5)-substituted analogues. *The Journal of Physical Chemistry B* 2010;114(32):10601–10611.
51. Liu Q-L, Wen D-D, Hang C-C, Li Q-L, Zhu Y-M. A Novel and Regiospecific Synthesis of 1-Aryl-1H-benzotriazoles via Copper (I)-Catalyzed Intramolecular Cyclization Reaction. *Helvetica Chimica Acta* 2010;93(7):1350–1354.
52. Wei X. Coupling activators for the oligonucleotide synthesis via phosphoramidite approach. *Tetrahedron* 2013;69(18):3615–3637.
53. Gillet LC, Alzeer J, Schärer OD. Site-specific incorporation of N-(deoxyguanosin-8-yl)-2-acetylaminofluorene (dG-AAF) into oligonucleotides using modified “ultra-mild”DNA synthesis. *Nucleic acids research* 2005;33(6):1961–1969.
54. Anderson KW, Tundel RE, Ikawa T, Altman RA, Buchwald SL. Monodentate Phosphines Provide Highly Active Catalysts for Pd-Catalyzed CN Bond-Forming Reactions of Heteroaromatic Halides/Amines and (H) N-Heterocycles. *Angewandte Chemie International Edition* 2006;45(39):6523–6527.
55. Szombati Z, Baerns S, Marx A, Meier C. Synthesis of C8-Arylamine-Modified 2'-Deoxyadenosine Phosphoramidites and their Site-Specific Incorporation into Oligonucleotides. *ChemBioChem* 2012;13(5):700–712.
56. Driver MS, Hartwig JF. Carbon–Nitrogen-Bond-Forming Reductive Elimination of Arylamines from Palladium(II) Phosphine Complexes. *J. Am. Chem. Soc.* 1997;119(35):8232-8245.